[American Journal of Science, Vol. 321, December, 2021, P. 1381–1444, DOI 10.2475/10.2021.01]

American Journal of Science

DECEMBER 2021

THE ROLE OF THE SOLID EARTH IN REGULATING ATMOSPHERIC O_2 LEVELS

DANIEL A. STOLPER*,†, JOHN A. HIGGINS**, and LOUIS A. DERRY***

ABSTRACT. **Solid-earth processes act as both sources and sinks for atmospheric O_2. They act as sinks by introducing reduced minerals and gases to the earth's surface that can remove O_2 from the atmosphere and ocean. They act as sources by exporting organic carbon and sedimentary pyrite to the mantle via subduction. Here we examine the relative sizes of igneous source and sinks of O_2 for the modern earth to determine their magnitudes and if they are in balance today. We find that igneous sinks for O_2 remove 1.83×10^{12} mol O_2/yr (±0.43, 1σ) while subduction indirectly releases 1.56×10^{12} mol/O_2 yr (±0.33, 1σ). This indicates that today igneous O_2 sinks are balanced by solid earth sources. We propose this balance is achieved by negative feedbacks associated with either low-temperature hydrothermal sinks for O_2, which are sensitive to deep-ocean O_2 concentrations, or the amount of organic carbon and pyrite buried in sediments and subducted, which are sensitive to dissolved O_2 concentrations. We also explore how igneous sinks for O_2 may have varied in the Neoproterozoic when atmospheric O_2 concentrations are thought to have been lower and the deep ocean anoxic. We find that despite these changes, the igneous O_2 sink was essentially the same as today: 1.78×10^{12} (±0.43, 1σ) mol O_2/yr. We explore how this sink would change as the deep ocean accumulated sulfate, became oxygenated, and began oxidizing oceanic crust such that there was an increase in the subduction flux of oxidants to the subarc mantle. We propose that significant changes to the O_2 cycle, both in terms of positive and negative feedbacks could occur during these transitions. For example, accumulation of sulfate in the deep ocean would increase the oxidation state of high-temperature hydrothermal fluids, decreasing the size of this O_2 sink and thus promoting an increase in atmospheric O_2. In contrast, the oxygenation of the deep ocean would have allowed hydrothermally derived H_2S to react with and consume O_2 instead of being titrated out via reactions with dissolved Fe^{2+}. Additionally, deep-ocean oxygenation would have initiated the oxidation of oceanic crust at low temperatures, creating new sinks for O_2. Finally, the oxidation of the subarc mantle via subduction of newly oxidized sediments and altered oceanic crust would have increased the oxygen fugacity of arc volcanic gases, decreasing their overall demand for O_2, allowing yet more O_2 to accumulate in the atmosphere. We place these changes into a conceptual framework and discuss their potential impact on the history of atmospheric and marine O_2 concentrations from the Neoproterozoic to late Paleozoic.**

Key words: earth history, hydrothermal, mantle, oxygen, redox, subduction, volcanism, weathering

* Department of Earth and Planetary Science, University of California, Berkeley, California 94720, USA
** Department of Geosciences, Princeton University, Princeton, New Jersey 08544, USA
*** Department of Earth and Atmospheric Sciences, Cornell University, Ithaca, New York 14853, USA
† Corresponding author: dstolper@berkeley.edu

INTRODUCTION

The partial pressure of atmospheric O_2, $P_{O_2}^{atm}$, is thought to have been relatively high and stable (~0.05–0.45 atm) over the past 400 million years (Berner and Canfield, 1989; Hansen and Wallmann, 2003; Bergman and others, 2004; Falkowski and others, 2005; Arvidson and others, 2006; Berner, 2006; Berner, 2009; Glasspool and Scott, 2010; Tappert and others, 2013; Lenton and others, 2018). In contrast, the atmosphere of the early earth (>2.5 billion years ago) is understood to have been essentially anoxic ($<10^{-5}$ current atmospheric levels) (for example, Rye and Holland, 1998; Farquhar and others, 2000; Pavlov and Kasting, 2002; Canfield, 2005; Lyons and others, 2014). The relatively high modern $P_{O_2}^{atm}$ (0.21 atm) vs. that in the Archean requires that over some time period in earth's past, atmospheric O_2 sources exceeded sinks such that O_2 accumulated. The relatively stable $P_{O_2}^{atm}$ (~0.05–0.45 atm) over the past 400 million years (or longer) further requires that over this time frame, the absolute magnitude of O_2 sources and sinks have been sufficiently similar to prevent excursions beyond this range.

O_2 is in net added to the atmosphere today due the sedimentary burial of reduced elements generated directly or indirectly by oxygenic photosynthetic organisms. The direct generation of O_2 occurs via burial of organic carbon synthesized by oxygenic photoautotrophs. The indirect addition of O_2 occurs via anaerobic dissimilatory metabolisms that transfer electrons from organic carbon to other redox sinks such as Fe^{3+} or sulfate that are then buried as minerals (for example pyrite). Examples of previous estimates for the size of this O_2 source based on organic carbon and pyrite sedimentary burial rates are 4.5 to 18.4 $\times$ 10^{12} mol O_2/yr (for example, Kump and Garrels, 1986; Holland, 2002; Hansen and Wallmann, 2003; Kasting and Canfield, 2012; Laakso and Schrag, 2014; Lenton and others, 2018). With ~3.7 $\times$ 10^{19} moles of O_2 in the atmosphere today,[1] these fluxes yield geological residence times of atmospheric O_2 of about 2 to 8 million years. We note that the oxygen in atmospheric O_2 is recycled (that is, converted back to water and then back to O_2) ~1,000 times faster by life on earth's surface during total (that is, gross) photosynthesis and respiration (yielding a residence time of ~1000 years; Bender and others, 1994). This faster cycling of O_2 by life has little effect on atmospheric O_2 levels as nearly all (>99.9%) of the photosynthetically derived organic carbon is aerobically respired rather than buried in sediments preventing the net accumulation of O_2 in the atmosphere.

Today, atmospheric O_2 sources are almost entirely related to the activity of life. Inorganic (that is, abiotic) O_2 sources such as H_2 escape from the atmosphere are estimated to contribute ~0.02 $\times$ 10^{12} moles of O_2/year today (Catling and others, 2001; Kasting and Canfield, 2012), which is 200 to 1000 times smaller in size than biologically associated geological O_2 fluxes.

The main sinks for O_2 on geologic timescales are the oxidation of organic carbon and pyrite in eroding sedimentary rocks and the oxidation of outgassed reduced gases derived from their breakdown during burial. Estimates for the size of this sink range from 4.5 to 15.5 $\times$ 10^{12} mol O_2/yr (for example, Kump and Garrels, 1986; Holland, 2002; Hansen and Wallmann, 2003; Kasting and Canfield, 2012; Laakso and Schrag, 2014; Lenton and others, 2018)—these yield geologic residence times for modern atmospheric O_2 of 8.2 to 2.4 million years. Reaction of O_2 with ancient organic carbon

[1] We note that estimates for the amount of O_2 in the atmosphere in geochemical studies typically vary from 3.6 $\times$ 10^{19} moles (for example, Kasting and Canfield, 2012) to 3.8 $\times$ 10^{19} moles (for example, Catling and Claire, 2005). The value of 3.7 $\times$ 10^{19} moles given here was derived from *Allen's Astrophysical Quantities*, 4th edition (Cox, 2002) as follows: they provide a (dry) mass of the earth's atmosphere of 5.136 $\times$ 10^{18} kg with a weight percent O_2 of 23.14%. This yields a total atmospheric mass of 1.19$\times$$10^{18}$ kg of O_2 (that is, 3.7 $\times$ 10^{19} moles).

and reduced minerals (and their metamorphic products) represent an O_2 sink directly tied to biological processes—these reduced species exist in sediments today due to the activity of oxygenic photoautotrophs. However, unlike modern O_2 sources where >99.5% of the O_2 produced is derived from the activity of life, there are also significant non-biologically associated O_2 sinks. These include mantle-derived reduced volcanic gases emitted to the atmosphere; reduced hydrothermal fluids created during alteration of oceanic crust and emitted to oceans in the vicinity of spreading centers; and the oxidative weathering of submarine and subaerial igneous rocks. As the source of electrons that reduce O_2 are derived directly from igneous rocks or gases, we term these sinks 'igneous O_2 sinks', but note that the processes involved in the transfer of these electrons to O_2 include uplift, erosion, low-temperature weathering, and metamorphism.

Estimates of the total size of modern igneous O_2 sinks vary from about 0.2×10^{12} to 3.1×10^{12} mol O_2/yr (Holland, 2002; Hayes and Waldbauer, 2006; Kasting and Canfield, 2012; Laakso and Schrag, 2014; Derry, 2015; Catling and Kasting, 2017; Daines and others, 2017; Laakso and Schrag, 2017; Miyazaki and others, 2018; Galvez, 2020). Direct comparison of these estimates is not straightforward as the various studies cited do not always include the same igneous sinks. For example, Hayes and Waldbauer (2006), who provide the lowest estimate (0.2–0.6 $\times$ 10^{12} moles O_2/yr), only considered reduced volcanic gases emitted from arc volcanoes. Nevertheless, we can put the magnitude of these estimates into context as follows. First, if these igneous O_2 sinks were left unchecked (that is, were not balanced by a concomitant O_2 source), all O_2 in the atmosphere would be removed within 12 to 185 million years depending on the sink size (0.2×10^{12} to 3.1×10^{12} mol O_2/yr). Second, maximum estimates of the igneous sink of $\sim 3 \times 10^{12}$ moles O_2/yr (Catling and Kasting, 2017; Galvez, 2020) approach the sizes of some estimates of the O_2 source generated via burial of organic carbon and pyrite: 4.5×10^{12} mol O_2/yr in Kump and Garrels (1986) and 6.4×10^{12} mol O_2/yr in the most recent version of the COPSE model (Bergman and others, 2004; Lenton and others, 2018). This suggests that estimates of modern O_2 igneous sink sizes may be sufficiently large to play a role in setting modern atmospheric O_2 concentrations.

A complexity worth noting in the discussion of igneous sinks is the importance of the identity of the mantle-derived species being oxidized. For example, if one mole of Fe^{2+} in an igneous rock is oxidized to Fe^{3+} by O_2 and then converted back to Fe^{2+} by dissimilatory iron reducing bacteria using organic carbon created by oxygenic phototrophic organisms, there will be no net change in $P_{O_2}^{atm}$. In contrast, if one mole of SO_2 is emitted from a volcano and oxidized to sulfate by atmospheric O_2, half a mole of O_2 will be consumed. However, if one mole of the S^{6+} in sulfate is then converted to S^{1-} in pyrite through dissimilatory sulfate reduction using electrons from organic carbon originally generated by oxygenic photosynthetic organisms, 1.75 moles of O_2 will be indirectly added to the atmosphere. This would result in a net release of 1.25 moles of O_2. Thus volcanic SO_2 emissions, depending on the fraction of sulfur either buried as sulfate minerals or accumulated as dissolved sulfate in the oceans vs. that buried as pyrite dictates whether volcanic SO_2 emissions are, in net, a source or sink for atmospheric O_2. Aspects of this are encapsulated by the '*f* ratio' described in Holland (2002).

A longstanding question is whether the size of the igneous O_2 sinks have changed with time and, as a result, played a role in the history of $P_{O_2}^{atm}$. For example, arguments have been made that the fO_2 (oxygen fugacity) of the mantle may have increased with time, volcanic eruptive pressures decreased, or volcanic eruptive temperatures decreased such that (in any of these cases) volcanic gases would have been more reducing in the Archean vs. the present (for example, Kasting and others, 1993;

Holland, 2002, 2009; Gaillard and others, 2011; Aulbach and Stagno, 2016; Nicklas and others, 2018; Moussallam and others, 2019b; Nicklas and others, 2019; Kadoya and others, 2020b). In turn, such changes would decrease the size of the volcanic O_2 sink with time. We note, however, that there remains vigorous debate on these proposals (for example Li and Lee, 2004; Kasting and others, 2012; Kadoya and others, 2020a). As an example, Holland (2009) assumed reduced gases from volcanism consumed ~3 to 6 $\times$ 10^{12} moles of O_2/yr 4.5 billion years ago, about 1 to 2x higher than current estimates for the modern igneous sink and that this sink has declined with time. Alternatively, Alcott and others (2019) assumed that the flux of reduced igneous species was capable of consuming 4.5 $\times$ 10^{13} moles of O_2/yr four billion years ago, which is 15$\times$ larger than the highest current estimate for the igneous sink in the modern, and that this flux has decreased monotonically with time.

Finally, the solid earth can also act as an indirect O_2 source through subduction (for example, Hayes and Waldbauer, 2006). Subduction of sedimentary organic carbon and pyrite is an indirect source of atmospheric O_2 as they are no longer available to be tectonically uplifted and oxidized by atmospheric O_2 during weathering. We note that volcanic outgassing of originally subducted organic carbon via volcanism is not an O_2 sink because CO_2 is the dominant volcanic carbon species. For example, CO_2 comprises on average 99.1% of carbon species emitted at arc volcanoes (based on compiled data given in Symonds and others, 1994), the parental melts of which are influenced by subducted materials. Hayes and Waldbauer (2006) examined the issue of organic carbon subduction and came to the conclusion that the flux of subducted organic carbon to the mantle has always been lower than the sedimentary burial flux of organic carbon. As a result, they calculate that the sedimentary organic carbon content of continental crust has increased continuously over earth's history, and thus that the total amount of organic carbon stored in continental crust has approximately doubled over the past billion years. Importantly, this burial is not envisioned to cause atmospheric O_2 levels to rise in lock step. Rather, they proposed that O_2 levels have been kept in check by the accumulation of oxidized elements derived from the oxidation of igneous rocks and gases over geologic time.

In this paper we address the question of the role played by the solid earth in setting $P_{O_2}^{atm}$ both in the modern and in the geologic past. To do this, we examine and evaluate the following questions:

(1) What is our understanding of the balance (or lack thereof) for the atmospheric O_2 cycle in the recent geological past (<1 million years)?
(2) What are the consequences of including vs. not including solid-earth/igneous O_2 sinks and sources in biogeochemical models of atmospheric O_2 on geological timescales?
(3) What is our best estimate of the sizes of the modern igneous O_2 sinks and solid-earth O_2 subduction sources?
(4) Finally and speculatively, which if any igneous sinks for O_2 would differ in the Proterozoic when $P_{O_2}^{atm}$ was lower vs. today and could such differences have played a role in changes in $P_{O_2}^{atm}$ over geologic time?

O_2 (im)balance for the modern

Models of $P_{O_2}^{atm}$ over the Phanerozoic invariably include negative feedbacks to ensure that $P_{O_2}^{atm}$ stabilizes at high levels (~0.05–0.45 atm; but not too high). As reviewed in Berner (2001), without such feedbacks, modeled $P_{O_2}^{atm}$ levels over the Phanerozoic commonly yield nonsensical values (for example, negative numbers; Lasaga, 1989). Such models incorporate a variety of different forms of negative

feedbacks (Berner, 1987, 2006, 2009; Kump, 1989; Van Cappellen and Ingall, 1996; Lasaga and Ohmoto, 2002; Bergman and others, 2004; Arvidson and others, 2006; Laakso and Schrag, 2014; Lenton and others, 2018). Additionally, such models commonly make the assumption that the modern cycle is in balance (for example, Lasaga and Ohmoto, 2002; Bergman and others, 2004; Laakso and Schrag, 2014; Laakso and Schrag, 2017; Lenton and others, 2018), although imbalances are sometimes allowed (for example, Derry and France-Lanord, 1996; Hansen and Wallmann, 2003; Li and Elderfield, 2013; Caves and others, 2016).

We begin our discussion with the question of whether O_2 sources and sinks in the near modern (here the past million years) are or are not in balance. Previous estimates of the near-modern differences between geological sources and sinks of O_2 are based on comparisons of the relative sizes of all O_2 sources vs. all sinks (for example, Holland, 1978, 2002; Hansen and Wallmann, 2003; Kasting and Canfield, 2012). Uncertainties are large on any individual source or sink term (often ~50% relative), which in turn leads to large uncertainties on the total source or sink size. As a commonly used example, Holland (2002) gives the total geologic source of O_2 to the atmosphere as 17.8×10^{12} mol O_2/yr with an uncertainty of $\pm 7.8 \times 10^{12}$. This uncertainty is ~40% of the total flux and is larger than some estimates of the total geologic sink for O_2. Although such estimates give an order of magnitude sense for the size of various O_2 fluxes, we consider the uncertainty to be too large to rigorously evaluate whether the modern O_2 cycle is in balance.

One constraint with stated precisions sufficiently small for this task is based on measurements of atmospheric O_2/N_2 ratios derived from ancient gases trapped in ice cores from the past 800,000 years (Stolper and others, 2016). This record indicates that $P_{O_2}^{atm}$ has declined over the past 800,000 years at a rate of 0.84%/myr (± 0.2, 1σ; relative to modern $P_{O_2}^{atm}$) equal to a decline of 0.31×10^{12} mol O_2/yr. Using the range of estimates for the size of geologic O_2 sources from above ($4.5–18.4 \times 10^{12}$ mol O_2/yr) and 3.7×10^{19} mol O_2 in the atmosphere, we can calculate that sinks exceed sources by 1.7 to 6.9%.

The net imbalance of 0.31×10^{12} mol O_2/yr calculated from the ice-core data is pertinent for two reasons. First, it provides support for the common assumption that the O_2 cycle, for whatever reason, is today close to being in balance such that sources and sinks balance to within a few percent. This supports but does not require that negative feedbacks exist that stabilize $P_{O_2}^{atm}$ on geological timescales. Second, as discussed above, typical estimates for the total size of the various igneous O_2 sinks are up to 10× larger than the imbalance indicated by the ice-core O_2/N_2 record (3.1×10^{12} vs. 0.31×10^{12} mol O_2/yr). If the total igneous sink is indeed significantly larger than the observed decline based on the ice-core record, then it follows that there must be a net sequestration of organic carbon or reduced minerals in continental crust or subduction zones to roughly balance the igneous sink of O_2.

MODELS OF $P_{O_2}^{atm}$ WITHOUT THE SOLID EARTH

Before estimating the sizes of the igneous O_2 sinks and sources, we first examine a simplified model framework in order to place these estimates into a quantitative context and highlight many of the issues that arise when considering igneous sinks for O_2 in the history of $P_{O_2}^{atm}$. Specifically, in this and the following two sections, we explore how the inclusion of igneous O_2 sinks and subduction sources affect models of atmospheric O_2. We first review model formulations that do not include igneous and solid-earth processes and then build up to models that incorporate these in later sections. The purpose in doing this is to provide an order-of-magnitude understanding of the importance of these various processes to the global carbon and oxygen cycles. It is not meant to simulate the full fluid+solid earth system in detail.

Most models of $P_{O_2}^{atm}$ do not include igneous O_2 sinks or removal of surface-derived carbon or sulfur to the mantle via subduction—for example these are not included in the commonly employed GEOCARBSULF model (Berner, 2006, 2009; Royer and others, 2014) and in the COPSE model (Bergman and others, 2004; Lenton and others, 2018; Lenton, 2020). Although these models vary in detail, they are governed by the following equations for tracking the carbon cycle where the amount of carbon in the atmosphere and ocean, $C_{ocn+atm}$, as a function of time is:

$$\frac{dC_{ocn+atm}}{dt} = F_{w;C_{inorg}} + F_{w;C_{org}} + F_{volc} - F_{b;C_{inorg}} - F_{b;C_{org}} \quad (1)$$

$F_{w;C_{inorg}}$ is the flux of carbon, C, into the system from weathering of inorganic carbonate minerals; $F_{w;C_{org}}$ is the flux into the system of carbon from oxidative weathering of ancient organic carbon; F_{volc} is the combined volcanic and metamorphic fluxes of carbon into the system; $F_{b;C_{inorg}}$ is the flux of carbon out of the system from burial of inorganic carbonate minerals in sediments; and $F_{b;C_{org}}$ is the flux of carbon out of the system from the burial of newly produced organic carbon in sediments.

In the GEOCARBSULF and COPSE models, the volcanic and metamorphic fluxes of carbon are sourced solely from the breakdown of sedimentary carbonate or organic carbon such that the emitted carbon has the same oxidation state as what was buried. As such, the models' combined atmospheric and sedimentary reservoirs are closed with respect to carbon (Lenton, 2020) and receive no new carbon from the mantle. More recent iterations of these models have attempted to address aspects of this assumption. For example, Williams and others (2019) (also see Tostevin and Mills, 2020) allow for a mantle input of CO_2 from mid-ocean ridges only (but not other mantle sources) but no subduction term such that the sedimentary reservoir must grow with time—they argue this is unimportant as the change in sedimentary carbon reservoirs over the time scales of hundreds of millions of years is negligible based on the work of Hayes and Waldbauer (2006).

A question is whether the amount of mantle-derived carbon added to the atmosphere from volcanism over the Phanerozoic (the timescale over which these models are typically run) is sufficiently small that it can be ignored and only the sedimentary reservoirs considered? We evaluate this as follows: Marty and Tolstikhin (1998) estimate that up to 5.7×10^{12} moles of mantled-derived carbon/yr is emitted to the atmosphere (this excludes sedimentary derived carbon emitted at arcs). Given an assumed modern sedimentary reservoir size of 6.25×10^{21} moles carbon (both carbonate and organic carbon) in the GEOCARBSUF and COPSE models (Bergman and others, 2004; Berner, 2006, 2009; Royer and others, 2014; Lenton and others, 2018), and the assumption that carbon is not subducted into the mantle (that is, if subducted, it is reemitted at arcs), this volcanic carbon flux would require that the total sedimentary inventory of carbon approximately doubled (97% growth) over the Phanerozoic. This is calculated by taking the modern sedimentary carbon inventory (6.25×10^{21} moles), subtracting 5.7×10^{12} moles of mantled-derived carbon/yr times 541 million years (the Phanerozoic) and comparing the two numbers. We consider such an increase sufficiently large that it will affect model assumptions. In other words, this simple calculation indicates that on timescales of hundreds of millions of years, the integrated flux of CO_2 from mantle degassing is a significant source of carbon to earth's surface and sedimentary reservoir.

A SIMPLE MODEL WITH IGNEOUS SOURCES OF CO_2 AND CONSTANT ATMOSPHERIC $P_{O_2}^{atm}$

We now extend this framework to consider a system that includes mantle CO_2 outgassing as a net source of carbon to the atmosphere and feedbacks that keep $P_{O_2}^{atm}$ constant. We do not allow for the net subduction of carbon into the mantle (that is, all subducted carbon is remitted at arcs at the same redox state as it was subducted). We also do not include igneous sinks for O_2. Equation (1) holds and now includes a mantle CO_2 source. $P_{O_2}^{atm}$ set by the difference in organic C burial vs. weathering fluxes:

$$\frac{dO_2}{dt} = F_{b;C_{org}} - F_{w;C_{org}} \tag{2}$$

We assume, as is typical, a 1:1 CO_2:O_2 ratio for organic carbon burial and oxidation. The change in the sedimentary organic carbon reservoir, $Sed_{C_{org}}$, vs. time is equal to:

$$\frac{dSed_{C_{org}}}{dt} = F_{b;C_{org}} - F_{w;C_{org}} \tag{3}$$

Thus, the change in atmospheric O_2 and $Sed_{C_{org}}$ are equal:

$$\frac{dO_2}{dt} = \frac{dSed_{C_{org}}}{dt} \tag{4}$$

The change in the sedimentary carbonate reservoir, $Sed_{C_{inorg}}$, is given by:

$$\frac{dSed_{C_{inorg}}}{dt} = F_{b;C_{inorg}} - F_{w;C_{inorg}} \tag{5}$$

We adopt the assumption that atmospheric O_2 levels are maintained through the operation of negative feedbacks (Berner, 1987, 2006, 2009; Kump, 1989; Van Cappellen and Ingall, 1996; Lasaga and Ohmoto, 2002; Bergman and others, 2004; Arvidson and others, 2006; Laakso and Schrag, 2014; Lenton and others, 2018) such that $\frac{dO_2}{dt} = 0$. We additionally assume operation of a silicate weathering feedback that keeps $C_{ocn+atm}$ constant (for example, Walker and others, 1981; Berner and Caldeira, 1997) such that $\frac{dC_{ocn+atm}}{dt} = 0$. Under these conditions, the following is true:

$$F_{volc} = \frac{dSed_{C_{inorg}}}{dt} = F_{b;C_{inorg}} - F_{w;C_{inorg}} \tag{6}$$

This equation can be understood as follows: because atmospheric O_2 concentrations are not changing, the sedimentary organic carbon reservoir also does not change with time (eq 4) and, as such, any input of carbon from the mantle to the ocean or atmosphere must be deposited as inorganic carbon. This then results in a net increase in the sedimentary carbonate reservoir. Put another way, given our model assumptions (mantle carbon source, no subduction of carbon, $\frac{dO_2}{dt} = 0$, and a silicate weathering feedback), all mantle-derived C added to the ocean and atmosphere leaves as carbonate minerals.

Finally, we assume that carbonate weathering is proportional to total carbonate mass in sediments (for example, Berner, 1991; Bergman and others, 2004):

$$F_{w;C_{inorg}} = k_{w;C_{inorg}} \times Sed_{C_{inorg}} \quad (7)$$

where $k_{w;C_{inorg}}$ is a rate constant. All equations above can also be derived for stable carbon isotopic compositions.

We solve equations (1) through (7) over the timescale of the Phanerozoic such that the current $Sed_{C_{org}}$ and $Sed_{C_{inorg}}$ reservoirs sizes are 4.9 and 1.35×10^{21} moles C (taken from the baseline COPSE reloaded model of Lenton and others, 2018). We use a mantle-derived volcanic outgassing flux of 5.7×10^{12} mol CO_2/yr (Marty and Tolstikhin, 1998) and C_{org} oxidative weathering flux of 7.5×10^{12} mol C_{org}/yr (Holland, 1978, 2002), which is also the C_{org} burial flux given our requirement that $\frac{dO_2}{dt} = 0$. Together, these set the carbonate reservoir size at 1.82×10^{21} moles C at the start of the Phanerozoic (that is, 4.9×10^{21} moles C minus 5.7×10^{12} mol CO_2/yr times 541 million years). We assume that at the start of the Phanerozoic (541 million years ago), 20% of carbon is buried as organic carbon and 80% as carbonate minerals (see typical carbon isotope mass balance arguments; for example, Hayes and others, 1999). This together with our other assumptions allows us to calculate that the initial carbonate weathering flux is 24.3×10^{12} mol C/yr and thus that $k_{w;C_{inorg}}$ is 1.34×10^{-8} yr^{-1}. For the isotopic modeling, we assume volcanic outgassing has a $\delta^{13}C$ of −5‰ and that the initial sedimentary reservoirs have a $\delta^{13}C$ of 0‰ for carbonates and −25‰ for organic carbon. Finally, we assume that newly deposited organic carbon is 25‰ lower in $\delta^{13}C$ than newly formed carbonate sediment. These are typical values used in models of carbon isotope mass balance (for example, Des Marais, 2001).

Figure 1 presents modeled changes in the relative carbonate reservoir size (fig. 1A), fraction of carbon based as organic carbon (labeled f_{org}; fig. 1B), and the $\delta^{13}C$ of newly deposited carbonate (fig. 1C) as a function of time. The total carbonate reservoir increases by 170% over the Phanerozoic while f_{org} decreases from 0.2 to 0.10. Despite this decrease, the absolute burial flux of organic carbon remains constant as required by the assumption that $\frac{dO_2}{dt} = 0$ and equation (4). The decrease in f_{org} is due to increases in the total influx of carbon at every time step. This occurs because as more carbonate is added to the sedimentary carbonate reservoir, more carbonate weathers due to the assumed dependence of carbonate weathering flux on the size of the carbonate sedimentary reservoir. This has the effect of lowering f_{org} due to increased fluxes of carbonate in and out of the system. Finally, the $\delta^{13}C$ of newly buried carbonate decreases by 1.9‰ over the 541 million years of modeled time. This decrease occurs because, as the carbonate reservoir grows and increasingly represents the total input and output of carbon into and out of the ocean and atmosphere, it necessarily approaches the isotopic value of the volcanic input term (−5‰).

Two important points emerge from this exercise. First, an earth system where carbon is not returned to the mantle via subduction, with a silicate weathering feedback, with constant $P_{O_2}^{atm}$, and with volcanic outgassing of CO_2 from the mantle would have experienced a large (order 100%) increase in the sedimentary carbonate reservoir over the Phanerozoic. Second, in this earth system, the imbalance with respect to carbon but not O_2 manifests itself as a decrease in f_{org} and the $\delta^{13}C$ of carbonate deposited over time. Although such decreases are usually associated with a decline in $P_{O_2}^{atm}$ (for example, Berner, 1991; Hayes and others, 1999; Canfield, 2005), that is not the case here.

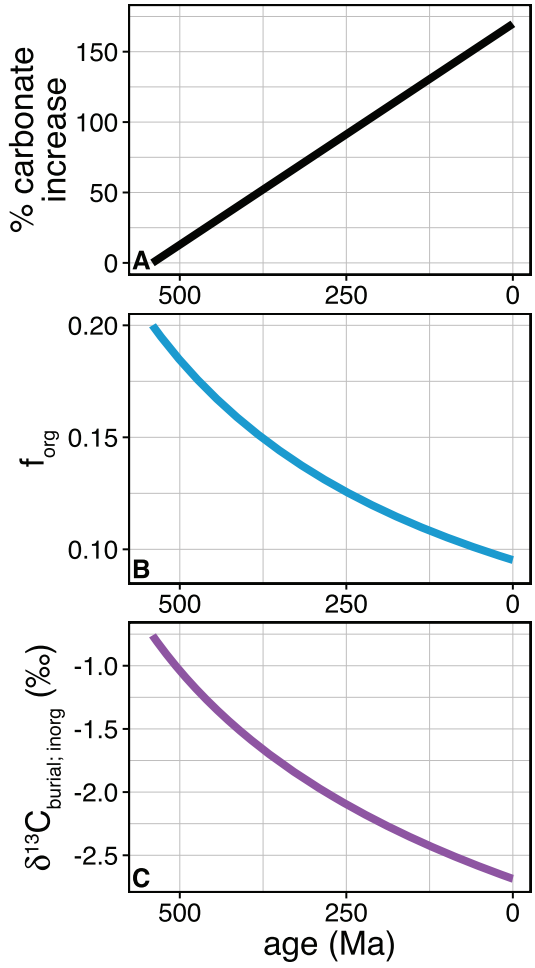

Fig. 1. Model output of a system in which no subduction of carbon occurs, $P_{O_2}^{atm}$ is constant, and CO_2 is released to the ocean and atmosphere from the mantle. See section *Models of $P_{O_2}^{atm}$ Without the Solid Earth* for details. (A) Percent change in total sedimentary carbonate relative to the initial value at 541 Ma. (B) Fraction of carbon buried as organic carbon (f_{org}). (C) Change in the $\delta^{13}C$ of carbonate buried at a given geologic age.

Models of $P_{O_2}^{atm}$ with Igneous Oxidation and Without Subduction

The next layer of complexity we consider is what happens when igneous sinks for O_2 are included in our calculations, but with the net subduction of carbon into the mantle still neglected. We modify equation (2) to include an igneous O_2 sink ($F_{igneous}$):

$$\frac{dO_2}{dt} = F_{b;C_{org}} - F_{w;C_{org}} - F_{igneous} \tag{8}$$

For clarity, we first only consider the role of carbon and then expand the model to include sulfur. When $\frac{dO_2}{dt} = 0$ and $F_{igneous}$ is a finite positive number, given equation (4), the following condition holds:

$$\frac{\mathrm{dSed}_{C_{org}}}{\mathrm{dt}} > 0 \tag{9}$$

Equation (9) shows that in order to balance the loss of O_2 to igneous sinks, the amount of organic carbon buried must exceed the amount oxidatively weathered. A similar sort of statement is articulated by equation (12) of Lécuyer and Ricard (1999) and discussed conceptually by Hayes and Waldbauer (2006). We note that without an igneous O_2 sink, the condition of equation (9) would generally be interpreted to indicate that atmospheric O_2 levels are increasing.

The question is how much do sedimentary organic carbon and pyrite reservoirs need to grow to keep $\frac{dO_2}{dt} = 0$ over the Phanerozoic when there is an igneous sink for atmospheric O_2? In other words, are the predicted increases in sedimentary organic carbon and pyrite required to balance typical estimates of the igneous O_2 sink size sufficiently small that they can be ignored, or are they geologically significant? To examine this, we use our toy model to calculate changes in sedimentary organic carbon and pyrite needed to balance the igneous O_2 sink over the Phanerozoic using the following simplifying assumptions. Specifically, (*i*) we perform our calculations under a range of igneous sink sizes from 1×10^9 mol O_2/yr up to the maximum suggested in previous studies (3.1×10^{12}; see discussion in the introduction). And (*ii*) we require that $\frac{dO_2}{dt} = 0$.

For this calculation, we use a modern C_{org} reservoir size of 1.35×10^{21} moles C (Lenton and others, 2018) and calculate the initial value at the start of the Phanerozoic by subtracting off the amount of organic carbon needed to balance the chosen size of the igneous O_2 sink—this must be calculated because models such as GEOCARB and the standard model of COPSE do not include igneous sinks of O_2, and instead move carbon and sulfur between oxidized and reduced sedimentary reservoirs. As such, as discussed above, the total carbon and sulfur in sediments stays constant by definition in these models. We calculate the relative growth in the sedimentary C_{org} size by ratioing the modern sediment C_{org} size to that calculated at 541 Ma. Results of this exercise are given in figure 2A. Given our choice of the modern C_{org} reservoir size (1.35×10^{21} moles C), the maximum allowable igneous O_2 sink size is 2.5×10^{12} moles O_2/yr. Larger sinks result in no sedimentary organic carbon at 541 Ma. Restricting ourselves to typical estimates of the igneous sink size of 1 to 2×10^{12} mol O_2/yr requires large increases in the size of the organic carbon reservoir of 1.67 to 5.09× over the Phanerozoic.

We now add pyrite burial and oxidation to the model by modifying equation (8):

$$\frac{\mathrm{dO_2}}{\mathrm{dt}} = \mathrm{F_{b;C_{org}}} - \mathrm{F_{w;C_{org}}} + \frac{15}{8}\mathrm{F_{b;S_{pyrite}}} - \frac{15}{8}\mathrm{F_{w;S_{pyrite}}} - \mathrm{F_{igneous}} \tag{10}$$

S_{pyrite} is the moles S from pyrite consumed during weathering or added to sediments during burial. The 15/8 relates the stoichiometry of O_2 reduced per mole S in pyrite oxidized (including Fe^{2+})—see equation (10) of Canfield (2005). We ignore other reduced sedimentary minerals as they are typically thought to be of secondary importance to the O_2 cycle (for example, Laakso and Schrag, 2014).

The change in total sulfur in the sedimentary pyrite reservoir is given by:

$$\frac{\mathrm{dSed_{S_{pyrite}}}}{\mathrm{dt}} = \mathrm{F_{b;S_{pyrite}}} - \mathrm{F_{w;S_{pyrite}}} \tag{11}$$

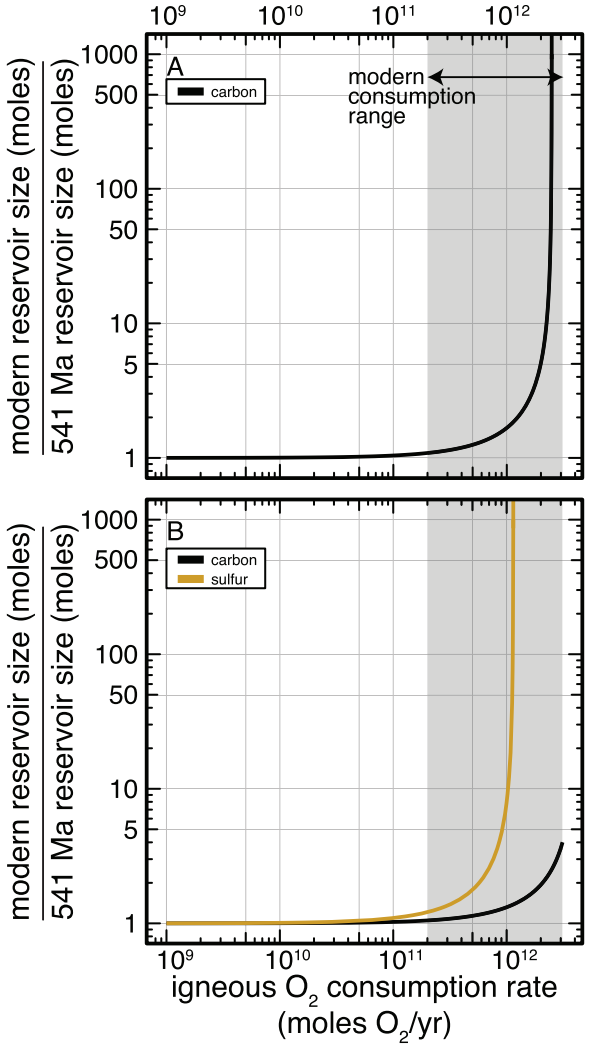

Fig. 2. Calculated relative increase in sedimentary organic carbon and pyrite reservoirs over the Phanerozoic required to perfectly balance the O_2 removed for a given igneous sink size. (A) Balance achieved only through organic carbon burial. (B) Balance achieved through combined organic carbon and pyrite burial. 60% of the O_2 burden is compensated by organic carbon burial and 40% via pyrite burial. Grey rectangles denote the typical range estimated for the igneous O_2 consumption rate ($0.2–3.1\times10^{12}$). See section *A Simple Model with Igneous Sources of CO_2 and Constant Atmospheric $P_{O_2}^{atm}$* for more details.

As such, the new condition under which both $\frac{dO_2}{dt} = 0$ and $F_{igneous}$ is a finite positive number is:

$$\frac{15}{8}\frac{dSed_{S_{pyrite}}}{dt} + \frac{dSed_{C_{org}}}{dt} > 0 \tag{12}$$

Equation (12) indicates that in order to balance the igneous O_2 sink, either the organic carbon or pyrite reservoirs (or both) must grow. We now perform the same calculations as above but include both organic carbon and pyrite burial. We fix the C:

S ratio of organic carbon:sulfur-in-pyrite such that 60% of the O_2 source is from C_{org} burial and 40% from pyrite burial. This ratio is based on typical estimates (37–44%; for example, Holland, 2002; Catling and Claire, 2005; Laakso and Schrag, 2014). We take the modern sedimentary C_{org} and sulfur-in-pyrite reservoir sizes from the output of the COPSE reloaded model as 1.35×10^{21} moles C in organic carbon and 1.32×10^{20} moles S in pyrite (Lenton and others, 2018).

Results from our calculations are given in figure 2B. For ranges of igneous O_2 sink sizes estimated for the modern ($0.2–3.1 \times 10^{12}$ moles O_2/yr), the C_{org} sedimentary reservoir size is estimated to have grown by 1.05 to 3.96× over the Phanerozoic. Thus the incorporation of pyrite burial resolves the issue encountered previously of there not being enough organic carbon in current sediments to balance the maximum igneous sink sizes estimated by previous studies. However, at the same time, once igneous O_2 consumption rates reach a value of 1.145×10^{12} mol O_2/yr, there is not enough sulfur in the sedimentary pyrite reservoir today (at least according to the value given by the baseline COPSE reloaded model; Lenton and others, 2018) to balance the igneous consumption flux. For igneous O_2 consumption rates of 1×10^{12} moles per year, which is at the lower end of published estimates for the modern, the model predicts that over the past 541 million years sedimentary organic carbon contents would have increased by 1.3× while sulfur in sedimentary pyrite would have increased by ~8×.

Precise quantitative conclusions from this modeling effort are challenging given the simplicity of the model and dependence on numerous model assumptions. Nevertheless, the key point is that inclusion of igneous O_2 sinks and mantle CO_2 sources but exclusion of net subduction of carbon and sulfur to the mantle in biogeochemical models indicate that sedimentary carbon (both carbonate and organic carbon) and sulfide inventories have to have grown significantly (10s to 100s of percent) over the Phanerozoic. We are not aware of any constraints on maximum or minimum allowable growth (or depletion) of sedimentary carbon and sulfur reservoirs over the Phanerozoic that could evaluate the reasonableness of the model estimates. But we consider these increases to be sufficiently large that, if they did occur, they would likely have impacted biogeochemical cycles and left a measurable signature in the geologic record.

THE ROLE OF SUBDUCTION IN THE O_2 CYCLE

Subduction of pyrite and organic carbon (and carbonate) into the mantle represents a mechanism to remove carbon and sulfur from the ocean/atmosphere system and thereby to prevent their net accumulation in continental crust. As such, subduction of organic matter and pyrite produced as a result of oxygenic photosynthesis represents a net source of O_2 to the atmosphere that could balance partly or wholly offset the loss of O_2 from igneous sinks. If subduction does not remove the required organic carbon and pyrite added to sediments each year to balance the igneous O_2 sinks, then either there must exist an unknown geologic source for O_2, sedimentary organic carbon and pyrite reservoir sizes must increase, or O_2 levels must fall (Hayes and Waldbauer, 2006).

We are aware of four quantitative biogeochemical modeling studies that incorporate both a subduction flux of organic carbon and/or pyrite as well as an igneous sink for O_2: (*i*) Hansen and Wallmann (2003) calculate that igneous sinks consume 2.24×10^{12} mol O_2/yr. Most of this sink is compensated for by subduction of organic carbon and pyrite ($+0.67 \times 10^{12}$ mol O_2/yr), net accumulation of sedimentary organic carbon and pyrite ($+0.57 \times 10^{12}$ moles/O_2), and via denitrification and other dissimilatory metabolisms ($+0.82 \times 10^{12}$ moles/O_2 yr). In total, this results in a net imbalance of -0.18×10^{12} mol O_2/yr. In the model of Hansen and Wallmann

(2003), subduction of sedimentary organic carbon and pyrite in terms of O_2 released to the atmosphere is only 30% of the size of the igneous O_2 sink. Thus, despite the inclusion of organic carbon and pyrite subduction in the model, the organic carbon and pyrite sedimentary reservoirs must still grow to achieve near balance in the O_2 cycle. (*ii*) In the MAGic model of Arvidson and others (2006) organic carbon subduction is considered as a sink for O_2 as opposed to a source as we have discussed above. Igneous sinks are balanced by a return flux of O_2 from the mantle to the atmosphere, which the authors acknowledge is unrealistic, but is required to balance the O_2 cycle. (*iii*) The model of Miyazaki and others (2018) assumes a modern igneous O_2 sink of 1×10^{12} mol/yr. This is perfectly balanced by adding excess organic carbon to sediments (the sulfur cycle is not considered) and then that excess is forced to be subducted to keep the sedimentary organic carbon reservoir size constant. (*iv*) Galvez (2020) calculated that hydrothermal processes associated with alteration of oceanic crust and the mantle lithosphere and SO_2 degassing from arc volcanism consume 2.7×10^{12} (± 1.1) mol O_2/yr. This was done following the approach of Lécuyer and Ricard (1999) and Evans (2012) in which the fluxes of reduced vs. oxidized elements in unaltered vs. altered crust and lithosphere are compared and differenced. SO_2 degassing fluxes from arcs were then added on top of this. They compared this number to literature estimates of organic carbon, pyrite, and iron subduction fluxes and found $\sim 2.3 \times 10^{12}$ mol O_2/yr are released due to subduction (note the approximate sign is as given in their work). They concluded this was consistent either with balance in the igneous sinks vs. subduction sources of O_2 or alternatively there was an imbalance in carbon burial vs. oxidation. Although the latter would allow for an imbalance in organic burial rates, Galvez (2020) notes some could be lost via consumption of organic carbon by magmatic processes, though this flux was not quantified.

Finally, as discussed above, Hayes and Waldbauer (2006) concluded that the subduction flux of organic carbon is less than the sedimentary burial flux such that that the sedimentary organic carbon reservoir has continuously grown over the Phanerozoic. The excess O_2 released from this imbalance is proposed to be removed via oxidation of igneous rocks and volcanic gases.

Taken together, the aggregate evidence does not clearly indicate that the igneous sinks are balanced by subduction of organic carbon and pyrite today. Furthermore, whether the igneous O_2 sink size differed in the past under different conditions (for example lower $P_{O_2}^{atm}$, anoxic deep oceans, *et cetera*) is also not clear. In the next section, we approach these problems by examining individual solid-earth sources and sinks of O_2 and establishing the geochemical boundary conditions that set the size of these fluxes today. Following this, we use these insights to explore how igneous sinks may have changed as the oxidation state of the atmosphere and ocean increased since the Proterozoic.

IGNEOUS SINKS FOR O_2

In this and the next section we attempt to address the following question: how are the igneous sinks for O_2 balanced? For example, is the subduction of sedimentary organic carbon and pyrite sufficient to offset the igneous sink for O_2? Alternatively, must sedimentary organic carbon and pyrite reservoirs experience net growth in order to keep $P_{O_2}^{atm}$ approximately constant over the Phanerozoic? To answer these questions, we require an estimate of (1) the total igneous sink of O_2 as well as (2) the source of O_2 from subduction, both with associated uncertainties. In this section we calculate the size of the igneous O_2 sink and then in the following section consider the size of the O_2 source linked to subduction.

In order to calculate the size of the total igneous O_2 sink and sources, we break these fluxes up into the following general categories. For sinks we consider (*i*)

hydrothermal systems, (*ii*) volcanic emissions, and (*iii*) subaerial weathering. For sources, we consider subduction of reduced carbon, sulfur, and iron. For each, we calculate the sizes of the O_2 source or sink using a Monte Carlo error propagation scheme (code provided in supplementary materials). In this approach, we establish the ranges and distribution type (for example, uniform or normal) of a given parameter and then calculate all parameters and the associated sink in 10^7 different iterations. From this, we calculate means and standard deviations of the various terms.

Aspects of such calculations have been included in previous studies (for example, Holland, 1978, 2002; Hansen and Wallmann, 2003; Hayes and Waldbauer, 2006; Evans, 2012; Derry, 2015; Galvez, 2020), but do not include the full range of identified possible sources and sinks of O_2. Such estimates of fluxes are inherently challenging because the omission of or incorrect assumptions about key processes will lead to inaccurate final calculated numbers regardless of the size of the provided uncertainty. Our strategy is to provide a full explanation of our assumptions. This approach allows us to consider, for a specific source or sink, how changes in O_2 concentrations in the atmosphere and ocean could change (or not change) its size and thus examine conditions outside of those in the modern. In table 1, we provide the summary of estimates for O_2 sources and sinks today.

Hydrothermal Systems

Low-temperature hydrothermal oxidation of iron and sulfur in oceanic crust.—Off-axis of mid-ocean ridge and back-arc spreading centers, seawater circulates through and reacts with oceanic crust at relatively low (<100°C) temperatures. During this circulation, dissolved O_2 oxidizes Fe^{2+} and S^{2-} in igneous rocks. This oxidation by O_2 is concentrated in aquifers in the extrusive basaltic section due to high permeabilities and is not thought to occur appreciably in deeper crustal sections (Bach and Edwards, 2003).

We focus first on the oxidation of iron. The amount of oxidized vs. total iron in a sample is quantified by $Fe^{3+}/(Fe^{2+}+Fe^{3+})$ ratios and given as $Fe^{3+}/\Sigma Fe$. Note that metallic iron is not considered. Differences in $Fe^{3+}/\Sigma Fe$ of altered basalts vs. that expected for pristine values can be used to calculate the amount of oxidation that has occurred due to fluid circulation as Fe^{3+} is insoluble and precipitates in secondary minerals. For example, submarine basalt $Fe^{3+}/\Sigma Fe$ increases from initial values of ~0.15 up to final values of 0.3 to 0.6 as these rocks age on the seafloor (Johnson and Semyan, 1994; Bach and Edwards, 2003).

We calculate the total amount of Fe^{2+} oxidized in the volcanic section per year and relate this to O_2 demands following the framework given in Bach and Edwards (2003) using the following equation:

$$\frac{dFe^{3+}}{dt} = [\text{spreading rate}] \times [\text{depth of oxidative alteration}] \times [\text{density of mafic crust}] \times [\text{wt.\% Fe}] \times \left[\frac{Fe^{3+}}{\Sigma Fe_{\text{final}}} - \frac{Fe^{3+}}{\Sigma Fe_{\text{initial}}}\right] \quad (13)$$

For the Monte Carlo calculations, the spreading rate is set to 2.5 to 3.5 km^2/year with a uniform distribution and is from Bach and Edwards (2003). This is similar to other estimates (for example, 2.7 ± 0.4 [1 standard deviation (σ)] in table 3 of Cogné and Humler, 2006). From this point on, whenever an uncertainty is given with ±1σ or ±1 s.e. (standard error), it indicates the distribution is assumed to be Gaussian in the

TABLE 1

Estimates of modern sinks for O_2 from igneous processes and sources from subduction

type	main category	subcategory	species	O_2/yr	±1σ
sink	hydrothermal	low temperature	Fe	4.51E+11	1.92E+11
		low temperature	S	2.22E+11	8.31E+10
		low temperature	total	6.73E+11	2.39E+11
		high temperature	H_2S	4.46E+11	3.02E+11
		high temperature	Fe	3.12E+10	2.22E+10
		high temperature	H_2	2.12E+10	1.42E+10
		high temperature	Mn	1.20E+10	7.57E+09
		high temperature	CH_4	8.58E+09	5.68E+09
		high temperature	total	5.19E+11	3.36E+11
		total		**1.19E+12**	**4.12E+11**
sink	volcanism	mid-ocean ridge	CO	3.78E+10	1.46E+10
		mid-ocean ridge	H_2	0.00E+00	
		mid-ocean ridge	$SO_2 + S_2 + H_2S$	0.00E+00	
		arc	CO	4.66E+09	2.24E+09
		arc	H_2	6.74E+10	2.56E+10
		arc	$SO_2 + S_2 + H_2S$	2.38E+11	5.17E+10
		hotspot	CO	2.20E+08	3.26E+07
		hotspot	H_2	5.04E+07	5.71E+06
		hotspot	$SO_2 + S_2 + H_2S$	1.55E+10	1.71E+09
		rift	CO	1.45E+10	4.67E+09
		rift	H_2	7.27E+08	7.94E+07
		rift	$SO_2 + S_2 + H_2S$	2.11E+10	3.69E+09
		all	CO	5.71E+10	1.55E+10
		all	H_2	6.81E+10	2.56E+10
		all	$SO_2 + S_2 + H_2S$	2.75E+11	5.19E+10
		arc	all	3.10E+11	5.78E+10
		hotspot	all	1.58E+10	1.71E+09
		rift	all	3.64E+10	5.95E+09
		mid-ocean ridge	all	3.78E+10	1.46E+10
		total		**4.00E+11**	**5.99E+10**
sink	subaerial weathering	all	Fe	1.62E+11	8.18E+10
			S	7.07E+10	3.11E+10
		total		2.33E+11	1.08E+11
sink	**total**			**1.83E+12**	**4.30E+11**
source	subduction		organic C	1.20E+12	2.43E+11
			S in pyrite	3.00E+11	1.14E+11
			Fe	6.01E+10	3.69E+10
	total			**1.56E+12**	**3.28E+11**
sources minus sinks	**total**			**2.61E+11**	**5.40E+11**

uncertainty propagation. Otherwise, the distribution is assumed to be uniform based on the given range. Any other situation is noted. The depth of oxidative alteration is set to 300 to 700 m, again from Bach and Edwards (2003). We assume a density of 2.71 ± 0.15 (1σ) g/cm^3 based on Jarrard and others (2003)—this excludes contributions of hydrothermally derived waters. Based on Bach and Edwards (2003), we assume the mean wt.% Fe in mid-ocean ridge basalts (MORB) is 8 ± 1.3 (1σ). This number (8%) agrees with independent estimates of 7.8% and 8.1% for MORB given in Keller and others (2015) and Gale and others (2013) respectively. We assume the $Fe^{3+}/\Sigma Fe_{inital}$ value is 0.14 ± 0.01 (1σ), which is based on X-ray absorption near edge structure (XANES) spectroscopic determinations of MORB glasses from Zhang and others (2018). Finally, we assume that $Fe^{3+}/\Sigma Fe_{final}$ is 0.3 to 0.6 based on the range suggested by Bach and Edwards (2003).

We estimate the mass of sulfur removed in the same manner:

$$\frac{dS^{2-}}{dt} = [\text{spreading rate}] \times [\text{depth of oxidative alteration}] \times [\text{density of mafic crust}] \times [\text{wt.\% S}] \times [\text{\% sulfur oxidized}] \quad (14)$$

In unaltered MORB, sulfur is speciated as S^{2-}. The wt.% sulfur is taken as 0.125 ± 0.02 (1σ) as given in Bach and Edwards (2003). The % sulfur oxidized is taken as 45 to 95% again from Bach and Edwards (2003). We note that during the Monte Carlo simulation, when the same term appears in multiple equations, an identical value is used for all calculations in that given Monte Carlo run.

We make the assumption that all of the iron and sulfur that is oxidized during alteration of MORB is oxidized by O_2. This results in a net O_2 demand of 0.45×10^{12} (±0.19; 1σ) mol/yr from iron oxidation and 0.22×10^{12} (±0.08; 1σ) mol/yr from sulfur oxidation. We can examine the reasonableness of these numbers by estimating whether a sufficient amount of O_2 is circulated through basaltic aquifers to allow for this amount of oxidation. Typical estimates of the low-temperature (that is, off-axis) flux of seawater through basaltic aquifers ranges from 3.7×10^{15} to 5.4×10^{17} kg fluid/yr (Elderfield and Schultz, 1996; Nielsen and others, 2006). The average deep-ocean (>1200 m depth) O_2 concentration is ~180 μmol/kg H_2O (Sarmiento and Gruber, 2006). Using the lower-end estimate of the off-axis water flux, 3.7×10^{15} kg H_2O per year, with 180 μmol/kg H_2O dissolved O_2, results in a flux of 0.67×10^{12} moles of O_2 delivered to off-axis systems each year, which is the same as our calculated mean O_2 demand of 0.67×10^{12} mol O_2/yr from combined iron and sulfide oxidation in MORB. As we are using the minimum estimate of the off-axis hydrothermal flux, this is a minimum flux estimate. Based on this we consider the assumption that the oxidation of the iron and sulfide solely by O_2 to be acceptable.

We note that our assumption that all oxidation of iron and sulfur in low-temperature hydrothermal settings is done by O_2 differs from that of Bach and Edwards (2003). Although they also assume that all sulfur oxidation is due to oxidation by O_2, they estimate that only up to half of all iron oxidation is from O_2 and nitrate reduction, with the rest occurring via oxidation of Fe^{2+} in minerals by water and release of H_2 (to maintain redox balance). This difference is in part because we assume deep ocean O_2 concentrations are ~180 μmol/kg H_2O vs. their assumed value of 100 μmol/kg H_2O. Importantly, for our purposes, this appears to lead to a distinction without a difference. For example, if H_2 generation by iron oxidation is as extensive as Bach and Edwards (2003) argue and the generated H_2 is emitted to the ocean, it will ultimately end up removing O_2 from the ocean or atmosphere either directly

(Greening and others, 2015) or indirectly by reaction with OH radicals (Ehhalt and Rohrer, 2009). H_2 escape to space consumes only ~0.05% of H_2 emitted to the atmosphere with the rest directly or indirectly removed by O_2 (Yung and others, 1989; Ehhalt and Rohrer, 2009) and is thus negligible. If, on the other hand, the H_2 is used to reduce sulfate to form sulfide (via sulfate reducing bacteria) and that sulfide is emitted to the ocean, then it will also be oxidized by O_2. If the sulfide reacts with Fe^{2+} (released from igneous rocks during alteration) and instead adds pyrite to the igneous rocks, it will also have no impact on our calculations because that added sulfur and iron must be removed later to get the final measured $Fe^{3+}/\Sigma Fe$ and sulfide contents in the altered rocks used above.

One way in which this generation of H_2 could result in iron oxidation without concomitant loss of O_2 is if the H_2 is used by denitrifying microorganisms to form N_2, which is inert with respect to O_2. If half of the iron oxidation is used to generate H_2 (see above discussion of Bach and Edwards, 2003) then 0.45×10^{12} moles/yr of H_2 are produced and could remove up to 0.18×10^{12} moles of nitrate per year. Typical deep-ocean nitrate concentrations are 32 μmol/kg seawater (Sarmiento and Gruber, 2006). Nitrate is removed from anoxic fluids circulating through basalts to near zero levels (for example, Wheat and Mottl, 2000). If we assume this removal is accomplished by reduction of nitrate by H_2, we can calculate a minimum low-temperature water flux of 5.6×10^{15} kg of H_2O per year to remove 0.18×10^{12} moles of nitrate. With 180 μmoles of O_2 per kg seawater in the deep ocean, such a water flux would provide 1.5× as much O_2 into the low-temperature hydrothermal as our calculations indicate is removed. As dentification occurs in anoxic environments and hydrolysis reactions are thought to require anoxic conditions (Neal and Stanger, 1983; Bach and Edwards, 2003), such O_2 would have to be removed before either process could occur. Thus, based on the above discussion, we believe there is sufficient O_2 delivered to low-temperature hydrothermal systems to meet the calculated O_2 demands. Even if incorrect, H_2 or sulfide released to the oceans would still consume O_2 such that our estimates for the total O_2 demand per year are still accurate.

Finally, we assume that the flux of dissolved reduced elements from low-temperature hydrothermal systems into the ocean is negligible. Our basis for this is as follows: 25°C springs from off-axis systems (specifically from the Juan de Fuca Ridge) have <0.1 to 6 μmol Fe^{2+}/kg H_2O and 1.3 μmol H_2S/kg H_2O (Mottl and others, 1998; Wheat and Mottl, 2000). If we assume that globally $\sim 1 \times 10^{16}$ kg of seawater flows through off-axis systems (for example, Elderfield and Schultz, 1996) then using 1.3 μmol H_2S/kg H_2O and the upper limit of 6 μmol Fe^{2+}/kg H_2O results in a flux of 1.3×10^{10} mol/yr H_2S and 6×10^{10} mol/yr Fe^{2+} into the ocean. Together, these would consume 0.041×10^{12} mol O_2/year, which we consider negligible given our final 1σ uncertainty for the total igneous O_2 sink is 10 × larger (see below). We note this is an approximate upper limit as it assumes all low-temperature off-axis fluids become anoxic—Fe^{2+} and H_2S will not accumulate in oxygenated fluids.

We note that this differs from recent estimates given in Thompson and others (2019) who, in their Table S3, calculate that today 10.5×10^{12} mol/yr Fe^{2+} are emitted to the ocean from low-temperature off-axis hydrothermal systems. Such would consume 2.6×10^{12} mol O_2/year, which is larger than our total estimate for all igneous sinks developed below. Their number was calculated based on their assumption that all low-temperature off-axis fluids contain 0.75 mmol Fe^{2+}/kg H_2O. As discussed above, the places where iron concentrations in off-axis systems have been measured indicate that the dissolved iron content of off-axis systems is likely ~1000 fold lower (0.1 to 6 μmol Fe^{2+}/kg H_2O; Mottl and others, 1998; Wheat and Mottl, 2000). As such, we retain our assumption that reduced element fluxes from off-axis systems are neglible for the modern O_2 budget.

High-temperature hydrothermal systems.—High-temperature (>250°C) hydrothermal fluids that circulate through oceanic crust (for example, black smokers), introduce reduced species to the ocean that will react with and consume dissolved O_2. There are two broad classes of high-temperature hydrothermal systems: mafic-hosted systems and ultramafic-hosted systems. These are considered separately here as ultramafic systems commonly have higher (~30×) H_2 and (~25×) CH_4 concentrations than mafic-hosted systems (for example, Elderfield and Schultz, 1996; Charlou and others, 2010) due to serpentinization reactions (for example, Früh-Green and others, 2004; Sleep and others, 2004). We calculate the O_2 demand for a given species vented from mafic and ultramafic systems according to the following equations. For mafic hydrothermal fluids we write:

$$\frac{dO_2}{dt} = [\%\ \text{mafic}] \times \left[\frac{\text{kg } H_2O}{\text{year}}\right] \times \left[\frac{\text{moles species}}{\text{kg } H_2O}\right] \times \left[\frac{\text{moles } e^-}{\text{mole species}}\right] \times \left[\frac{\text{mole } O_2}{4 \text{ moles } e^-}\right] \tag{15a}$$

For ultramafic hydrothermal fluids we write:

$$\frac{dO_2}{dt} = [\%\ \text{ultramafic}] \times \left[\frac{\text{kg } H_2O}{\text{year}}\right] \times \left[\frac{\text{moles species}}{\text{kg } H_2O}\right] \times \left[\frac{\text{moles } e^-}{\text{mole species}}\right] \times \left[\frac{\text{mole } O_2}{4 \text{ moles } e^-}\right] \tag{15b}$$

In these equations, the % mafic and % ultramafic terms are the percentage of the total high-temperature fluid flux (in kg H_2O/year), that go through the mafic and ultramafic systems. These are subject to the constraint of closure:

$$[\%\ \text{mafic}] + [\%\ \text{ultramafic}] = 100\% \tag{16}$$

The [moles species/kg H_2O] term is the concentration of a given reduced species in the emitted water, the electrons (e^-) per mole species are the number of electrons required to oxidize it to its ultimate form in the deep ocean, and 4 moles of electrons are required to reduce 1 mole of O_2 to two moles H_2O.

We estimate the ultramafic proportion of the high-temperature hydrothermal fluid flux following Keir (2010). In this approach, the percent of oceanic basement serpentinized is a proxy for the percent of hydrothermal fluids flowing through ultramafic rocks. Only slow spreading systems (<4 cm/yr full spreading rate) are considered as these systems expose ultramafic rocks to high-temperature circulation systems. Keir (2010) estimates 8% of high-temperature hydrothermal fluids circulate through ultramafic systems. Alternatively, Alt and others (2013) estimate 2.3 to 4.6% (by volume) of oceanic crust is serpentinized. Based on these studies, we estimate of 2.3 to 8% of hydrothermal fluids transit ultramafic systems.

Estimates for high-temperature hydrothermal fluid fluxes are typically of order 1×10^{13} kg H_2O/yr (Elderfield and Schultz, 1996), but with order-of-magnitude uncertainty. This is an important parameter as it appears in the flux estimates for all reduced species emitted to the ocean from high-temperature hydrothermal systems. We use a lower-end estimate of 0.17×10^{13} kg H_2O/yr based on models of thallium

isotopes in hydrothermal systems (Nielsen and others, 2006), and upper estimate of 6×10^{13} kg H_2O/yr based on ^3He flux arguments given in Keir (2010).

The following reduced species are considered in this calculation: H_2S, H_2, CH_4, Mn^{2+}, and Fe^{2+}. For mafic systems, we use concentration ranges based on measured maximum and minimum values from black-smoker fluids given in table 14 of Elderfield and Schultz (1996) (as originally given in Kadko and others, 1994). For ultramafic systems, we use concentration ranges based on the maximum and minimum measured concentrations from the Rainbow, Logatchev, and Ashadze hydrothermal fields given in Charlou and others (2010).

Based on these, we arrive at an O_2 demand from high-temperature hydrothermal systems of 0.52×10^{12} (± 0.34; 1σ) mol O_2/yr with 94% from mafic systems and 6% from ultramafic systems. 86% of this O_2 consumption is derived from the emission of H_2S. The source of H_2S (based on sulfur isotope arguments) is thought to be dominantly sulfide leached from igneous rocks (~67–75%) with the remainder derived from the reduction of seawater sulfate at elevated (>250°C) temperatures (for example, Shanks and others, 1995). Even though some of the sulfur is originally sourced from seawater sulfate, we consider this an igneous sink as the seawater-derived sulfate is reduced via oxidation of igneous elements.

Hydrothermal summary.—In summary, the calculated total demand of O_2 from low- and high-temperature hydrothermal systems is 1.19×10^{12} (± 0.41; 1σ) mol O_2/yr (fig. 3). 94% of the O_2 sink is controlled by three terms: low-temperature iron oxidation (38%), low-temperature sulfide oxidation (19%), and high-temperature hydrothermal sulfide emission (37%; 99% of which is from mafic-hosted systems).

We note that we do not include in our estimates oxidative serpentinization of the lithospheric mantle associated with slab bending at subduction zones. Such processes are excluded under the assumption that the fluids that enter and react with the sublithospheric mantle (and generate H_2 formed at the expense of iron oxidation) are not re-emitted back to the ocean in hydrothermal circulation systems. Instead, we assume they are subducted into the mantle in the form of hydrated minerals and that any H_2 produced reacts with and reduces oxidized phases to form reduced minerals like awaruite (Ni_3Fe).

We note that this assumption differs from estimates in Evans (2012) and Galvez (2020) who consider serpentinization of lithospheric mantle to cause the net oxidation of the lithospheric mantle and thus act as an O_2 sink. For example, Evans (2012) estimates up to 1.68×10^{12} (± 1.31) mol O_2/yr could be consumed by lithospheric serpentinization while Galvez (2020) estimates 0.62×10^{12} (± 0.36) mol O_2/yr could be consumed. These are based on estimates of the amount of serpentinized lithospheric mantle that exists and its $Fe^{3+}/\Sigma Fe$. Such estimates generally carry large uncertainty due to poor knowledge of the degree of lithospheric mantle serpentinization. Regardless, we argue and proceed here with the assumption that lithospheric serpentinization does not act as a direct sink of O_2 as the H_2 produced from iron oxidation must escape through >6 km of oceanic crust without reacting with other phases. We consider this unlikely and are unaware of any evidence of largescale emissions of H_2 (or CH_4 produced from H_2) to the ocean from fluids directly derived from serpentinization of the lithospheric mantle. Instead, where serpentinization derived fluids are observed being emitted to the ocean near subduction zones, they are typically associated with serpentinization of the forearc from fluids assumed to be derived from dewatering of sediments and basalts (not the lithospheric mantle) (for example, Mottl and others, 2004; Ohara and others, 2012).

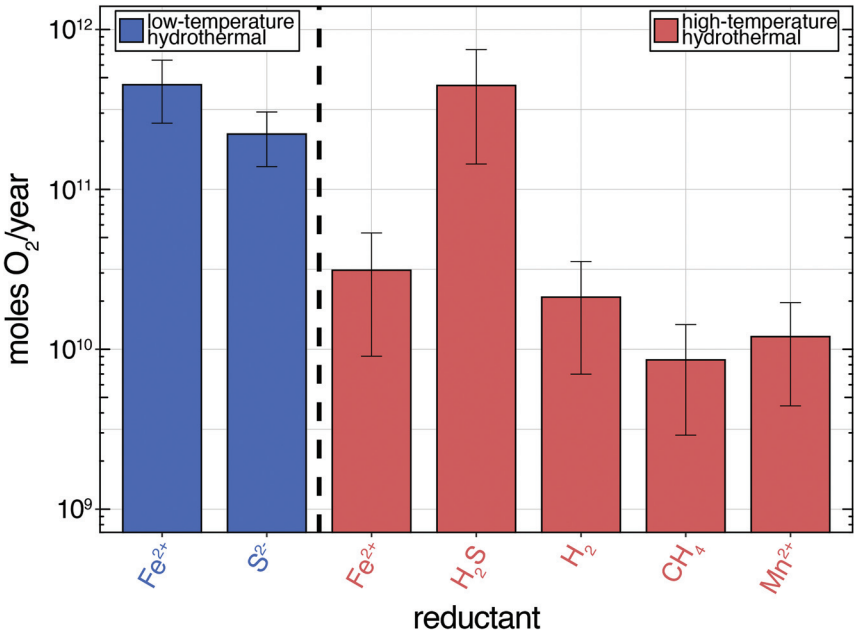

Fig. 3. Comparison of calculated moles of O_2 consumed per year for the modern based on the oxidation of various species associated with high- and low-temperature hydrothermal alteration of oceanic crust. Error bars are $\pm 1\sigma$.

Volcanic Degassing

A variety of reduced volcanic gases including H_2, CO, SO_2, S_2, and H_2S remove O_2 from the atmosphere either via direct reaction or indirectly via O_2-derived oxidants (for example, hydroxyl radicals). These gases are emitted at mid-ocean ridges, continental rifts, arc volcanoes, and hotspot (that is, intraplate) volcanoes. Here we estimate global outgassing fluxes of these gases as a function of the volcanic source. Before doing so, we outline assumptions we make for all systems.

We assume that the overall amount of O_2 volcanic gases can remove from the atmosphere (that is, their reducing power) is set by how reducing the melt (or rocks) were that were last in chemical equilibrium with the gas. This reducing power is set by the oxygen fugacity (fO_2), temperature, and pressure of the melt. Following separation from the melt, the gas's reducing power remains fixed. For example, let us assume that after a gas separates from a melt, some CO converts to CO_2, which is redox balanced by reduction of H_2 to H_2O via the reaction $CO + H_2O \leftrightarrow H_2 + CO_2$. The presence of one molecule of CO or one molecule of H_2 in a volcanic gas will consume the same amount of O_2. As such, these later gas-phase reactions, due to considerations of redox balance, do not affect the overall ability of the gas to remove O_2 from the atmosphere. This is true despite changes in gas fO_2 as a function of temperature and pressure during adiabatic decompression. We demonstrate this quantitatively in figure 4 where a gas with 95% H_2O and 1% CO_2 decompresses adiabatically from 50 bar and 1200°C to 1 bar and 800°C in isolation (that is, not in contact with a melt). Although the fO_2 of the gas increases by 6 log units relative to the nickel-nickel oxide buffer (NNO; fig. 4B) the total amount of O_2 that could be oxidized in grams per gram volcanic gas emitted remains constant (fig. 4D) A similar result and argument was recently presented

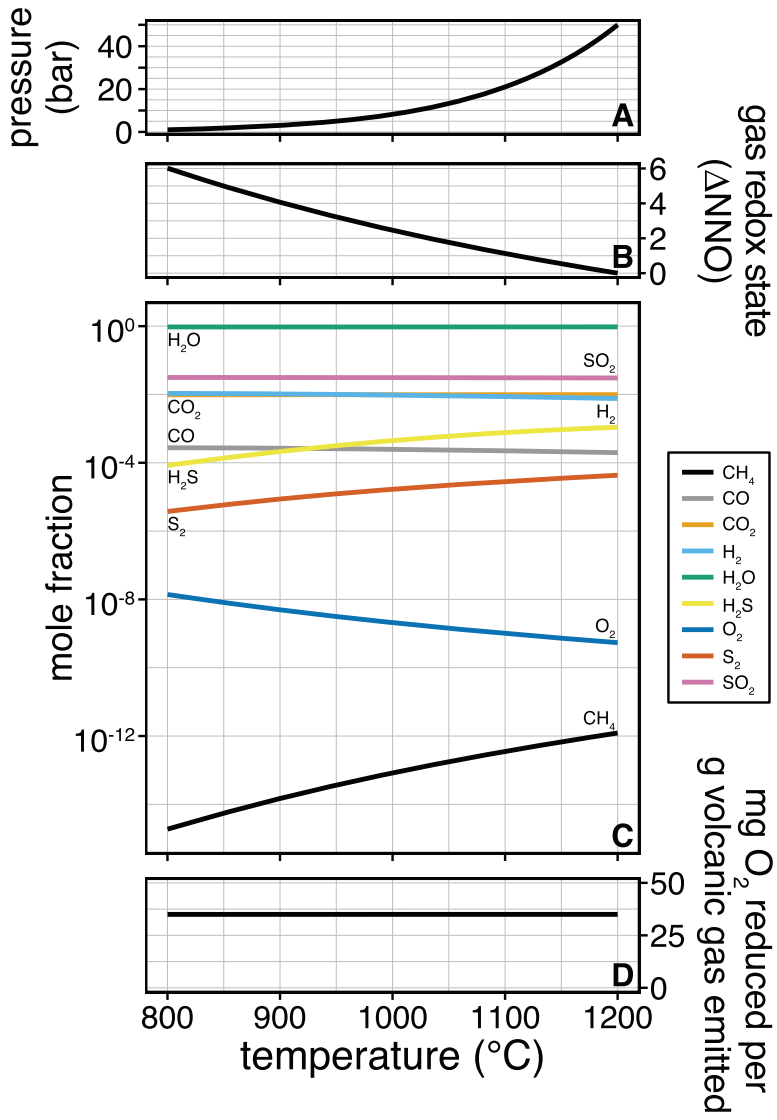

Fig. 4. Calculation of changes in gas composition from cooling during adiabatic decompression of a volcanic gas associated with (A) changes in pressure, (B) fO_2 relative to the NNO buffer, (C) gas composition, and (D) oxidative capacity with respect to O_2. Despite these changes, the total amount of O_2 that can be reduced per unit mass volcanic gas emitted does not change (D).

in Kadoya and others (2020a) and differs from those presented in Moussallam and others (2019b).

We take the approach of estimating gas fluxes by anchoring our calculations to gases with relatively well-constrained modern degassing fluxes, such as CO_2, H_2O, and SO_2, and calculating abundances of other gases based on expected ratios using thermodynamic relationships. We note that our approach of using a flux that is well constrained and multiplying it by a ratio to find the flux of another species, though indirect, is a common way that geochemical fluxes of various species are calculated. The equations are as follows:

$$F_{H_2;i} = F_{H_2O;i} \times \frac{fH_2;i}{fH_2O;i} \quad (17)$$

$$F_{CO;i} = F_{CO_2;i} \times \frac{fCO;i}{fCO_2;i} \quad (18)$$

$$F_{S_2;i} = F_{SO_2;i} \times \frac{fS_2;i}{fSO_2;i} \quad (19)$$

$$F_{H_2S;i} = F_{SO_2;i} \times \frac{fH_2S;i}{fSO_2;i} \quad (20)$$

In equations (17) to (20), F is a flux in moles per year, f is a fugacity and i represents a given volcanic source such as arcs or mid-ocean ridges.

We calculate the fugacity ratios in equations (17) to (20) by setting the fO_2, temperature, and pressure of the gas when it erupted using the D-Compress computer program (Burgisser and others, 2015).

We use the following temperature ranges in our calculations: for arc gases we use a range of 850 to 1200°C based on the range given in Moussallam and others (2019b). For hotspot volcanism, we use a range of 1100 to 1220°C based on MgO thermometry of glasses from Kilauea (see supplementary information of Sides and others, 2014). For mid-ocean ridges, we use a typical temperature of 1200°C. For continental rifts we use a temperature of 1100°C based on volcanic emissions from the Nyiragongo volcano from the East African Rift (Sawyer and others, 2008).

For arc fO_2, we use a uniform range of +1 to +2 log units above the quartz-fayalite-magnetite buffer (QFM) based on ranges for Marianas arc glasses (Brounce and others, 2014). We use an fO_2 of +1 log units relative to the QFM buffer for hotspot volcanism based on the least degassed Hawaiian sample from Brounce and others (2017). For MORB, we use a range of −0.35 to 0 log units relative to QFM based on XANES determinations of MORB (Zhang and others, 2018). We use an fO_2 0.25 log units below the QFM buffer for continental rifts again based on studies of Nyiragongo (Sawyer and others, 2008).

We assume gases from arcs and hotspots are 90% H_2O and 1% CO_2 with the rest solved for by the D-Compress program. These are based on typical values of high-temperature emissions (for example, Symonds and others, 1994). For continental rifts, we assume gases are 30% CO_2 and 60% H_2O based on typical gases at Nyiragongo (Sawyer and others, 2008). As will be discussed, for mid-ocean ridges, we only account for CO and CO_2 degassing. CO/CO_2 ratios are defined solely by temperature, fO_2 and pressure and thus we do not define the mid-ocean ridge gas composition.

For mid-ocean ridges, we assume eruption occurs at 200 bar (that is, at the bottom of the seafloor). For subaerial degassing from arcs, hotspots, and continental rifts, we assume the minimum pressure of eruption to be 1 bar. This assumption fails for high-elevation volcanoes, but we consider it acceptable. It is thought that gases can cease to be in equilibrium with melts at pressures above atmospheric via bubble-induced isolation of gases from their surrounding melts in a volcanic conduit (Burgisser and others, 2012; Oppenheimer and others, 2018). We take the maximum pressure at which a gas separates from a melt to be 5 bar based on data and models of the pressures at which gas bubbles burst at Erebus (Burgisser and others, 2012). We note that 5 bar (specifically 5 atm) was used by Catling and Kasting (2017) for calculations of arc gas speciation as well. Eruption pressure is unimportant for calculations of

H_2/H_2O and CO/CO_2 ratios for arc gases as they vary little (<0.2% relative) from 1 to 5 bars. However, relative SO_2, S_2, and H_2S ratios vary strongly from 1 to 5 bar (Burgisser and Scaillet, 2007). For example, for a gas with 90% H_2O and 1% CO_2, temperature of 1000°C, and fO_2 of 0 log units relative to the nickel-nickel oxide (NNO) buffer, the H_2S/SO_2 ratio at 1 bar is 0.011 while at 5 bar is 0.053, that is, a 5× difference. Given that one mole of H_2S consumes 4 time more O_2 than one mole of SO_2, such differences matter for our calculations.

Sulfur outgassing fluxes.—Volcanic sulfur degassing fluxes are best constrained for SO_2 emissions which can be measured both from the ground and space (Oppenheimer and others, 2011). We use the recent estimates of subaerial SO_2 outgassing fluxes from Fischer and others (2019) for arc, hotspot, and continental rift volcanism as given in their table 3. No uncertainty is given by them for the final fluxes. However, uncertainties for CO_2 fluxes are given, which are largely based on measured C/S ratios combined with SO_2 fluxes. The uncertainty for total CO_2 emissions from these systems is ±10.9% relative (±1 s.e.), which we also use as the relative uncertainty for SO_2 emissions here with a normal distribution.

Based on this, for arcs, we use a total average SO_2 outgassing flux of 4.26×10^{11} mol/yr (±0.47, 1σ). This is similar to previous estimates of 1.25 to 5.6×10^{11} mol SO_2/yr emitted from arcs (Wallace, 2005). The H_2S/SO_2 range used is 1.24×10^{-5} to 2.6×10^{-1} and the S_2/SO_2 range is 2.75×10^{-7} to 2.9×10^{-2}. Given that these ranges span many orders of magnitude, we use a log-uniform distribution for arc H_2S/SO_2 and S_2/SO_2 ratios in the Monte Carlo calculations.

For hotspot volcanism, we use a total average SO_2 outgassing flux of 0.30×10^{11} mol/yr (±0.03, 1σ). The H_2S/SO_2 range used is 0.00125 to 0.0158 and S_2/SO_2 range is 2.0×10^{-5} to 4.8×10^{-4}.

For continental rifts, we use an SO_2 flux of 0.21×10^{11} mol SO_2/year (±0.02, 1σ). We estimate H_2S/SO_2 and S_2/SO_2 ratios using uniform ranges of 0.063 to 0.28 and 0.025 to 0.093 respectively.

We do not include sulfur degassing from mid-ocean ridges as it is generally thought that in water-poor melts (that is, <0.5 wt.% water) such as for the parental melts of MORBs, sulfur does not degas until eruption depths shallower than 1000 to 200 meters are reached (Moore and Schilling, 1973; Killingley and Muenow, 1975; Wallace and Edmonds, 2011). As MORBs typically erupt at water depths equal to or greater than 2000 meters, one would not expect significant sulfur degassing from these systems (for example, see fig. 4A of Wallace and Edmonds, 2011). For the same reasons, we do not include a sulfur flux from diffuse gas emissions of continental rifts as these gases are thought to originate from the upper mantle or lower crust and travel along faults to reach the surface.

These result in a total estimated sink from volcanic sulfur degassing of 0.275 ± 0.052 (1σ) $\times 10^{12}$ mol O_2/yr. Of this, 87% is from arcs, 6% from hotspots, and 8% from continental rifts.

CO outgassing fluxes.—We estimate CO outgassing fluxes using CO_2 outgassing fluxes combined with thermodynamically calculated CO/CO_2 ratios. For arcs, hotspots, and continental rifts, we use CO_2 fluxes from Fischer and others (2019). Uncertainties on CO_2 emissions are taken as 10.9% relative (1 s.e.; see sub-subsection *Sulfur outgassing fluxes*).

For arcs, we use a CO_2 flux of 1.12×10^{12} mol/yr (±0.12, 1σ). We estimate a CO/CO_2 ratio for arcs gases of 0.0016 to 0.0151.

For hotspot volcanism, we use a CO_2 flux of 0.030×10^{12} mol/yr (±0.003, 1σ). We estimate a CO/CO_2 ratio of 0.012 to 0.017.

CO_2 outgasses from continental rifts during active and passive volcanism and through diffuse seepage. We use a volcanic flux of 0.033×10^{12} mol CO_2/yr (±0.004,

1σ). We calculate a CO/CO_2 value of 0.05 for continental rift volcanic gases. This has no range as CO/CO_2 ratios do not depend strongly on the total pressure (which we allow to vary), just fO_2 and temperature (which we do not vary for continental rift systems).

Diffuse seepage of CO_2 from continental rift systems has recently been proposed to be a significant source of volcanic CO_2 to the atmosphere (Lee and others, 2016a; Brune and others, 2017; Foley and Fischer, 2017; Hunt and others, 2017). For example, Hirschmann (2018) estimates a flux of 1.7 to 5.8×10^{12} mol CO_2/yr from diffuse outgassing at continental rifts, which we use here with a uniform distribution. The diffuse CO_2 is emitted through soils near active faults and has interacted with both igneous and sedimentary rocks at temperatures lower than its emission temperature, which allows for modification of the ultimate CO/CO_2 ratio of the emitted gas. Consequently, we do not take our typical approach in assuming a thermodynamic CO/CO_2 ratio associated with the original magmatic emission. Instead, we use the average measured CO/CO_2 values of diffuse emissions along the East African Rift from Lee and others (2016a). Assuming a value of 0 for CO measurements below baseline, we arrive at a mean CO/CO_2 ratio of 0.0073 ± 0.0009 (±1 s.e.).

Finally, for mid-ocean ridges we use the recent estimate of CO_2 fluxes from Le Voyer and others (2019) of 0.47 to 2.09 mol CO_2/yr. We estimate a CO/CO_2 ratio range of 0.047 to 0.071.

These calculations yield O_2 burdens from CO outgassing of 0.0571×10^{12} (±0.0155; 1σ) mol O_2/yr. Of this, 8% is from arcs, 66% from mid-ocean ridges, <1% from hotspots, 24% from diffuse outgassing along continental rifts, and 1% from active and passive continental rift volcanism.

H_2 outgassing fluxes.—We estimate volcanic H_2 fluxes using H_2O fluxes from a given system and multiplying those fluxes by thermodynamically calculated H_2/H_2O ratios. As above, we use the H_2O degassing fluxes given in Fischer and others (2019) with a normally distributed 10.9% 1σ relative uncertainty.

For arcs we use a flux of 3.592×10^{13} mol H_2O/yr (±0.39, 1σ). We calculate H_2/H_2O ratios to be 0.0014 to 0.0061.

For hotspot volcanism, we use a flux of 1.71×10^{10} mol H_2O/yr (±0.19, 1σ). We use an H_2/H_2O range of 0.0056 to 0.0062.

For continental-rift volcanism, we use a flux of 6.06×10^{10} mol H_2O/yr (±0.66, 1σ). We use an H_2/H_2O ratio of 0.024.

We do not consider H_2O fluxes (and thus H_2 fluxes) from mid-ocean ridges as eruption depths and thus pressures are too high for H_2O to degas. For example, models indicate that MORB parental magmas do not significantly outgas H_2O (<10% loss) unless erupted at depths shallower than 100 meters (Dixon and Stolper, 1995) whereas eruption depths are typically 2000 meters. For the same reasons, we do not include an H_2O flux from diffuse rift gas emissions as it has been assumed that these gases originate from the upper mantle or lower crust and travel along faults to reach the surface.

Based on this we find that volcanic H_2 degassing from volcanoes consumes on average 0.0681 ± 0.0256 (1σ) $\times 10^{12}$ mol O_2/yr. Of this, 99% is from arcs, <0.1%, from hotspots, and 1% from continental rifts.

CH_4.—We do not include methane fluxes from high-temperature volcanic systems as they are negligible given that CH_4/CO_2 ratios at chemical equilibrium are typically 10^{-10} or less (based on the thermodynamic calculations discussed above).

Potential complexities.—We consider two potential issues in our approach: (1) For arcs, continental rifts, and hotspots, we only include fluxes from subaerial volcanoes and (2) our hotspot fluxes are derived from active hotspots and do not account for the punctuated nature of flood basalt volcanism.

(1) Volcanism in modern continental rifts and hotspots is dominantly subaerial and so use of subaerial fluxes is acceptable for these. However, arc volcanoes are commonly submerged and, due to elevated water contents in melts, are largely degassed even at eruption depths of 2000 m below sea level (for example, Wallace and Edmonds, 2011). Our estimates for arc fluxes are based on measured emissions from subaerial volcanoes and do not include submarine emissions. We are unaware of any global estimates of volcanic emissions from submarine arc volcanoes. We attempted to evaluate the relative importance of subaerial vs. submarine volcanic emissions as follows: de Ronde and others (2003) estimates that 21,690 km of subduction zones contain submarine volcanoes and that 45% of all volcanoes in these subduction zones are submarine (this is based on the average of their table 1 values). Given a total subduction zone length 51,310 km (Bird, 2003) and the assumptions that (*i*) arc gas emissions are directly proportional to subduction zone length and that (*ii*) the proportion of submarine vs. subaerial arc volcanoes are directly related to their relative gas contributions, we can estimate that 81% of arc volcanic emissions are subaerial and 19% are submarine. Despite the admittedly crude nature of this calculation, it indicates that most (>80%) arc volcanic emissions are subaerial in origin and supports our assumption that it is acceptable here to exclude submarine arc emissions given the limited knowledge of their total gas fluxes.

(2) A potential issue with our estimate for hotspot emissions is that it is based on measurements of outgassing fluxes from modern hotspot volcanoes and thus necessarily neglects the episodic eruptions of large-scale flood basalts (there are no flood basalts actively erupting). We examined this issue as follows. The SO_2 and CO_2 fluxes for hotspots we use are based on determinations of Hawaii, Reunion, and the Galapagos. (Fischer and others, 2019). Water emissions were only given for Hawaii. Based on average magmatic production rates for the past 20 million years given in table 5 of Mjelde and others (2010), these three systems generate on average 0.38 km^3/yr of magma. Estimates of intraplate magmatic rates (both intrusive and extrusive) inclusive of episodes of flood basalts from Crisp (1984) yield average Phanerozoic intraplate magma production rates of 1.93 to 4 km^3/yr. These are 5.1 to 10.5× higher than those used here. If we upscale our estimate of the hotspot igneous volcanic sink size by 5.1 to 10.5× to correct for this, this would increase our igneous sink size by between 0.06 to 0.15 × 10^{12} moles O_2/year. However, such an upscaling is not straightforward as some hotspot volcanism occurs underwater, and as discussed, above, hotspot submarine eruptions typically occur at too deep of water depths for significant outgassing of sulfur species and H_2O (which are 99% of the hotspot sink calculated here). For example, the Ontong Java Plateau, due to being emplaced at the seafloor, is not thought to have degassed sulfur during eruption (Reekie and others, 2019). Given this complexity, we do not attempt an upscaling of our hotspot emissions to account for episodic flood-basalt volcanism. However, the additional O_2 removed by such an upscaling, as given below, is less than the $\pm 1\sigma$ uncertainty on our total igneous O_2 sink and does not alter our conclusions.

Volcanic outgassing fluxes summary.—All told, volcanic outgassing is estimated to consume 0.400 ± 0.060 × 10^{12} mol O_2/yr. When broken down by source, arcs account for 78% of this sink, hotspots 4%, rifts 9%, and mid-ocean ridges 9%. In terms of molecules, sulfur species account for 69% of the sink, H_2 17% and CO 14%. This is summarized in figure 5 as a function of volcanic source (fig. 5A) and molecule type (fig. 5B).

Continental Outgassing of H_2 and CH_4

Sherwood Lollar and others (2014) estimate an abiotic production rate of 0.36 to 2.27×10^{11} mol H_2/yr in continental rocks derived, for example, from water radiolysis or hydration of igneous or metamorphic minerals. To our knowledge, it is not known how much of this H_2 is released to the atmosphere vs. reacts or is retained at depth. Given this uncertainty, we have not included this process as an O_2 sink. Its inclusion would increase the O_2 sink by at most 0.114×10^{12} mol O_2/yr (which, as will be presented below, is $<1\sigma$ of the final uncertainty on the total igneous sink, and thus does not change our conclusions).

For methane, 1.4 to 4.6×10^{11} moles of methane are estimated to be emitted to the atmosphere per year from geothermal systems (see table 6.3 of Etiope, 2015) and consume 0.28 to 0.92×10^{12} moles of O_2 per year. Sources of the methane include thermogenic and microbial processes as well as abiotic methane generated via the inorganic reduction of CO_2 or CO (Etiope and Sherwood Lollar, 2013), the latter of which is an igneous O_2 sink. The fraction of abiotic methane in these systems is poorly constrained (Etiope and Sherwood Lollar, 2013). Fiebig and others (2019) have recently argued there is no evidence that demands the presence of abiotic methane in these systems. Given this uncertainty, we do not include abiotic continental methane as an igneous sink for O_2.

Subaerial Oxidation of Continental Igneous and Metamorphic Crust by Atmospheric O_2

Reduced minerals in continental igneous and metamorphic crust can be oxidized by atmospheric O_2 during uplift, erosion, and weathering. We include metamorphic rocks to ensure that meta-igneous rocks are also taken into account in our calculations. We estimate the igneous O_2 sink from continental iron and sulfur oxidation following the approach of Holland (1978). Specifically, we estimate igneous rock weathering rates and the amount of Fe^{2+} or sulfur oxidized per gram rock. These are given by the following equations:

$$\frac{dFe^{3+}}{dt}_{\text{continental}} = [F_{\text{riverine sediment}}] \times [\%\ \text{igneous} + \text{metamorphic}] \times [\text{wt.}\%\ \text{Fe}] \times \left[\frac{Fe^{3+}}{\Sigma Fe_{\text{final}}} - \frac{Fe^{3+}}{\Sigma Fe_{\text{initial}}}\right] \tag{21}$$

and

$$\frac{dS^{2-}}{dt}_{\text{continental}} = [F_{\text{riverine sediment}}] \times [\%\ \text{igneous} + \text{metamorphic}] \times [\text{wt.}\%\ \text{S}] \times \left[\frac{S^{2-}}{\Sigma S_{\text{initial}}}\right] \tag{22}$$

$F_{\text{riverine sediment}}$ is the mass flux of sediments through rivers and the '% igneous+metamorphic' is the amount derived from weathering of such rocks. Initial values are the values before weathering while final values are those of sediments deposited and isolated from the atmosphere. For iron, we allow for incomplete oxidation (that is, $Fe^{3+}/\Sigma Fe_{\text{final}}$ in eq 21 need not equal 1) while for sulfur we assume complete oxidation. We do not include other redox-sensitive elements such as Mn or trace elements due to poor constrains on their oxidation states before and after weathering

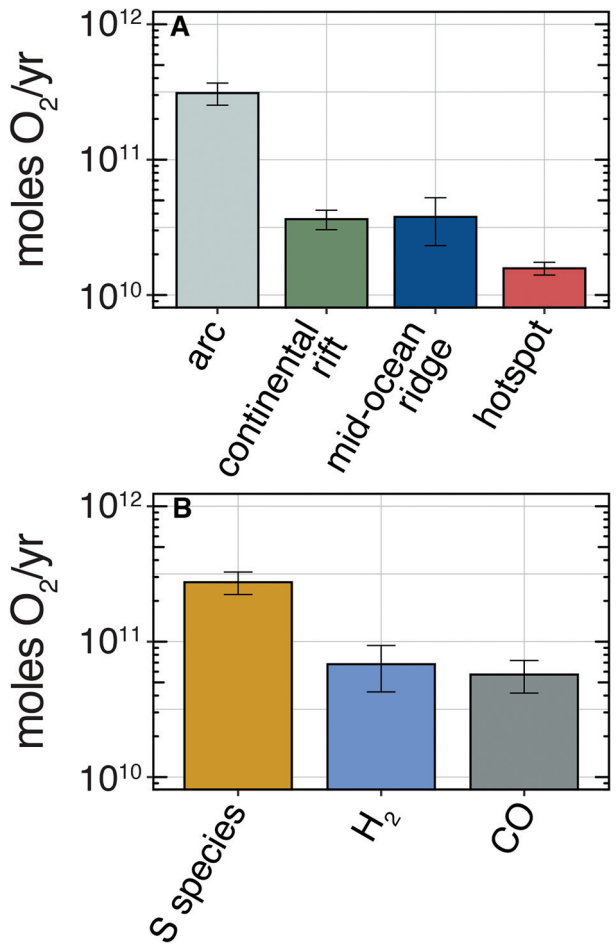

Fig. 5. Moles of O_2 consumed each year for the modern due to volcanism organized by (A) volcanic source and (B) species. Error bars are $\pm 1\sigma$.

and low contents relative to iron. For example, molar Mn/Fe ratios from igneous and metamorphic continental rocks (Hartmann and others, 2012) are typically 0.02 and thus negligible to the overall O_2 budget.

We use the pre-anthropogenic sediment flux ($F_{\text{riverine sediment}}$) from Syvitski and Kettner (2011) of $15.1 \pm 0.5 \times 10^{15}$ g/yr. We assume the uncertainty is $\pm 1\sigma$. We are inherently making the assumption that this pre-anthropogenic flux is a good approximation of a steady-state system. This could be an issue if pre-anthropogenic but still near-modern sediment fluxes are not in a steady state due to, for example, changes in climate from the last glacial period. However, we consider this the best available estimate for pre-anthropogenic sediment fluxes.

We use the current relative exposure of igneous and metamorphic rocks, 29.8% from Hartmann and others (2012), as our upper limit for the concentration in the sedimentary mass flux derived from these rocks. For the lower limit, we use the minimum estimate from Veizer and Mackenzie (2014) that 5% of sediments are newly derived from igneous/metamorphic rock weathering. This is based on Sm/Nd model

ages (Veizer and Jansen, 1985). In summary, we assume 5 to 29.8% of sediments in rivers are newly generated by the weathering of igneous and metamorphic rocks.

We estimate the weight percent iron in various types of igneous and metamorphic rocks from the compilation of Hartmann and others (2012) weighted by their exposed surface area. This yields a value of 3.97% iron by weight which is in agreement with Rudnick and Gao (2014) for average continental crust of 3.92 wt.% iron. We use a value of 4 ± 0.4% (1σ) with an assumed (by us) ±10% relative uncertainty.

Based on the compilation of Hartmann and others (2012), the mean initial $Fe^{3+}/\Sigma Fe$ value of exposed igneous and metamorphic rocks (weighted based on their exposure area) is 0.34. We assume a ±10% relative uncertainty (±0.034, 1σ) for this term. Our lower limit for the final $Fe^{3+}/\Sigma Fe$ of sediments is the average $Fe^{3+}/\Sigma Fe$ of exposed sediments from Hartmann and others (2012) of 0.55. This is a lower limit as iron in sediments may have originally been more oxidized during transport and then reduced following deposition during diagenesis. For an upper limit, we use the $Fe^{3+}/\Sigma Fe$ of oxidized sediments from the deep ocean, which is 0.82 (Chester and Jickells, 2012). Together, this yields a range for final $Fe^{3+}/\Sigma Fe$ values of 0.55 to 0.82.

For sulfur, we again use the compilation Hartmann and others (2012) which yields an average sulfur content of exposed igneous and metamorphic rocks of 0.056 wt.%. We assume a ±10% (1σ) relative uncertainty. This is similar to average sulfur contents of upper continental crust of 0.062 wt.% (Rudnick and Gao, 2014). From Hartmann and others (2012), 77% of this sulfur is speciated as S and the rest as SO_3. We assume the sulfur speciated as S is actually sulfide (that is, 2−). We again assume a 10% (1σ) relative gaussian uncertainty for these terms. Finally, we assume all sulfur is oxidized to sulfate during erosion and transport. This is supported by the rapid oxidation of pyrite during weathering (Petsch and others, 2000) and dearth of detrital pyrite following the oxygenation of the atmosphere ~2.4 billion years ago (for example, Johnson and others, 2014).

These yield total O_2 sinks for continental igneous and metamorphic rock oxidation of 0.233 ± 0.108 (1σ) × 10^{12} mol O_2/yr. 70% is from iron oxidation and 30% from sulfur oxidation (fig. 6)

Igneous Sink Summary

All told, we estimate a total igneous sink of 1.83 × 10^{12} mol O_2/yr (±0.43, 1σ). Of this, 37% is from low-temperature hydrothermal alteration of oceanic crust, 28% from high-temperature hydrothermal fluid emissions, 22% from subaerial volcanism, and 13% from subaerial oxidation of igneous and metamorphic rocks (fig. 7). In figure 8, we provide histograms of the distributions for these sinks. Our value is less than that given recently in Galvez (2020) of 2.7 × 10^{12} mol O_2/yr (±1.1, 1σ), though the two overlap within ±1σ uncertainty. Given the different approaches, it is difficult ascertain the full cause of the disagreement. However, as discussed above, at least 0.62 × 10^{12} of the 0.87 × 10^{12} mol O_2/yr disagreement is due to their inclusion of lithospheric serpentinization as a sink of O_2.

SOLID-EARTH SOURCES OF O_2

In this section we take up the following question: how much organic carbon, sulfur in pyrite, and Fe^{2+} is subducted each year? We do this to compare the solid-earth O_2 source term associated with subduction to the igneous O_2 sink calculated above. Galvez (2020), motivated by the same question, made a similar comparison using literature estimates of subduction fluxes. Here we calculate these fluxes ourselves by estimating the amount of sediment subducted each year and the weight percent organic carbon, sulfur in pyrite, and Fe^{2+} derived from reduction of Fe^{3+} in that sediment. This is again done using a Monte Carlo approach in which distributions for these

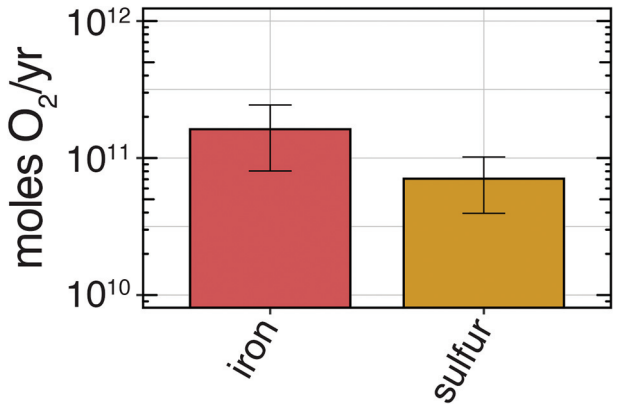

Fig. 6. Moles of O_2 consumed per year for the modern during subaerial weathering of continental igneous and metamorphic rocks due to iron and sulfur oxidation. Error bars are ±1σ.

values are estimated and sampled from 10^7 Monte Carlo iterations. We solve the following specific equations:

$$F_{C_{org};\,subduction} = F_{sediment} \times [C_{org}] \tag{23}$$

$$F_{S_{pyrite};\,subduction} = F_{sediment} \times [S_{pyrite}] \tag{24}$$

$$F_{Fe^{2+};\,subduction} = F_{sediment} \times [Fe^{2+}] \tag{25}$$

Estimates of Sedimentary Mass Fluxes into Subduction Zones

We first establish bounds on sediment subduction fluxes based on estimates by others at specific subduction zones. Following Evans (2012), we scale all prior estimates to an assumed total global length of subduction zones. We use the value of 51,310 km from Bird (2003). For our lower bound, we use the estimate of Plank and Langmuir (1998) of 1.3×10^{15} g/yr sediment subducted over an examined subduction zone length of 29,700 km. This flux accounts for removal of sediments to accretionary prisms, but not for potential underplating. Scaling this up to a total subduction length of 51,310 km from 29,700 km yields 2.25×10^{15} g/year.

For our upper bound, we use the estimate of Scholl and von Huene (2007) (which is an update of von Huene and Scholl, 1991) of 1.1 km^3/yr of sediment subducted along an examined 42,250 km of subduction zones. This value is corrected for sediment added to accretionary prisms but not underplating. To convert this volume to a mass, we estimate a typical dry-weight (that is, matrix) density of sediment outboard of subduction zones of 2.86 g/cm^3 based on table 2 in Plank and Langmuir (1998)—this is a weighted average for all subduction zones with the weighting based on the total volume of sediment approaching the trench per year. Using this density, the 1.1 km^3/year of sediment from Scholl and von Huene (2007) scaled to a total subduction zone length of 51,310 km from 42,250 km equates to a zero-porosity mass of 3.82×10^{15} g/yr of sediment subducted.

Based on these considerations, we use a range of 2.25 to 3.82×10^{15} g/yr for total sediment subduction fluxes. A question is whether this estimate is reasonable and internally consistent with other model assumptions made here. We evaluate this as follows: in the subsection *Subaerial Oxidation of Continental Igneous and Metamorphic Crust*

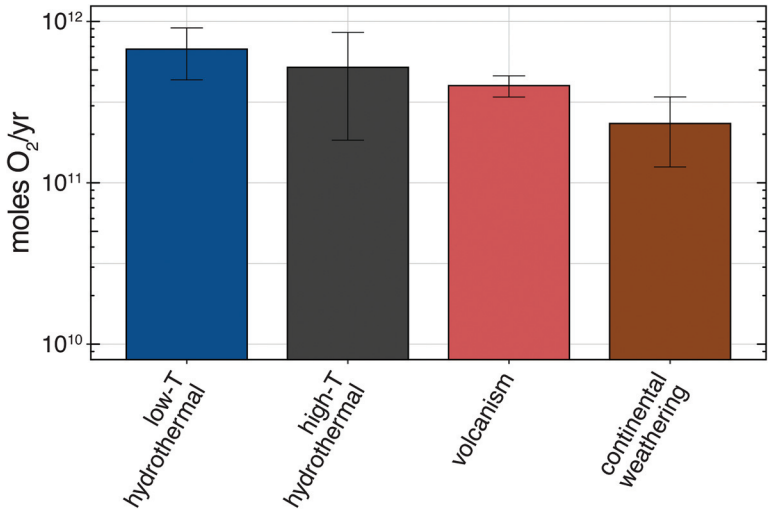

Fig. 7. Summary of the O_2 consumption rates of various igneous O_2 sinks for the modern. Error bars are $\pm 1\sigma$.

by Atmospheric O_2 we calculated 2.6×10^{15} g/yr (± 1.1, 1σ) of new sediment is produced via weathering of igneous and metamorphic rock. As this is within the range of our estimate for sedimentary subduction fluxes, our calculations indicate that the amount of new sediment produced vs. subducted each year is within uncertainty. Although whether or not the sedimentary reservoir is currently net accumulating or net being destroyed is not known, at the very least our various calculations do not imply the presence of a large imbalance in the sediment cycle. Based on this, we consider our estimates of subduction fluxes to be, to first order, both reasonable and internally consistent.

Estimates of the Subduction Flux of Sedimentary Organic Carbon

Here we estimate the subduction flux of organic carbon. This calculation requires us to estimate the typical weight percent organic carbon in subducting sediments. We follow Wallmann (2001) and categorize sediments as either pelagic or terrigenous with different representative organic carbon contents. Pelagic sediments form in the open ocean whereas terrigenous sediments are derived from the erosion of continents and deposited in shallower waters. Terrigenous sediments are introduced to subduction zones by, for example, river deltas and turbidites. This distinction acknowledges the fact that deep-sea (that is, pelagic) sediments typically have less organic carbon in them compared to near-shore environments receiving higher fluxes of continental material (for example, Canfield, 1994). We use Plank and Langmuir's (1998) estimate that 82% of subducted sediment is terrigenous and the rest (18%) is pelagic. We have removed the structural water content of subducted sediments in doing this apportionment. We assign an arbitrary $\pm 10\%$ uncertainty to this term and assume a uniform distribution (72–92%) to the terrigenous flux and solve for the pelagic flux in each Monte Carlo iteration by assuming pelagic fluxes bring the sum to 100%.

Again, following Wallmann (2001), we assign a weight percent total organic carbon (TOC) to the pelagic and terrigenous sediments. We use the estimates from Emerson and Hedges (1988) of 0.34 wt.% for open-ocean (that is, pelagic) sediments and 1.02 wt.% for continental margin (that is, terrigenous) sediments. Both estimates

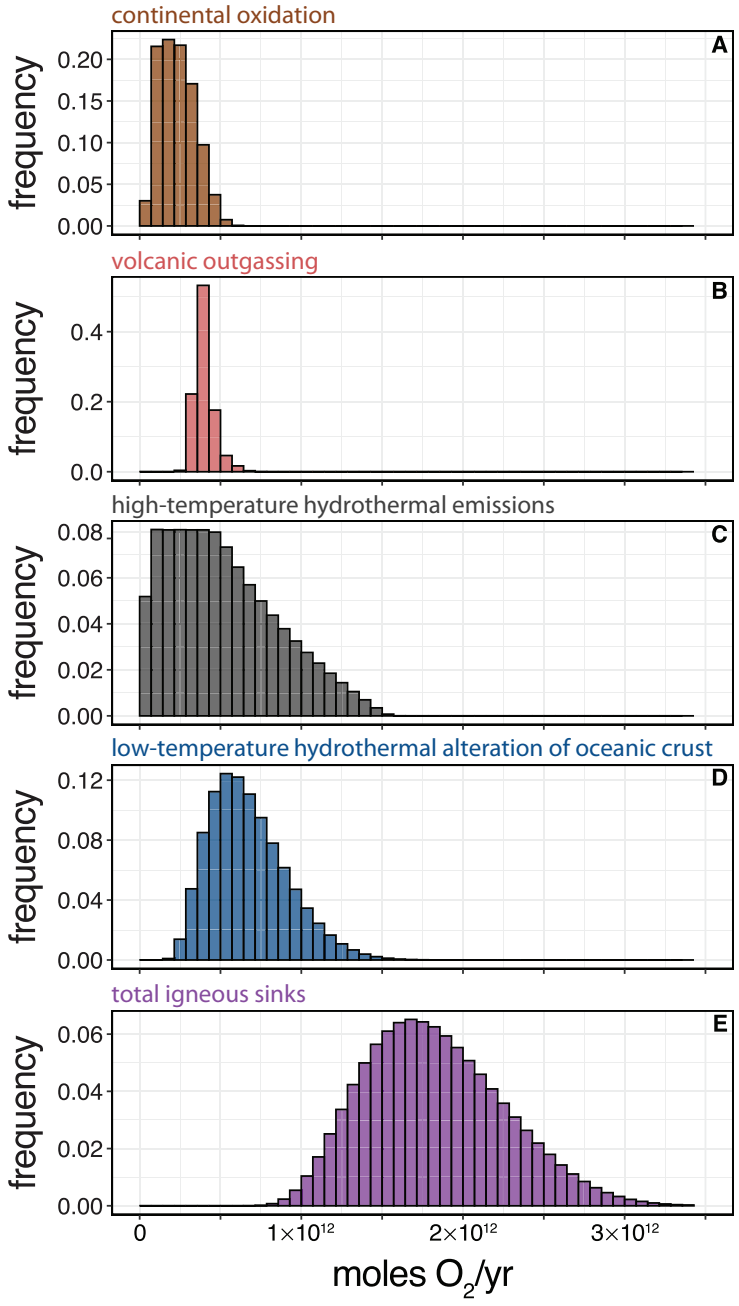

Fig. 8. Histograms of calculated distributions for igneous O_2 sinks (as frequencies).

are for sediments in the sedimentary mixed layer (top 10–20 cm). In order to establish an uncertainty range, we estimated these numbers in a second, independent manner. We use the compilation of marine sedimentary TOC contents in dry weight percent

TABLE 2

Estimates of sizes of modern and Neoproterozoic igneous O_2 sinks and their differences

	modern igneous sink O_2/yr	±1σ	Neoproterozoic igneous sink O_2/yr	±1σ	difference (Neoproterozoic minus modern)	±1σ
low-T hydrothermal	6.73E+11	2.39E+11	0	-	-6.73E+11	2.39E+11
high-T hydrothermal	5.19E+11	3.36E+11	5.19E+11	3.21E+11	-4.19E+08	2.25E+11
volcanism	4.00E+11	5.99E+10	1.03E+12	2.59E+11	6.29E+11	2.23E+11
subaerial weathering	2.33E+11	1.08E+11	2.33E+11	1.08E+11	0	-
total	**1.83E+12**	**4.30E+11**	**1.78E+12**	**4.26E+11**	**-4.51E+10**	**3.97E+11**

from Seiter and others (2004). These are from the top 0 to 15 cm of cores and thus are directly comparable to the TOC estimates of Emerson and Hedges (1988). For continental margin sediments, we calculate the median TOC content of samples deposited at water depths less than 100 m. We use the median rather than the mean to prevent aliasing towards samples with high TOC contents because distributions show a tail to high TOC contents. This yields a median TOC weight percent for continental margins of 0.69% (based on 698 determinations). For the pelagic sediments, we use the median organic carbon weight percent for depths greater than 2000 meters, yielding a pelagic TOC weight percent of 0.55% (based on 1802 determinations). Based on this, we use a uniform distribution of TOC for pelagic sediments of 0.34 to 0.55 wt. % and 0.69 to 1.02 wt.% for terrigenous sediments.

These TOC contents are for the bioturbated sedimentary mixed layer. The organic carbon in these sediments will be further oxidized before ultimately exiting the mixed layer and being buried more deeply. Emerson and others (1987) estimate that 30 to 50% of this mixed layer organic carbon can be further oxidized in continental-margin settings (that is, terrigenous sediments) and 20 to 40% can be further oxidized in open-ocean settings. We use these estimates with uniform distributions to estimate the amount of organic carbon further oxidized in the mixed layer before burial to deeper depths.

With these constraints, we use the following equation to estimate organic carbon subduction fluxes:

$$F_{C_{org};\,subduction} = F_{sediment} \times \begin{pmatrix} \left[\%_{terrigenous\ \ sediment}\right] \times \left[C_{org}\right]_{terrigenous} + \\ \left[\%_{pelagic\ \ sediment}\right] \times \left[C_{org}\right]_{pelagic} \end{pmatrix} \quad (26)$$

where $F_{Corg;\ subduction}$ is the subduction flux of organic carbon in g/yr, $F_{sediment}$ is the sediment subduction flux in g/yr, $[\%_{terrigenous\ sediment}]$ and $[\%_{pelagic\ sediment}]$ are the relative amounts of pelagic vs. terrigenous sediment, and $[C_{org}]$ is the residual weight percent organic carbon in terrigenous or pelagic sediments that remains following oxidation during burial in sediments.

The weight percent organic carbon in terrigenous or pelagic sediments is calculated as

$$\left[C_{org}\right]_{terrigenous} = \left[C_{org}\right]_{terrigenous\ initial} \times \left[\%\ preserved\right]_{terrigenous} \quad (27)$$

with an equivalent equation for pelagic sediments.

Based on this, we estimate that 1.20×10^{12} (± 0.24, 1σ) moles of organic carbon are subducted each year releasing an equivalent amount of O_2. This translates into an average weight percent of organic carbon in subducting sediments of 0.48% (± 0.06; 1σ). This is not the mean organic content of marine sediments, but is instead weighted heavily towards the terrigenous-derived sediment endmember that has higher organic contents than pelagic sediment. For example, we calculate that 88% ($\pm 5\%$, 1σ) of the subducted organic carbon is derived from terrigenous sediments and the rest from pelagic sediments. Is this subduction flux a reasonable number? Though difficult to evaluate, we can at least compare this (1.20×10^{12} (± 0.24, 1σ) to previous estimates of the moles organic carbon subducted per year: 0.2×10^{12} (Holser and others, 1988), 0.54×10^{12} (Wallmann, 2001), 0.72×10^{12} ($\pm 0.39 \times 10^{12}$) (Evans, 2012), 0.95×10^{12} (Clift, 2017), 1.5×10^{12} (Lasaga and Ohmoto, 2002), and 1.1-2.9 $\times 10^{12}$ (Bebout, 1995). Thus our estimate, 1.2×10^{12} moles organic carbon subducted is within the admittedly wide range of previous estimates ($\sim$0.2–2.9 $\times 10^{12}$ moles organic carbon/yr).

A similar exercise has recently been done by Clift (2017). They did this following the general approach of Plank and Langmuir (1998) whereby sediment fluxes and, in this case, organic carbon contents were estimated for specific subduction zones and totaled to find a global average subduction flux. Their final number, 0.95×10^{12} mol C_{org}/yr is within $\pm 2\sigma$ of our estimate. This differs from our approach of using a single global number for organic carbon contents of subducting sediments and should in principle, result in a more accurate estimate of subduction fluxes. However, it requires accurate estimates of carbon contents of sediments entering specific subduction zones, which are variable both as a function of sediment depth below the seafloor at a given location and along strike (House and others, 2019). For example, different assumptions about sediment fluxes and carbon contents results in an order of magnitude difference in carbon subduction fluxes at the Sunda trench (Clift, 2017; House and others, 2019). As such, we take the simpler approach here of estimating global numbers and expect that improved estimates will require a study of subduction zones on a case-by-case basis.

Our calculations of organic carbon subduction fluxes depend on three important assumptions that we now evaluate. First, we assumed that it does not matter whether the deposited organic matter was synthesized 'recently' (that is, it is similar in age to the sediment being deposited) or represents relict fossil organic carbon that escaped oxidation during uplift, erosion, and redeposition. This assumption is acceptable if the organic carbon being subducted would be reactive to O_2—that is, it could be oxidized upon uplift. This is probably a reasonable assumption as ancient organic carbon preserved in sediments is known to oxidize during erosion (Petsch and others, 2000) and during sediment transport (for example, Bouchez and others, 2010). A caveat to this is that graphite is generally thought to be less susceptible to oxidation during uplift and transport compared to other more labile forms of ancient sedimentary organic carbon (commonly termed 'petrogenic' carbon) (for example, Galy and others, 2008; Bouchez and others, 2010; Sparkes and others, 2020). Thus, subduction of 'inert' graphite with respect to O_2 would not result in the net release of O_2 to the atmosphere. Rather such graphitization itself would be a net source of O_2 regardless of whether that graphite is subducted or buried in a sedimentary basin. Here, we proceed with the assumption that most organic carbon that is uplifted is oxidizable and thus subduction of this organic carbon

represents a net O_2 source. This assumption is supported by the recent work of Canfield and others (2021) who showed that recycled graphite (that is, graphite that survives sedimentary weathering and is redeposited in new sediments) is rarely found in Proterozoic marine sediments despite lower atmospheric O_2 levels compared to today. Thus, based on these results, graphite is likely mostly oxidized during uplift, transport, and redeposition in sediments.

Second, we assume that all microbial respiration occurs in the sedimentary mixed layer. Put another way, we assume that degradation of organic carbon below the mixed layer by anaerobic metabolisms (for example, from sulfate reduction) can be neglected. In deep-sea sediments with low accumulations rates (for example, 0.001 cm/yr), sulfate reduction rates are 100 to 1000× lower than aerobic respiration rates (Canfield, 1989) supporting the assumption that most respiration in deep-sea pelagic sediments occurs in the mixed layer (where oxic respiration occurs). In settings with higher sedimentation rates, sulfate reduction becomes important, and at the highest sediment rates (>0.1 cm/yr), aerobic respiration and sulfate reduction consume approximately equal amounts of organic carbon (Canfield, 1989). This consumption of organic carbon by both aerobic and sulfate reducing organisms dominantly occurs in the depth interval we are using for the mixed layer (<20 cm burial depth in sediments). For example, in Danish fjords, Jørgensen (1982) found that for samples taken at water depths <200 m (that is, shelf sediments) 75 to 95% of sulfate reduction occurred in the top 15 cm of the sediment. Additionally, methanogenesis (which typically occurs deeper than the sedimentary mixed layer) is estimated to consume 5 to 10× less organic carbon than sulfate reduction (Canfield, 1993). Based on this, the assumption that the vast majority of respiration occurs in the mixed layer whether by aerobic or anaerobic metabolisms appears to be reasonable. However, the exclusion of potentially deeper organic carbon respiration makes our estimate an upper limit on organic carbon contents of subducting sediments (assuming all other assumptions are accurate).

Third, we assume that all organic carbon that enters a subduction zone and that is not diverted to the accretionary prism or underplated will reach the mantle. However, as the organic matter is heated, it can decompose to liquid and gaseous hydrocarbons that could escape back to the ocean and atmosphere (for example, along a decollement). The amount of carbon lost from subducting sediments is generally thought to be small based on studies of ultra-high-pressure metamorphic rocks derived from subduction zones. For example, Bebout (1995) estimates that >75% of organic carbon is retained in subducting sediments while Cook-Kollars and others (2014) estimate that potentially 80 to 90% is retained. Given this, we do not correct for any potential loss of organic carbon during subduction but recognize that this assumption may need to be revisited in the future.

Estimates of Sedimentary Sulfur Subduction Fluxes

Here we estimate sulfide-in-pyrite subduction fluxes. We assume that all pyrite in sediments is derived from in-situ reduction of sulfate to sulfide using electrons from organic carbon (for example, via dissimilatory sulfate reducing microorganisms) and that no detrital sulfide minerals are present in marine sediments—as such all pyrite that is subducted is an O_2 source. This is consistent with the observation that pyrite is efficiently oxidized during uplift and transport (for example, Petsch and others, 2000; Johnson and others, 2014).

We estimate the amount of pyrite being subducted following Hansen and Wallmann (2003). Rather than estimate pyrite contents in marine sediments (which are poorly constrained), we instead estimate an average S/C ratio in which the sulfur (S) and carbon (C) are in pyrite and organic carbon respectively and multiple this

S/C ratio by organic carbon subduction fluxes to estimate sulfur-in-pyrite subduction fluxes:

$$F_{S_{pyrite};\,subduction} = \frac{S}{C} \times F_{C_{org};\,subduction} \tag{28}$$

This approach is based on the well-known correlation between organic carbon and sulfur contents of marine sediments (Berner, 1982; Berner and Raiswell, 1983). Using the data of Berner (1982), the S/C ratio of marine sediments is 0.38 ± 0.12 (1σ). We use this ratio with the mean organic carbon wt.% of subducting sediments calculated above (subsection *Estimates of the Subduction Flux of Sedimentary Organic Carbon*; 0.48% ±0.06, 1σ) to estimate the average sulfur-in-pyrite weight percent of subducting sediments and multiply this by the sediment subduction flux. In doing this, we are assuming that the S/C ratio for pelagic and terrigenous-derived sediments are similar—we consider this an acceptable assumption as the S/C ratio used from Berner (1982) is derived from a variety of oxygenated marine environments indicating similar trends across different depositional settings. Based on this, we estimate a sedimentary sulfur (in pyrite) content of 0.18 ± 0.06% (1σ) by weight and sedimentary pyrite sulfur flux of $0.17 \pm 0.07 \times 10^{12}$ mol S/yr. This is an O_2 source of 0.30×10^{12} (±0.11, 1σ) mol/yr. The potential size of the O_2 source from the subduction of the Fe^{2+} in pyrite is not included in this estimate and is taken up in the next section. Note that the relative uncertainty on the S/C ratio is sufficiently large that the Monte Carlo simulations occasionally generate negative S/C values in the overall distribution. As such values have no meaning, we assign any such negative values a value of 0 before performing any calculations.

We now compare our estimate of pyrite sulfur subduction fluxes to previous estimates. Hansen and Wallmann (2003) estimate a sulfur-in-pyrite subduction flux of 0.075×10^{12} mol/yr, 44% the size of that calculated here (0.17×10^{12} mol S/yr). This disagreement results from different sediment subduction fluxes. They used a sediment subduction flux of 1.2×10^{15} g/year from Plank and Langmuir (1998). When the sediment subduction flux of Plank and Langmuir (1998) is scaled to account for global subduction zone lengths vs. only the length of trenches Plank and Langmuir (1998) examined, this flux increases to 2.25×10^{15} g/year. This rescaling results in an 88% increase in sediment subduction flux and thus a similar increase in sulfur subduction fluxes, largely eliminating the mismatch (0.14×10^{12} with the rescaling vs. 0.17×10^{12} mol S/yr here).

An alternative estimate of sedimentary sulfur-in-pyrite subduction fluxes is from Evans (2012) who estimate that sediments contain 1.15 wt.% sulfur in pyrite and a subduction flux of sulfur-in-pyrite of $0.62 \pm 0.33 \times 10^{12}$ mol/yr, which is 3.6× larger than our estimate. This difference largely arises because Evans (2012) assumed that all of the iron in sediments that could become pyritized (25% of iron; see Canfield, 2004) has converted to pyrite, and, as the author notes, this represents an upper bound for sulfide subduction fluxes. Galvez (2020) used this upper bound in their estimate of subduction fluxes. Finally, Holser and others (1988) estimates a subduction flux of 0.07×10^{12} mol S/yr based on estimates of sedimentary sulfur contents and the assumption that subduction rates equal generation rates of oceanic crust. Consequently, previous estimates of sulfur-in-pyrite subduction fluxes vary by a factor of 9, indicating the challenge of estimating this number. Despite this, our estimate falls in between previous estimates and is at least consistent, to an order of magnitude, with previous estimates.

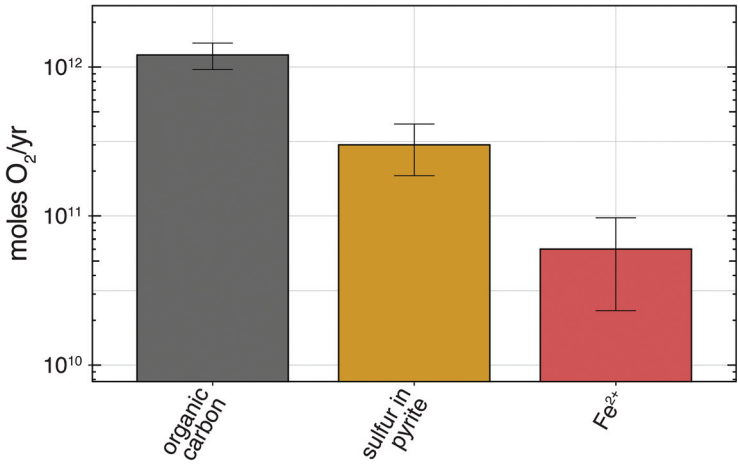

Fig. 9. Summary of the O_2 release rates due to subduction of various elements and species for the modern. Error bars are $\pm 1\sigma$.

Estimates of Weight Percent Fe^{2+} in Subducting Sediments

Iron subducted as Fe^{2+} in sediments represents a net source of O_2 if that iron was first originally Fe^{3+} and was reduced in sediments to Fe^{2+} using electrons ultimately derived from the oxidation of organic carbon. According to the compilation of Hartmann (2012), the typical $Fe^{3+}/\Sigma Fe$ of exposed continental igneous and metamorphic rocks is 0.34 while continental sediments have $Fe^{3+}/\Sigma Fe$ of 0.55. We assume these rocks are representative of terrigenous sediments preserved in the rock record that ultimately enter subduction zones. We assumed above that the iron in these continental sedimentary rocks could have been oxidized during weathering and transport to a minimum $Fe^{3+}/\Sigma Fe$ of 0.55 and maximum of 0.82 before being reduced back to a value of 0.55 (see section *Subaerial Oxidation of Continental Igneous and Metamorphic Crust by Atmospheric O_2)*. Based on this we assume that the relative amount of Fe^{2+} vs. all iron in terrigenous sediments that represents a source of O_2 during subduction is between 0 to 0.27 and is always 0 in pelagic sediments. Finally, we assume the total iron content of both sediment types is 4 ± 0.3 (1σ) wt.% based on the mean and standard deviation given in Plank and Langmuir (1998) for the typical composition of subducting sediments. We then use the same relative terrigenous vs. pelagic contents of sediments that was used for the organic carbon subduction calculations above to estimate the amount of Fe^{2+} subducted per year.

Based on all this, we calculate that subduction of Fe^{2+} results in a net source of O_2 of 0.060×10^{12} moles of O_2 per year (± 0.037, 1σ).

Subduction Summary

In total, we estimate that subduction of sedimentary organic carbon, pyrite, and iron results in the net release of 1.56×10^{12} (± 0.33, 1σ) mol O_2/yr. Of this, 77% is from the subduction of organic carbon, 19% from the subduction of sulfur in pyrite, and 4% from the subduction of iron (fig. 9). Histograms of the distributions are given in figure 10. Galvez (2020) estimated that 2.3×10^{12} mol O_2/yr are released by subduction (no uncertainty is given) with equal contributions from organic carbon and pyrite burial. As discussed above this estimate is based on the assumption that the maximum amount of iron in sediments that could be pyritized, is pyritized, which contributes to the difference between the two estimates.

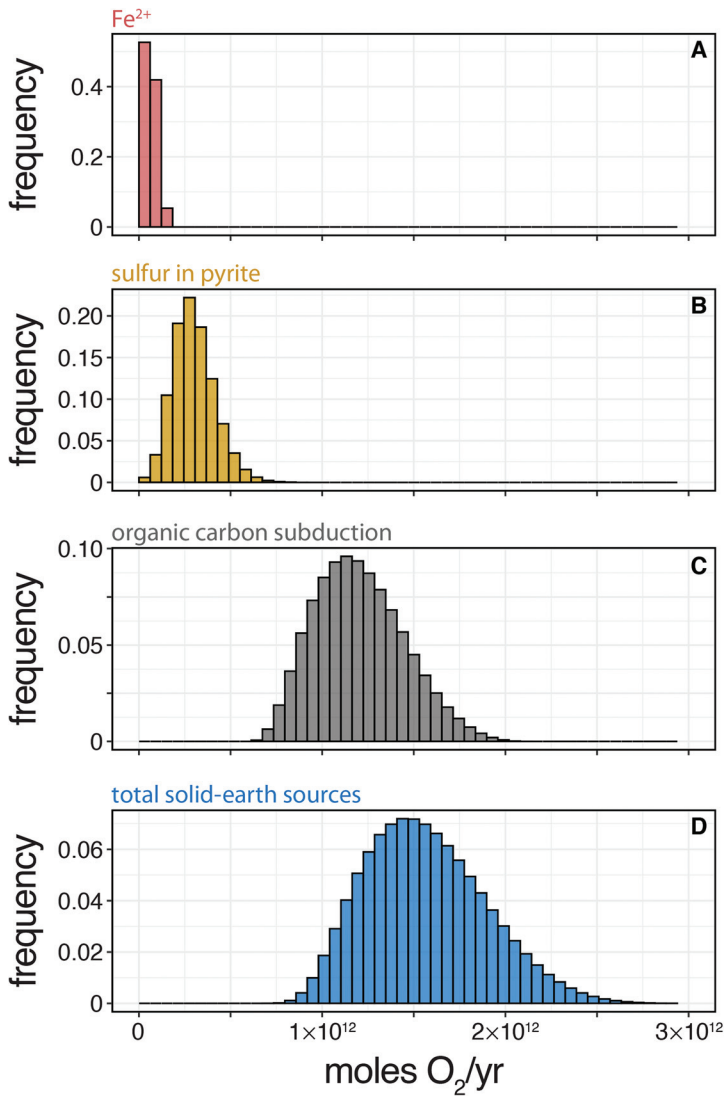

Fig. 10. Histograms of calculated distributions for O_2 sources associated with subduction for the modern (as frequencies).

O_2 SINKS VS. SOURCE

In the above sections we developed estimates of the various total sizes of sources and sinks of O_2 associated with igneous and solid-earth processes. Here we discuss their relative differences (or lack thereof) and potential geochemical mechanisms that control their relative sizes

Balance in the Solid-Earth O_2 Cycle?

We estimated that the solid earth removes 1.83×10^{12} mol O_2/yr (± 0.43, 1σ), while subduction returns 1.56×10^{12} mol O_2/yr (± 0.33, 1σ) (fig. 11). Both estimates are within $\pm 1\sigma$. An overlay of the distributions of the total igneous atmospheric O_2 sources and sinks is given in figure 12 and shows this overlap visually. The difference

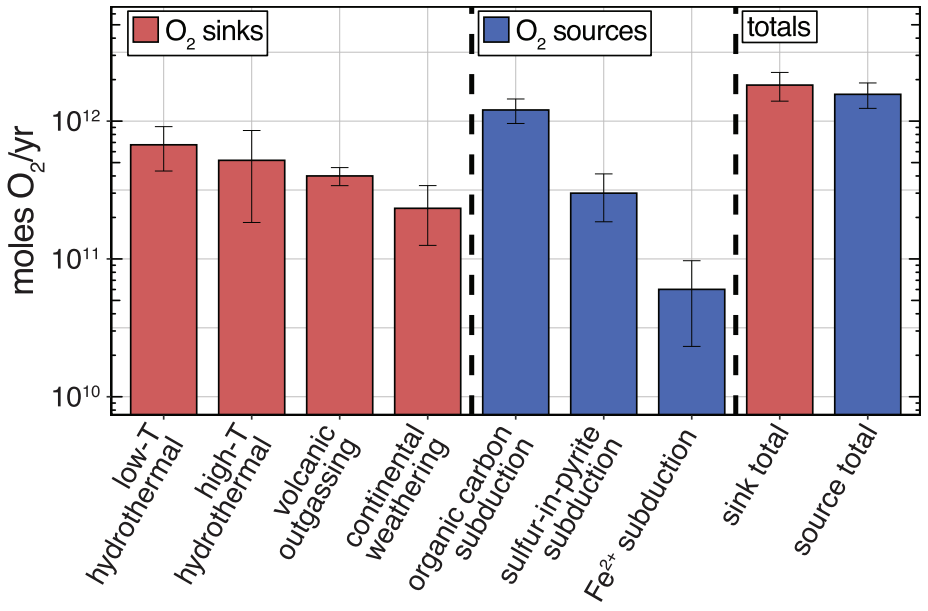

Fig. 11. Summary of the sizes of various solid-earth sources and igneous sinks of O_2 for the modern. Error bars are $\pm 1\sigma$.

is -0.26×10^{12} mol O_2/yr (± 0.54, 1σ) such that solid-earth processes are, in net, a sink for O_2. However, the difference is within 1σ of 0. It is similar to that given by the ice-core record of O_2/N_2 ratios from the past 800,000 years: -0.31×10^{12} mol O_2/yr (Stolper and others, 2016).

The critical point of these calculations and a key conclusion of this work is that based on our analysis, the relative sizes of the igneous sources and sinks are indistinguishable within $\pm 1\sigma$ uncertainty. Put another way, it appears that igneous O_2 sinks are, within uncertainty, balanced by the solid-earth sources. Another way to show this statistically is as follows: if we take the Monte Carlo outputs for all source and sink calculations, 32% of the time igneous O_2 sources are greater than sinks and thus, despite the difference generally being such that sinks are larger than sources, there is a substantial chance that the opposite is true. This is an important point as it indicates that today at least, the solid-earth O_2 cycle is effectively in balance. Now, it must be pointed out that the uncertainty on the difference between sources and sinks is large ($\pm 0.54 \times 10^{12}$ mol O_2/yr, 1σ) and, as such, larger imbalances are possible. But we consider the simplest interpretation of the calculations to be that the igneous O_2 sources and sinks balance within uncertainty.

Negative Feedbacks in the Solid-Earth O_2 Cycle?

A fundamental question is why igneous sources and sinks of O_2 to the atmosphere would be in (near) balance. One possibility is that this is simply chance, which, though relatively unsatisfying, cannot be excluded. Alternatively, the balance reflects a system of stabilizing (negative) feedbacks similar to those proposed for atmospheric CO_2 and the geologic carbon cycle on million-year timescales (for example, Walker and others, 1981). To explore this possibility, we examine how igneous sources and sinks of O_2 could depend on atmospheric or marine O_2 levels. We do this first for the modern and then, in the following section, consider the Precambrian.

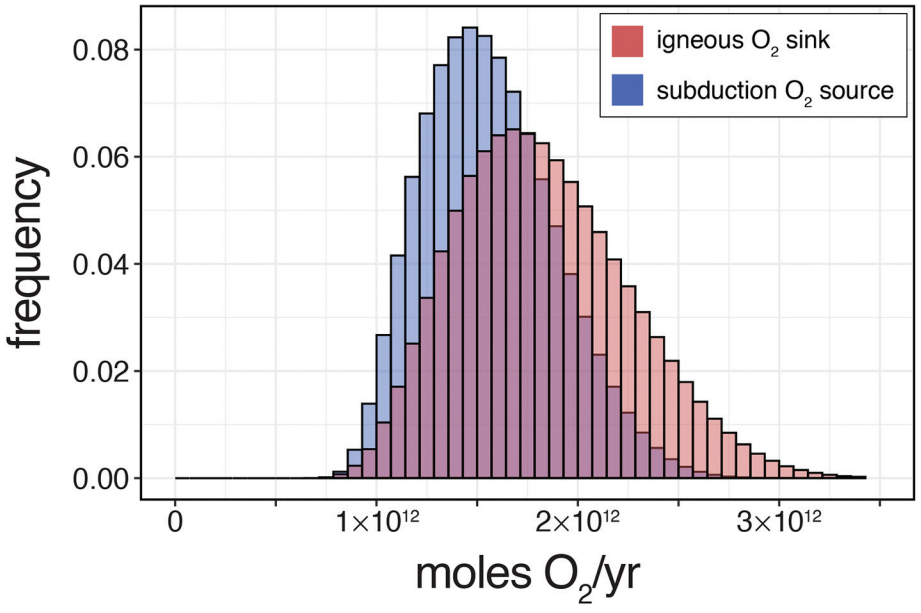

Fig. 12. Overlay of calculated distributions of modern igneous atmospheric O_2 sinks and subduction sources (as frequencies).

The high-temperature hydrothermal sink for O_2 is insensitive to atmospheric and marine oxygen levels as long as the deep-ocean is oxygenated, and all emitted reduced constituents are oxidized by O_2 dissolved in seawater (as opposed to deposited on the seafloor). This system thus cannot serve as a negative feedback for $P_{O_2}^{atm}$ today. The presence vs. absence of sulfate in the ocean has been proposed to modulate the composition and reducing power of these hydrothermal fluids (Kump and Seyfried, 2005), which will be discussed later for the Precambrian. However, over the Phanerozoic, sulfate levels have been sufficiently high ($>\sim$5–10 mmol/kg seawater; Lowenstein and others, 2003) that we assume that the reducing power of high-temperature hydrothermal systems is insensitive to any likely fluctuations in Phanerozoic marine sulfate levels.

Volcanic emissions are also unlikely to be strongly sensitive to atmospheric and marine O_2 concentrations. This is the case for emissions from hotspots, mid-ocean ridges, and continental rifts as these gases are derived from melts of the mantle, the fO_2 of which are not strongly influenced by recent surface processes. For arc volcanoes, the situation is more complicated. Igneous arc rocks are more oxidized than mid-ocean ridge equivalents (Gill, 1981; Ballhaus and others, 1990; Carmichael, 1991; Lécuyer and Ricard, 1999; Kelley and Cottrell, 2009). It is generally thought that this difference reflects the subduction of oxidized sediments and altered oceanic crust that oxidizes that subarc mantle, resulting in more oxidized melts and therefore, more oxidized gases (Arculus, 1985; Ballhaus and others, 1990; Wood and others, 1990; Parkinson and Arculus, 1999; Kelley and Cottrell, 2009; Evans and Tomkins, 2011; Evans and others, 2012; Bénard and others, 2018; Muth and Wallace, 2021)—however this view that igneous arc parental melts are more oxidized than MORB parental melts is not universal (Lee and others, 2005, 2010, 2012; Dauphas and others, 2009; Mallmann and O'Neill, 2009; Lee and others, 2010, 2012). The redox state of

island arc igneous rocks has not changed measurably over the past 540 million years (that is, over the Phanerozoic; Stolper and Bucholz, 2019) suggesting this term is not controlled by changes in atmospheric or marine O_2 concentrations over the Phanerozoic. We relax this assumption in the section on the Precambrian.

Finally, we do not consider that oxidation rates of igneous rocks during weathering are highly sensitive to atmospheric O_2 levels for typically assumed Phanerozoic levels (>0.05 atm). This is based on the observation that paleosols show similar trends in degree of iron oxidation and retention in Mesoproterozoic vs. Phanerozoic examples (Rye and Holland, 1998; though see Planavsky and others, 2018 for an alternative view on this) despite ~100× fold lower Mesoproterozoic atmospheric O_2 levels vs. modern (for example, Lyons and others, 2014).

The low-temperature oxidative alteration of oceanic crust is potentially sensitive to marine O_2 levels as the amount of O_2 circulated through off-axis systems sets the maximum size of the O_2 sink in these systems. Assuming off-axis oxidation rates scale with the amount of deep-ocean O_2, then increases in marine O_2 levels will increase the amount of oxidative weathering that occurs and act as a negative feedback to increasing marine O_2 levels.

Additionally, the subduction of organic carbon, pyrite, and reduced iron could also act as a stabilizing (that is, negative) feedback with respect to O_2 levels. In our calculations, 88% of the O_2 sourced from subduction is derived from the subduction of terrigenous sediments (vs. pelagic sediments), which are derived from near-shore sedimentary systems. The burial of organic carbon and pyrite in such coastal systems is generally thought to inversely scale with and play a key role in regulating $P_{O_2}^{atm}$ (Kump, 1989; Van Cappellen and Ingall, 1996; Lasaga and Ohmoto, 2002; Bergman and others, 2004; Arvidson and others, 2006; Laakso and Schrag, 2014). As such, the amount of organic carbon and pyrite in subducting sediments could also inversely scale with $P_{O_2}^{atm}$ for the same reasons they do in near-shore sediments. For example, if insufficient carbon and pyrite are subducted to balance igneous O_2 sinks, $P_{O_2}^{atm}$ will fall resulting in increased accumulation of organic carbon and pyrite in near-shore sediments. This in turn will increase the amount of organic carbon and pyrite subducted until balance is reached between solid-earth O_2 sources and igneous sinks. The linkage between these processes likely operates over timescales similar to those of tectonic cycles (order tens to hundreds of millions of years). Thus, we do not expect that igneous sources and sinks will ever exactly balance, but rather, as found here, are commonly in near balance.

Balance in the Sulfur Cycle?

In the calculations above, we estimated a total input of sulfur bearing species from igneous processes of 0.87×10^{12} mol S/yr (± 0.17, 1σ). For high-temperature hydrothermal fluids, a proportion of the emitted sulfur is derived from seawater sulfate that was converted to sulfide. Though this sulfur removes O_2, it does not net change the sulfur content of the ocean and thus is not a true sulfur input. As discussed above, ~67 to 75% of the emitted sulfur is leached from igneous rock and the rest derived from seawater sulfate (for example, Shanks and others, 1995). Reducing the high-temperature hydrothermal S flux by 30% yields a total igneous sulfur input of 0.80×10^{12} mol S/yr (± 0.13, 1σ). As a comparison point, a recent estimate of total non-anthropogenic sulfur emitted from rivers to the ocean is 3.4×10^{12} mol S/yr (Burke and others, 2018).

Above, we estimated a total sulfur-in-pyrite subduction flux in sediments of 0.17×10^{12} mol S/yr (± 0.07, 1σ), which leaves an excess flux of 0.63×10^{12} mol S/yr (± 0.14, 1σ) to the ocean. Such an imbalance is important as, if the sulfate remaining in the ocean is converted to pyrite and buried in sediments, it would act as an igneous

O_2 source. Importantly, sulfur is also removed from the ocean and subducted into the mantle in altered oceanic crust both via alteration of mafic rocks and via serpentinization of ultramafic rocks during hydrothermal circulation on ridge flanks and during plate flexure at subduction zones (for example, Alt, 1995; Alt and others, 2013; Coggon and others, 2016). Although such uptake can oxidize igneous rocks, this is not an O_2 sink if the sulfur is retained in the rock either as sulfate or sulfide—it is a sink of oxidants that can oxidize the mantle but, based on the accounting done here, will not directly affect atmospheric O_2 when removed from the ocean.

To quantify these additional igneous sulfur sinks, we first use recent estimates of hydrothermal sulfur uptake fluxes during alteration of mafic oceanic crust from the study of the Macquarie ophiolite (Coggon and others, 2016). This ophiolite formed from mid-ocean ridge oceanic crust (as opposed to a back-arc setting); it is relatively young (<12 million years); and it is complete (that is, it goes from basalts to gabbros) (see Varne and others, 2000 and references therein). As such, it is ideally suited to estimate subduction fluxes of oceanic crust. Coggon and others (2016) estimate a net uptake of between 0.19 to 0.27×10^{12} mol S/yr to altered oceanic crust (that is, the difference in all sulfur removed vs added). In order to avoid underestimating the absolute sulfur uptake, we must add our hydrothermal sulfur fluxes to these numbers. In other words, we must add back 70% of the high temperature sulfur flux and all of the low temperature sulfur flux that were leached from oceanic crust during alteration. This equates to an extra 0.27×10^{12} mol S/yr (± 0.11, 1σ). Second, Alt and others (2013) estimate that low and high temperature serpentinization during alteration of oceanic crust takes up 0.013 to 0.146×10^{12} mol S/yr of which 23 to 29% is derived from seawater sulfate and 0.007 to 0.049×10^{12} mol S/yr during serpentinization associated with slab bending at subduction zones.

Assuming uniform uncertainty for the various estimates from Coggon and others (2016) and Alt and others (2013) and a normally distributed uncertainty for our hydrothermal sulfur flux (corrected for 30% seawater sulfate in the high-temperature flux) yields a total sulfur uptake flux into oceanic crust of 0.55×10^{12} mol S/yr (± 0.12, 1σ). This is within 1σ uncertainty of our estimate for the excess sulfur added to the ocean from igneous sulfur sources, 0.63×10^{12} mol S/yr (± 0.14, 1σ). This indicates that the sulfur cycle, to our best estimate, is also in balance (within $\pm 1\sigma$) through the dual action of sulfur uptake in subducted sediments and subducted altered oceanic crust. The calculated imbalance of 0.08×10^{12} mol S/yr, assuming complete conversion to pyrite, would result in a source of 0.14×10^{12} mol O_2/yr from the sulfur. Inclusion of this would increase our igneous related source to 1.70×10^{12} mol O_2/yr (± 0.46), within 1σ uncertainty of the original estimate of 1.56×10^{12} mol O_2/yr (± 0.33, 1σ) and the estimated igneous O_2 sink of 1.83×10^{12} mol O_2/yr (± 0.43, 1σ).

THE LATE PROTEROZOIC VS. THE PHANEROZOIC

Following the oxygenation of the atmosphere at the start of Proterozoic ~2.3 to 2.5 billion years ago, the Proterozoic atmosphere is generally thought to have had lower-than-modern, but non-negligible O_2 concentrations. Typical (though debated) estimates are of order 1% of modern (see review in Planavsky and others, 2018). These lower-than-modern atmospheric O_2 concentrations are associated with both an anoxic deep ocean and lower-than-modern marine sulfate concentrations. At some point towards the end of the Proterozoic through early Paleozoic (that is, before 400 million years ago), it is thought that atmospheric O_2 levels rose, marine sulfate concentrations increased, and the deep ocean became oxygenated. A common (though not universal) view is that O_2 (Shields-Zhou and Och, 2011; Lyons and others, 2014; Blamey and others, 2016; Tostevin and Mills, 2020) and marine sulfate levels (Kah

and others, 2004; Spear and others, 2014; Turner and Bekker, 2016; Blättler and others, 2020) rose to some degree in the late Neoproterozoic before a second increase in $P_{O_2}^{atm}$ and a large-scale oxygenation of the deep ocean in the early Paleozoic (Dahl and others, 2010; Sperling and others, 2015; Wallace and others, 2017; Stolper and Keller, 2018).

In this final section, we speculate on how changes from an anoxic and lower sulfate ($\sim$<1 mmol/kg seawater; Fakhraee and others, 2019) deep ocean at the end of the Proterozoic to an oxygenated higher sulfate (> a few mmol/kg seawater; Blättler and others, 2020) deep ocean may or may not have affected igneous sinks of O_2. In order to conduct this examination quantitively, we again employ our Monte Carlo calculation framework for various igneous O_2 sinks modified given these changes in boundary conditions. Calculated sizes for various sinks for the Precambrian are given in table 2 along with differences vs. the modern.

In examining the Neoproterozoic system, we focus solely on how the igneous sinks may have changed because these can be analyzed based on how inorganic reactions change due to shifts in boundary conditions. We do not attempt to analyze how subduction fluxes would change as the amount of organic carbon, reduced sulfur, and reduced iron buried in Proterozoic marine sediments is, in our estimation, poorly constrained. We consider this equally true for the response of marine biogeochemical cycles to these processes. As such, we focus on the igneous sink.

Subaerial Weathering

In the discussion on paleosols in the subsection *Balance in the Solid-Earth O_2 Cycle?*, we assumed oxidative subaerial weathering of igneous rocks has not depended on $P_{O_2}^{atm}$ since the Mesoproterozoic and thus this sink for O_2 should remain constant from the Neoproterozoic to early Phanerozoic (Rye and Holland, 1998; though see Planavsky and others, 2018 for a different view). We also assume that the weathering fluxes of subaerial volcanic rocks have remained constant through time—over the Phanerozoic, sediment fluxes show no clear change vs. time (Husson and Peters, 2017). Although large changes in sediment fluxes have been invoked to have occurred between the Precambrian and Cambrian (associated with the so-called Great Unconformity), recent studies have interpreted this either as a large-scale increase in sediment deposition (Husson and Peters, 2017) or an erosive event (Keller and others, 2019). Given this uncertainty, we leave constant the sedimentary erosion rates associated with the calculation of the subaerial oxidative weathering of igneous and metamorphic rocks. As subaerial weathering of igneous rocks is estimated here to only represent 13% of the modern igneous O_2 sink (subsection *Igneous Sink Summary*), even large changes to this term are unlikely to alter on our interpretations. More quantitative constraints on how this O_2 sink has changed over the Mesoproterozoic to today will likely require models that incorporate changes in erosion rates of igneous rocks over time coupled to sediment uplift and transport to oxidation kinetics or iron- and sulfur-bearing igneous minerals as a function of $P_{O_2}^{atm}$ from 0.1 to 100% of modern as have been done for pyrite (Johnson and others, 2014) and organic carbon (Daines and others, 2017; Miyazaki and others, 2018).

Hydrothermal Systems

Low-temperature hydrothermal systems.—Following Laakso and Schrag (2014), Daines and others (2017), and Miyazaki and others (2018), we assume that without any O_2 in the deep ocean, there will be no oxidative consumption of O_2 during low-temperature hydrothermal alteration of oceanic crust. In making this assumption, we

are implicitly assuming that oxidation of Fe^{2+} in igneous minerals by water and associated release of H_2 does not occur substantially during low-temperature hydrothermal circulation of anoxic seawater through oceanic crust. This is supported by the low $Fe^{3+}/\Sigma Fe$ (~0.25) of Precambrian submarine basalts relative to Phanerozoic equivalents (>0.3) (Stolper and Keller, 2018).

We do not include any fluxes of reduced elements from off-axis fluids. As discussed above, this is supported by the low amount of Fe^{2+} and H_2S found in 25°C springs from off-axis systems with <0.1 to 6 μmol Fe^{2+}/kg H_2O and 1.3 μmol H_2S/kg H_2O (Mottl and others, 1998; Wheat and Mottl, 2000).

High-temperature hydrothermal systems.—Kump and Seyfried (2005) proposed that high-temperature hydrothermal fluids were more reducing in a low-sulfate Precambrian ocean vs. in the modern because, in the absence of sulfate, fluid fO_2 would be similar to QFM (for example, Sleep and Bird, 2007). The H_2S fugacity is then set by the fluid fO_2 and chemical equilibrium with pyrrhotite. Kump and Seyfried (2005) provide calculations of H_2S and Fe^{2+} concentrations in the fluid at 400°C and 400 and 500 bar and H_2 concentrations at 400°C and 400 bar for systems with and without sulfate.

Based on this, we recalculate our high temperature hydrothermal fluxes assuming equilibration of fluids at QFM for mafic hosted system. We use the same fluid fluxes as in the modern—in doing this we are not correcting for any potential changes in hydrothermal fluxes due to changes in mantle heat flow (this is discussed farther below). For serpentinizing systems, we do not change the concentrations. In mafic-hosted systems, for Fe^{2+}, we use a range based on the maximum and minimum concentrations at 400°C at 400 and 500 bar calculated by Kump and Seyfried (2005): 17.5 to 80 mmol/kg fluid (vs. 0.75 to 6.5 used here for the modern). We recalculate H_2 and H_2S concentrations with the recent calibration of their solubility and activity coefficients from Scheuermann and others (2020) at 400 and 500 bar and 400°C (their eqs 11 and 13) along with fugacities from the online SUPCRT program using the slop07.dat database (Geopig, 2010). Water densities were calculated assuming a seawater salinity of 3.2 wt.% NaCl using the SoWat program (Driesner and Heinrich, 2007; Driesner, 2007). This results in ranges of H_2 concentrations of 7.8 and 9.1 mmol/kg fluid (vs. 0.05 to 1 used here for the modern) and 9.9 and 10.8 mmol/kg fluid for H_2S (vs. 2.9 to 12.2 used here for the modern).

Based on these calculations, we estimate a total potential sink for high-temperature hydrothermal system in the Precambrian of 1.13×10^{12} moles O_2/yr (±0.63, 1σ) as compared to the calculated modern value of 0.52×10^{12} moles O_2/yr (±0.34, 1σ). However, as Fe^{2+} and H_2S do not co-exist in marine fluids (ultimately forming pyrite), we assume that all emitted H_2S is titrated in the deep ocean as, ultimately, pyrite, and thus does not reach the upper ocean where it could react with O_2 derived from the atmosphere. We assume H_2S is removed given that the deep-ocean is generally assumed to have been ferruginous in the Neoproterozoic (for example, Lyons and others, 2014). In this case, without the sulfide, the Precambrian high-temperature hydrothermal sink is 0.52×10^{12} moles O_2/yr (±0.32, 1σ), which is identical within ±1σ to the modern sink. Thus, in this scenario, switching from an anoxic to oxygenated deep ocean would cause no net change in the high-temperature hydrothermal O_2 sink size. As will be developed, temporal changes may occur during deep-ocean oxygenation. We note that if the ocean were sulfidic and the iron titrated out instead, the hydrothermal sink would be 0.77×10^{12} moles O_2/yr (±0.42, 1σ), and thus larger than (but still within ±1σ of) the modern sink.

As discussed above, in doing these calculations, we are assuming that the hydrothermal flux of water in the Neoproterozoic vs. today are sufficiently similar that no rescaling is required—this requires knowledge of both the thermal history of the

mantle and how this translates into the amount of mid-ocean ridge volcanism. A previous attempt linearly scaled hydrothermal fluxes to heat flow changes and, based on their model, predicted that hydrothermal circulation at 750 million years was 10 to 40% higher than today (Halevy and Bachan, 2017). We have not incorporated such changes in the model above as we consider the geological constraints on the hydrothermal flux of fluids through time to be limited. If included, these would increase the hydrothermal sink by 0.05 to 0.2 $\times$ 10^{12} moles O_2/yr, which is within the 1σ uncertainty of the final O_2 sink.

Volcanism

The amount of O_2 consumed by volcanism is a function of the total flux and the redox state of emitted gases. For mid-ocean ridge and continental rift volcanism, we assume no difference in Neoproterozoic vs. modern redox state based on the lack of any secular change in reconstructed mantle fO_2 from the Mesoproterozoic to today (Li and Lee, 2004; Aulbach and Stagno, 2016; Nicklas and others, 2018, 2019; Kadoya and others, 2020b). Hotspots are derived from heterogeneous mantle sources (as reviewed in Hofmann, 2003). We assume that although individual hotspots may vary in redox state (for example, Moussallam and others, 2019a), they will not vary systematically over time. Arc redox is allowed to vary with time as discussed below.

We also assume that volcanic outgassing fluxes from mid-ocean ridges, continental rifts, and hotspots have not, on average, changed significantly over the past billion years. On long (billion-year timescales) mantle outgassing rates are commonly assumed to scale with mantle potential temperature such that secular mantle cooling (for example, Herzberg and others, 2010) has caused decreased outgassing (Hayes and Waldbauer, 2006; Halevy and Bachan, 2017; Krissansen-Totton and others, 2018). This assumption results in outgassing rates that were 12 to 35% higher 1 billion years ago vs. today (Hayes and Waldbauer, 2006; Halevy and Bachan, 2017; Krissansen-Totton and others, 2018). In contrast, studies based on reconstructions of subduction zone and continental rift length find that CO_2 outgassing rates do not change smoothly with time with variations of up to a factor of 2 over the Phanerozoic. In such reconstructions the modern and Neoproterozoic are times of the lowest outgassing rates (Mills and others, 2019), though the Neoproterozoic from 750 to 541 Ma varies from 1 to 1.5x of modern. Given this uncertainty, we assume outgassing rates and C, S, and H contents did not change over the past billion years. As estimated above, modern non-arc-related volcanism consumes 0.09 $\times$ 10^{12} ($\pm$0.02, 1σ) mol O_2/yr. Increasing this by 12 to 35% results in increases of 0.01 to 0.03 $\times$ 10^{12} mol O_2/yr, which is insignificant given an estimated modern igneous O_2 sink of 1.83 $\times$ 10^{12} mol O_2/yr ($\pm$ 0.43, 1σ).

As discussed above, modern igneous arc rocks are more oxidized than mid-ocean ridge igneous rocks. As noted previously, the leading hypothesis for the driver of this difference is that the subduction of oxidized altered oceanic crust and sediments into the mantle oxidizes the source of parental arc melts (Arculus, 1985; Ballhaus and others, 1990; Wood and others, 1990; Parkinson and Arculus, 1999; Kelley and Cottrell, 2009; Evans and Tomkins, 2011; Evans and others, 2012; Bénard and others, 2018; Muth and Wallace, 2021). Based on this, it has been proposed that in the Precambrian when the deep ocean was anoxic, subducted sediments and altered oceanic crust would have been more reduced (due to limited interaction with oxygenated waters) vs. today. As a result, a smaller flux of oxidants would be delivered to the subarc mantle resulting in more limited oxidation of the source of parental arc melts (Evans and Tomkins, 2011; Richards and Mumin, 2013; Stolper and Keller, 2018). These proposals are consistent with the recent observation that $Fe^{3+}/\Sigma Fe$ and V/Sc ratios of island arc igneous rocks (both proxies for the fO_2 of the parental melt)

increase between the Neoproterozoic and the early Phanerozoic (Stolper and Bucholz, 2019). This was interpreted to indicate that the oxygenation of the deep ocean and/or increases in marine sulfate concentrations resulted in an increase in the subduction flux of oxidized sediments and oxidized altered oceanic crust, which in turn caused the subarc mantle to become more oxidized.

Based on this discussion, we recalculated the volcanic outgassing sink for O_2 under the assumption that before increases in marine sulfate and/or oxygenation of the deep ocean, the subarc mantle fO_2 was similar to that of modern MORB. Above, this was assumed to be between -0.35 to 0 log units relative to QFM (Zhang and others, 2018) and we use this here leaving all other arc parameters (temperature, pressure, elemental composition) unchanged. For sulfur in Precambrian arcs, this results in an H_2S/SO_2 range of 0.012 to 29.489 and the S_2/SO_2 range is 0.00211 to 0.548. Given that these ranges span many orders of magnitude, we use a log-uniform distribution for Precambrian arc H_2S/SO_2 and S_2/SO_2 ratios in the Monte Carlo calculations. For H_2 emissions, we find an H_2/H_2O range of 0.015 to 0.028, which we sample with a uniform distribution. For CO emissions, we find a CO/CO_2 range of 0.016 to 0.070, again sampled with a uniform distribution.

In order to calculate the emissions of the various species we require either estimates for outgassing fluxes of one S-, C-, and H-bearing species each (as done for the modern), or an estimate of total S, C, and H emissions. Estimates of ancient S, C, and H emissions from arcs either for total emissions or of specific species are unconstrained. Here, we take the approach of assuming that total outgassing fluxes of C, S, and H species were the same in the Neoproterozoic as today. Although this is almost certainly incorrect to some degree, we consider this a simple and, as will be developed, justifiable starting point.

We begin with hydrogen fluxes. Today arcs have elevated H_2 fluxes relative to other volcanic sources due to high water contents. This water is derived from molecular water or hydrated minerals in subducted alerted oceanic crust and sediments. We are unaware of a reason why over the past ~1 billion years the amount of water in altered oceanic crust and sediments would differ vs. today, and so we consider our assumption of constant arc H_2O emissions over the past billion years to be an acceptable working hypothesis. Based on this we estimate that H_2 emissions in the Precambrian consumed 0.38×10^{12} moles O_2/yr (± 0.08, 1σ) vs. a modern sink of 0.07×10^{12} moles O_2/yr (± 0.03, 1σ). The net difference is 0.31×10^{12} moles O_2/yr (± 0.08, 1σ).

Like H_2O, carbon emissions from arcs are thought to be elevated relative to other volcanic sources due to the introduction of subducted carbon to the subarc mantle (as reviewed in Kelemen and Manning, 2015). The advent of pelagic carbonate sedimentation in the Mesozoic could have led to more subduction of carbonate resulting in increased arc CO_2 emissions in the Mesozoic and Cenozoic vs. the Precambrian (Volk, 1989; Berner, 1991), invalidating our assumption that CO_2 fluxes are largely unchanged (on average) over the past billion years. Additionally, how rates of carbonization of oceanic crust differs as a function of ocean chemistry is not known. Our calculated O_2 demand from CO outgassing from Precambrian arcs is only 0.02×10^{12} mol O_2/yr (± 0.008, 1σ), or only 1.4% of the total Precambrian O_2 igneous demand. As such, even large uncertainties in the arc CO_2 outgassing flux are relatively unimportant for our purposes.

Our calculated O_2 sink size from arc-derived volcanic sulfur in the Precambrian is 0.54×10^{12} mol O_2/yr (± 0.25, 1σ) or 30% (± 11, 1σ) of the total Precambrian igneous O_2 sink. This is $0.30 \pm (\pm 0.21, 1\sigma)$ 10^{12} mol O_2/yr larger than the equivalent Phanerozoic sink. This increase is driven entirely by the change in the fO_2 of the source melts and not total sulfur degassing fluxes (which was held constant). If we

assume sulfur degasses completely from arc volcanic rocks, then sulfur degassing fluxes are set by the sulfur content of the parental melt, which is in turn set by the amount of sulfur in the mantle source, the partition coefficient for sulfur between the solid residue and the melt, and the degree of melting. For sulfur, this is complicated as sulfur speciates in melts as either (or both) sulfide or sulfate as a function of fO_2 (Jugo, 2009), and the two have different partition coefficients (Chowdhury and Dasgupta, 2019). Chowdhury and Dasgupta (2019) recently modeled that for various assumed sulfur contents of the mantle source and for typical arc melt fractions (>15%), parental arc melts will contain similar amounts of sulfur regardless of whether the sulfur was originally present as sulfate (that is, high source fO_2) or sulfide (low source fO_2). This is because these melt fractions are sufficient to exhaust most of the sulfur present in the source. Assuming this to be correct, the key control on total arc sulfur degassing fluxes is the average sulfur content of the subarc mantle.

Modern mantle sources of parental arc melts are thought to be enriched in sulfur relative to the ambient upper mantle (for example, Métrich and others, 1999; de Hoog and others, 2001) due to the transfer of sulfur from the slab to the subarc mantle either by oxidized sulfate-bearing fluids (see review in Wallace, 2005) or by reduced sulfide bearing fluids (Li and others, 2020). If sulfate in altered oceanic crust is an important source of sulfur to the subarc mantle, the lower sulfate concentrations in the Precambrian deep ocean vs. today may have lowered transfer of sulfur to the subarc mantle, thus lowering total sulfur contents of arc volcanic gases. However, Canfield (2004) proposed that anoxic deep-ocean waters, which stabilize pyrite, may have led to an increase in subduction fluxes of sedimentary sulfur in the Precambrian. This proposal was based on a sulfidic deep-ocean existing, as opposed to a ferruginous (that is, Fe^{2+} bearing) deep-ocean as is now commonly assumed for the Neoproterozoic (for example, Lyons and others, 2014). However, pyrite is also stabilized in such systems and so ferruginous conditions may also have led to increased sedimentary pyrite subduction. Regardless, there are sufficiently large uncertainties in the modern sulfur budget of subduction zones such that estimates in the past contain significant uncertainty. As such, we proceed with the working hypothesis that total sulfur arc outgassing fluxes were constant on average over the past billion years. This assumption requires verification, and if wrong, may have implications for the history of arc magmatism, the marine sulfur cycle, and atmospheric O_2 levels.

All told, we calculate a total O_2 consumption rate from volcanism in the Precambrian before the oxygenation of the deep ocean to be 1.03×10^{12} mol O_2/yr (± 0.26, 1σ), which is 0.63×10^{12} mol O_2/yr (± 0.22, 1σ) in excess of the Phanerozoic calculation. In all Monte Carlo simulations, the Precambrian volcanic sink is larger than the modern sink (figs. 13C, H, and M).

Differences between Igneous O_2 Sink Sizes in the Precambrian vs. Phanerozoic

Combining the various igneous sink estimates and excluding the H_2S emitted from high-temperature hydrothermal vents, we calculate a total Precambrian sink size of 1.78×10^{12} mol O_2/yr (± 0.43, 1σ). This is effectively the same as the modern sink size of 1.83×10^{12} (± 0.43) (fig. 14). Calculated distributions for each sink in the modern, Neoproterozoic, and the difference between the two (Neoproterozoic minus modern) are given in figure 13 and table 2.

We find that the loss of the low temperature hydrothermal sink in the Precambrian is compensated for by an increased arc volcanic sink due to the lower fO_2 of the subarc mantle. As such, at least over the past billion years, it is not obvious that, on average, the total igneous sink for O_2 has changed particularly in magnitude. This is distinct from previous studies. For example, Holland (2009) estimated that the O_2 demand from reduced volcanic gases declined by ~0.5 to 0.25×10^{12} mol O_2/yr over

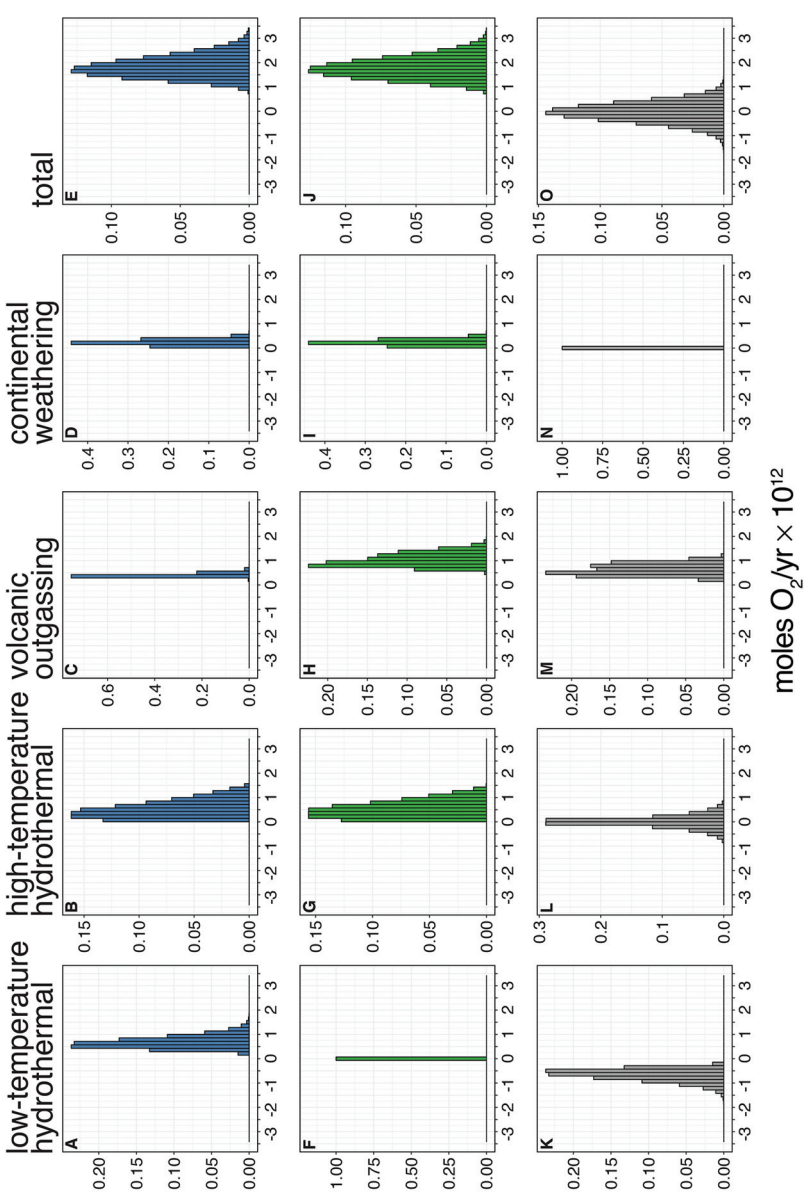

Fig. 13. Calculated distributions for igneous O_2 sinks in the modern (top row), Neoproterozoic (middle row), and difference between the two (bottom row; Neoproterozoic minus modern). Each column is arranged by type. Distributions can be directly subtracted as the same underlying random distributions are used in both.

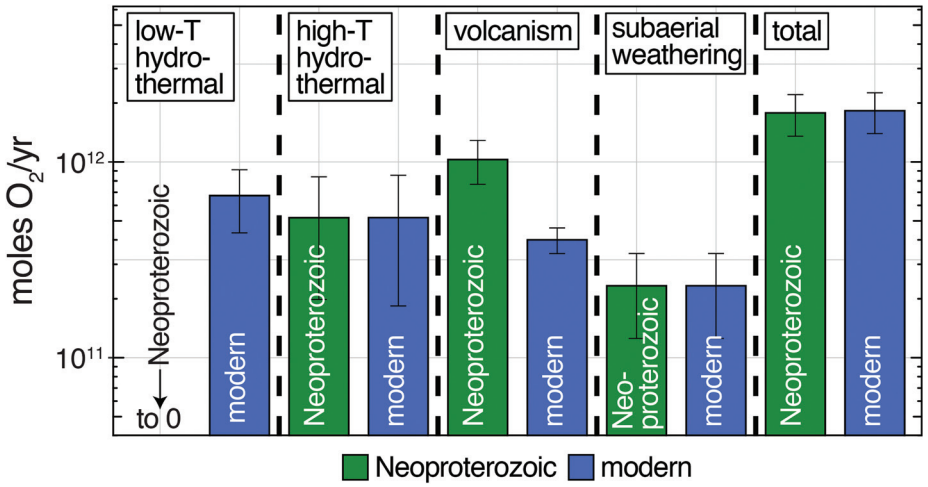

Fig. 14. Estimated size of O_2 sinks in the early Neoproterozoic vs. the modern. Error bars are $\pm 1\sigma$. The Neoproterozoic low-T hydrothermal sink is assumed to be 0 mol O_2/yr. The subaerial weathering of igneous rocks is assumed to be the same in the Neoproterozoic vs. modern. For the Neoproterozoic high-temperature (high-T) hydrothermal sink, we have not included the emitted H_2S in our calculation.

the past billion years. Similarly, Alcott and others (2019) assumed igneous sinks decreased over the past billion years by between 1 to 11 $\times$ 10^{12} mol O_2/yr. In contrast, other models assume deep-ocean oxygenation in the Phanerozoic caused an increase in igneous O_2 sinks by order 1 $\times$ 10^{12} mol O_2/yr (Laakso and Schrag, 2014; Daines and others, 2017; Miyazaki and others, 2018).

Potential Feedbacks During The Transition From An Anoxic To Oxygenated Deep Ocean

Here we explore how igneous sinks may have responded to changes in deep-ocean sulfate and O_2 levels during the transition from the Neoproterozoic to Paleozoic with an emphasis on positive and negative feedbacks associated with these changes. In doing this, we will focus solely on the potential response of the igneous system (both in terms of positive and negative feedbacks). However, it must be kept in mind that there are numerous biogeochemical cycles in the earth system that may respond to the changes in both sulfate and oxygen levels and that in turn generate feedbacks of their own (for example, Lenton and Watson, 2004; Laakso and Schrag, 2014; Mills and others, 2014; Lenton and others, 2016, 2018; Daines and others, 2017; Reinhard and others, 2017; Fakhraee and others, 2019; Alcott and others, 2019; Laakso and others, 2020).

We begin with increases in atmospheric O_2 and marine sulfate levels in the Neoproterozoic. It is commonly argued based on sulfur isotopes, presence/absence of gypsum/anhydrite-bearing evaporite sequences, the chemical composition of fluid inclusions preserved in evaporites, and the isotopic compositions of evaporites that seawater sulfate increased sometime between the Tonian (1000–720 Ma) and Ediacaran (635–541), from order 1 mmol/kg seawater to 6 to 10 mmol/kg seawater, though the precise details remain uncertain (Kah and others, 2004; Spear and others, 2014; Turner and Bekker, 2016; Fakhraee and others, 2019; Blättler and others, 2020; Laakso and others, 2020). What drove this sulfate increase remains unknown. One proposed explanation for this increase is that there was an increase in the sulfate input flux to the ocean due to oxidative weathering of sulfides exposed during the Neoproterozoic Pan-African orogeny or associated with post-

glacial weathering (Halverson and Hurtgen, 2007; Laakso and others, 2020). Another hypothesis assumes that increases in marine O_2 concentrations changed the location of sulfate reduction to sediments from the water column and also increased sulfide oxidation rates, thus increasing marine sulfate concentrations (Fakhraee and others, 2019).

Over the Neoproterozoic, atmospheric O_2 levels are also commonly argued to have increased (Shields-Zhou and Och, 2011; Lyons and others, 2014; Blamey and others, 2016; Tostevin and Mills, 2020), but they are generally not thought to have reached levels sufficient to oxygenate the deep ocean until the Paleozoic (Dahl and others, 2010; Sperling and others, 2015; Wallace and others, 2017; Stolper and Keller, 2018; Tostevin and Mills, 2020). What caused the increases in atmospheric O_2 remains uncertain. A non-exhaustive list of proposed explanations includes: perturbations to biogeochemical cycles due to major climatic perturbations, such as snowball earth episodes (Sahoo and others, 2012; Laakso and Schrag, 2014; Laakso and Schrag, 2017), evolution and expansion of eukaryotic algae (Lenton and others, 2014; Brocks and others, 2017) or sponges (Sperling and others, 2007; Love and others, 2009), changes in terrestrial weathering (Lenton and Watson, 2004; Mills and others, 2014), formation and weathering of large igneous provinces (Horton, 2015), formation and erosion or weathering of mountain ranges (Derry and others, 1992; Campbell and Allen, 2008), accumulation and increased degassing of near-surface carbon reservoirs on continental crust (Lee and others, 2016b), or a reorganization of biogeochemical cycles (Reinhard and others, 2017; Alcott and others, 2019; Laakso and others, 2020).

Here we do not attempt to identify which if any of these hypotheses is correct. Rather we assume that the observations driving these hypotheses are correct with the following relative timeline: First, marine sulfate levels began increasing from below to above 1 micromole/kg seawater followed later by the oxygenation of the deep ocean such that during the sulfate increase, the deep ocean remained either anoxic or weakly oxic.

What occurs as sulfate concentrations begin to increase in the ocean? If we assume that some of this sulfate reaches the deep ocean and enters high-temperature hydrothermal systems, the redox state of these fluids, based on the model of Kump and Seyfried (2005), will become more oxidizing (figs. 15A vs. 15B) lowering dissolved Fe^{2+} and H_2 concentrations of hydrothermal fluids to modern values. As the deep ocean is thought to have remained anoxic and ferruginous during this transition, H_2S would still be titrated out in the deep ocean. This change in high temperature hydrothermal results in a change in the igneous sink from 1.78×10^{12} (± 0.43, 1σ) to 1.34×10^{12} (± 0.28, 1σ) mol O_2/yr. Given correlated uncertainties, the net decrease in the igneous O_2 sink is 0.45×10^{12} (± 0.28, 1σ) mol O_2/yr. This change occurs rapidly on geologic timescales as the typical residence time of water in high-temperature hydrothermal systems is only a few years (for example, Kadko and Moore, 1988). This change (0.45×10^{12}) is 24% of the modern igneous O_2 sink, and, without a compensatory change in O_2 sources or sinks, would allow O_2 to rise to modern levels in 83 million years. We note that this analysis assumes that sulfate and Fe^{2+} can coexist in the deep ocean. This is not a detail and, as discussed below, matters for this transition.

Although it is often assumed that sulfate and Fe^{2+} cannot co-exist (as reviewed in Johnston and others, 2010), there is no thermodynamic reason this is not the case (hydrated ferrous sulfate salts are stable). The combined presence of sulfate and Fe^{2+} in Proterozoic deep oceans requires that in the open ocean there was insufficient organic carbon available to fully convert the sulfate to sulfide or that for other reasons

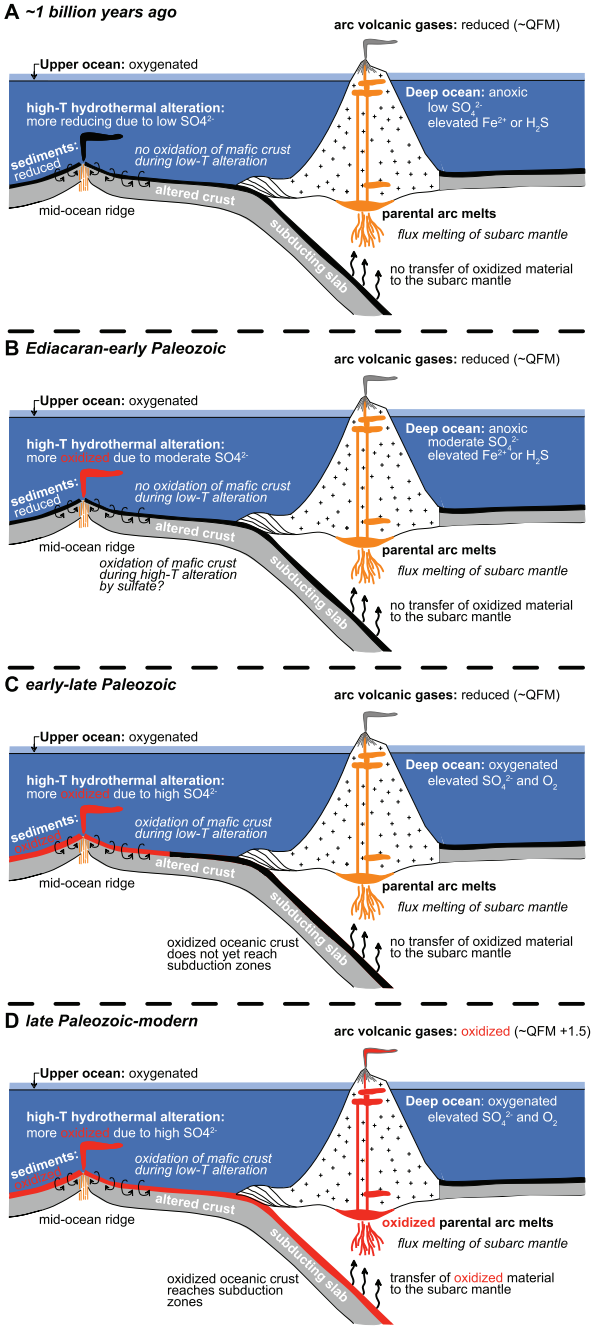

Fig. 15. Schematic of how changes in ocean O_2 and sulfate levels could impact igneous O_2 sinks. Modified from Stolper and Bucholz (2019).

sulfate reduction rates were lower—these possibilities are discussed in Johnston and others (2010). That this occurred has been argued to be the case in the Neoproterozoic deep ocean with both sulfate at up to 3 mmol/kg seawater and Fe^{2+}

coexisting due to spatial heterogeneities in organic carbon delivery and ultimately lower primary productivity rates limiting sulfate reduction rates (Planavsky and others, 2011). Additionally, Laakso and others (2020) recently modeled that Ediacaran sulfate levels increased due to changes in sulfide weathering associated with Neoproterozoic Pan-African orogenesis, but that sulfate reduction rates were still sufficiently low that the deep ocean remained ferruginous despite increased marine sulfate concentrations. As such, the scenario proposed above is consistent with prior work on the history of deep ocean sulfate and Fe^{2+} concentrations.

On this basis, adding sulfate to the deep ocean but keeping it anoxic (and ferruginous) results in a geologically rapid decrease in the igneous O_2 sink by about 0.5×10^{12} mol O_2/yr. One consequence of this change could be to allow O_2 levels to begin accumulating (or accumulate faster) in the atmosphere following the sulfate increase. As O_2 levels increase in the atmosphere, more O_2 will dissolve in surface waters that sink to form deep-ocean water masses, increasing the flux of O_2 to the deep ocean. However, in order to oxygenate the deep ocean, this flux of O_2 must exceed the amount of respiration that occurs in the ocean (Sarmiento and others, 1988; Canfield, 1998; Lyons and others, 2014). Deep-ocean oxygenation is thought to occur only once O_2 levels in the atmosphere are above 15 to 50% of modern (Canfield and others, 2007; Canfield, 2014).

An alternative explanation for the rise in sulfate is that the sulfate increase is due to increased oxygenation of the oceans (Turner and Bekker, 2016) which changed sulfate reduction and oxidative recycling rates such that sulfate accumulated in the ocean (Fakhraee and others, 2019). If the oxygenation only occurs on the shelves as opposed to in the deep waters feeding submarine hydrothermal systems and sulfate reduction in the open ocean is limited due to limited open-ocean primary production rates, then sulfate and iron could still co-exist and the scenario developed above would hold. However, based on box-model calculations, Fakhraee and others (2019) argued that for sulfate levels to rise to mmol/kg seawater concentrations requires sufficient increases in ocean oxygenation such that mid- and deep-ocean anoxia was limited. This would require O_2 in much of the deep ocean, even at low concentrations. This matters here as, in this condition, the sulfide emitted from hydrothermal systems would no longer be titrated out as pyrite with dissolved Fe^{2+}, but instead oxidized by O_2 in the deep ocean. Thus, if deep ocean oxygenation and marine sulfate increases occur simultaneously, the high-temperature hydrothermal sink would take on the values seen today such that igneous sinks would not measurably change going from 1.78×10^{12} (± 0.43, 1σ) prior to this to 1.78×10^{12} (± 0.44, 1σ).

Here, we favor and proceed with the assumption that deep-ocean oxygenation did not cause the increased sulfate concentrations given that current records indicate that sulfate levels increased to low millmol/kg seawater concentrations in the Ediacaran (Fakhraee and others, 2019; Blättler and others, 2020) while the deep-ocean did not transition to elevated oxygen concentrations until the Paleozoic (Tostevin and Mills, 2020). This requires either that sulfate increases were not directly caused by changes in marine oxygen concentrations (Laakso and others, 2020) or that any increases in oxygen concentrations did not occur in the deep ocean (for example, they were restricted to shelf environments).

Regardless, once the deep ocean becomes oxygenated, O_2 will begin entering low temperature hydrothermal systems and oxidize reduced igneous rocks (fig. 15C). This then introduces a negative feedback that scales with deep-ocean O_2 content and could act to slow down the accumulation of O_2 in the ocean and atmosphere. Additionally, the oxygenation of the deep-ocean will allow the sulfide emitted from high-temperature hydrothermal systems to begin reacting with oxygenated deep waters as opposed to being titrated out as iron sulfide minerals. The addition of this

H_2S sink from both mafic and ultramafic systems would immediately increase the igneous sink by up to 0.45×10^{12} mol O_2/yr (± 0.30, 1σ). As a result, once O_2 begins reaching deep-water masses and persisting in the deep ocean, two new igneous sinks will be turned on that will slow further accumulation of O_2. The timescales of these new O_2 sinks will be on the order of 1000 years for reactions with H_2S (the mixing time of marine water masses) and order 10-million-year timescales via oxygen-dependent rates of low-temperature oxidation of oceanic crust (Bach and Edwards, 2003).

The introduction of O_2 and sulfate into the deep ocean begins the oxidation of igneous oceanic crust by these species. The O_2 will also cause marine sediments to become increasingly oxidized (figs. 15B and C—note here we are displaying pelagic sedimentation, but similar changes will occur for terrigenous sediments deposited under higher oxygen concentrations). Together, these will increase the flux of oxidants to the subarc mantle. Depending on what the oxidant is for the subarc mantle (for example, sulfate and/or other oxidized elements such as iron), determines whether this oxidation begins with increases in marine sulfate concentrations (fig. 15B) or deep-ocean O_2 accumulation (fig. 15C). Additionally, both could increase the oxidant flux to the subarc mantle at different times. In figure 15, for schematic purposes, we assume subarc oxidation begins following deep-ocean oxygenation.

Regardless of the identity of the oxidant, subduction of this oxidized material will (in our interpretation) cause the subarc mantle to become more oxidized. This in turn will elevate the fO_2 of parental arc melts, increasing the fO_2 of volcanic gases and ultimately lowering their consumption of atmospheric O_2 (fig. 15D). That such a change occurred is supported by two observations discussed previously: (*i*) From the Neoproterozoic to Early Phanerozoic, $Fe^{3+}/\Sigma Fe$ ratios of submarine basalts increase indicating that the oxygenation of the deep ocean resulted in an increased oxidation of oceanic crust (Stolper and Keller, 2018). (*ii*) Over the same time interval, $Fe^{3+}/\Sigma Fe$ and V/Sc ratios of island arc rocks increase (Stolper and Bucholz, 2019). As both $Fe^{3+}/\Sigma Fe$ and V/Sc are proxies for the fO_2 of the parental arc source magmas, these increases were interpreted to indicate that the subarc mantle became more oxidized at this time (Stolper and Bucholz, 2019). The modeled change in the fO_2 of the subarc mantle causes a decrease in igneous O_2 sinks (from volcanism) for the Precambrian vs. the modern of 0.63×10^{12} mol O_2/yr (± 0.22, 1σ), which is sufficient to allow for the accumulation of all the O_2 currently in the atmosphere in 59 million years assuming all other fluxes remain constant. Furthermore, the proposed oxidation of the subarc mantle and associated increase in fO_2 of volcanic gases is a positive feedback. This is because this change in fO_2, in the framework proposed here, causes emitted arc gases to consume less O_2 allowing more O_2 to accumulate. This in turn will increase the extent of oxidation of sediments and altered crust, further increasing the fO_2 of the subarc mantle, and so on.

The change in the fO_2 of the subarc mantle is expected to be delayed by of order one hundred million years relative to changes in marine sulfate and O_2 concentrations (figs. 15B and C vs. D). This is because oxidation of the subarc mantle first requires the oxidation of oceanic crust and sediments, then transport via subduction and transfer to the subarc mantle, and for enough transport and transfer to occur to oxidize the subarc mantle. The timescale to oxidize oceanic crust has been estimated to be ~20 million years (Bach and Edwards, 2003) and only occurs in crust typically younger than ~20 million years old that is open to circulation (sedimentation closes off this flow) (Hart and Staudigel, 1978; Coogan and others, 2016). This crust then must reach a subduction zone, which takes ~50 million years (for example, mean ages of oceanic crust are 40 to 70 myr; Müller and others, 2016). Finally, enough oxidized material must be subducted to oxidize the subarc mantle, which has been modeled to take one to one hundred million years (Evans and Tomkins, 2011). Based on

this, we consider that it takes of order one hundred million years for the signal of altered and oxidized oceanic crust to be expressed in the fO_2 of arc volcanic gases.

These long timescales are potentially significant for the history of atmospheric O_2 because, as discussed above, it has been proposed that although marine sulfate and atmospheric O_2 concentrations increased towards the end of the Neoproterozoic, it was not until ~400 Ma that $P_{O_2}^{atm}$ reached sufficient levels (15–50% of modern; Canfield and others, 2007; Canfield, 2014) to oxygenate the deep ocean. Furthermore, some recent studies have proposed that deep- and surface-ocean O_2 levels continued to increase from the Paleozoic to the Mesozoic (Stolper and Keller, 2018; Lu and others, 2018). The cascade of feedbacks discussed above, and their different timescales may offer mechanisms to help explain both the magnitude and timing of these changes. For example, an increase in atmospheric O_2 levels and sulfate levels in the Neoproterozoic may have been sufficient to cause oxidizing conditions in high-temperature systems and thus lower the O_2 consumptive flux of these systems. This could have resulted in an increased accumulation of O_2 in the atmosphere over of order ~50 million years leading to the eventual oxygenation of the ocean tens of millions of years following this initial rise (figs. 15A–C). Following this oxygenation, further increases in O_2 levels would have been limited by three solid-earth negative feedbacks. First, low-temperature hydrothermal circulation would begin consuming O_2 in the deep ocean (fig. 15C). Second, H_2S from high-temperature hydrothermal systems would begin reacting with dissolved O_2 in the deep ocean. Third, increased O_2 in the deep ocean would lower the burial and eventual subduction of organic carbon and pyrite in sediments. All three of these feedbacks would increase the imbalance between the igneous O_2 sink and solid-earth source, putting the geologic brakes on the build-up of O_2 in the ocean and atmosphere.

On a time scale of order 100 million years, changes in the oxygen fugacity of arc gases due to the slow oxidation of the subarc mantle would lower the O_2 burden from volcanism and allow O_2 to further accumulate long after the initial rise of atmospheric O_2 and marine sulfate (figs. 15C vs. D). This delay could help explain one of two observations about the history of atmospheric and marine O_2 levels. First, if sulfate is the oxidant of the subarc mantle, then the subarc mantle will begin becoming oxidized in the Ediacaran when marine sulfate levels increased. The initial rise in O_2 in the early Phanerozoic (<541–~400 Ma) could have been amplified by the changes in high-temperature hydrothermal circulation. Then, towards the end of the early Paleozoic (~400 Ma), changes in volcanic outgassing (which take order 100 million years to occur) may have been expressed helping amplify increases in O_2 and the eventual oxygenation of the ocean. Second and alternatively, if oxidation of the oceanic crust and sediments does not begin in earnest until the oxygenation of the deep ocean in the Paleozoic, then the proposed increases in marine O_2 (and inferred relationship to atmospheric O_2) from the late Paleozoic to Mesozoic may be in part due to the order ~100-million-year delay between oxygenation and changes in arc fO_2. We summarize these thoughts with figure 15.

The point of all of this is not to argue that changes in igneous processes are the only causes of changes in atmospheric and marine and O_2 levels over the Neoproterozoic through early Phanerozoic. As discussed above, there are a diverse range of other ideas on why sulfate and O_2 concentrations have changed with time including changes in tectonic regimes, snowball earth episodes, evolution, diversification, or expansion of different forms of life, and changes in biogeochemical cycles. Rather, our simple point is this: based on our analysis, igneous O_2 sinks are not expected to be constant given changes in marine O_2 and sulfate concentrations from the Neoproterozoic to Paleozoic and can both act as positive and negative feedbacks to changes in marine O_2 on geologically relevant timescales. Thus, they likely have a

role to play in the relative timing and delay in atmospheric vs. ocean oxygenation in the Neoproterozoic vs. Paleozoic and perhaps even the purported increase in O_2 over the Paleozoic through to the Mesozoic. If correct, it would indicate that changes in the surface biogeochemistry influenced and were in turn influenced by changes in igneous processes during the rise of O_2 to near modern levels. A useful avenue for future work could be to create a coupled model of the mantle and fluid earth in which elements are exchanged between the two, redox states can evolve, and biogeochemical cycles respond to such changes. Such is beyond the scope of this work but represents a next step to explore the qualitative proposals above quantitatively.

SUMMARY AND CONCLUSIONS

We summarize the key points of our work here:

(1) Typical estimates for the magnitude of the modern O_2 igneous sink vs. the observed imbalance of O_2 sources and sinks based on ice-core records require that most of the igneous sink be balanced by other sources.

(2) Incorporation of mantle sources of CO_2 and igneous sinks for O_2 without subduction in models of atmospheric $P_{O_2}^{atm}$ would predict that both the carbonate and organic carbon sedimentary reservoirs and pyrite reservoirs grew significantly through geologic time. Incorporation of a subduction flux can remove this requirement.

(3) We estimated that today igneous processes remove 1.83×10^{12} mol O_2/yr (± 0.43, 1σ), while subduction returns 1.56×10^{12} mol O_2/yr (± 0.33, 1σ). Thus, at the $\pm 1\sigma$ level, solid-earth O_2 sources and sinks are in balance. We propose that this balance could be achieved through negative feedbacks associated with either or both (*i*) the O_2 dependence of oxidation of oceanic crust during low-temperature hydrothermal alteration; Or (*ii*) the regulation of sedimentary organic carbon and pyrite burial fluxes by $P_{O_2}^{atm}$, which in turn influence sedimentary subduction fluxes of organic carbon and pyrite.

(4) We examined how the igneous O_2 sink size may have differed in the Neoproterozoic vs. today given an anoxic deep ocean and low marine sulfate levels. We calculated that the Neoproterozoic igneous sink was 1.78×10^{12} (± 0.43, 1σ). We proposed that these various sinks respond differently to the oxygenation of the deep ocean and changes in marine sulfate levels. Specifically, introduction of sulfate into the deep ocean is proposed to cause a rapid decrease in the igneous sink size. Once the ocean is oxygenated, the low-temperature alteration of oceanic crust becomes a negative feedback that increases as O_2 concentrations increase. Additionally, H_2S from high-temperature hydrothermal systems begins to be oxidized by marine O_2, increasing the size of the igneous O_2 sink. Finally, oxidation of oceanic crust either by O_2 or sulfate can act as a positive feedback by oxidizing the subarc mantle and increasing the fO_2 of arc volcanic gases. This is proposed to have a delay of order 100 million years between the onset of oxidation and change in the fO_2 of arc gases. Together, these changes may act to both accelerate and delay initial changes in atmospheric and marine O_2 concentrations with implications for the pace and timing of changes in atmospheric and marine O_2 concentrations from the Neoproterozoic through Paleozoic.

ACKNOWLEDGMENTS

We thank T. Plank and E. Stolper for helpful conversations and S. Crowe, J. Krissansen-Totton, L. Kump, and W. Seyfried Jr. for clarifications. N. Pester is thanked

for help using the SUPCRT database. We additionally thank two anonymous reviewers for constructive reviews as well as comments from the Associate Editor, N. Planavsky. DAS acknowledges support from an Esper Larsen Jr. Research Grant from UC Berkeley. JAH acknowledges support from Princeton University.

REFERENCES

Alcott, L. J., Mills, B. J. W., and Poulton, S. W., 2019, Stepwise Earth oxygenation is an inherent property of global biogeochemical cycling: Science, v. 366, n. 6471, p. 1333–1337, https://doi.org/10.1126/science.aax6459

Alt, J. C., 1995, Sulfur isotopic profile through the oceanic crust: Sulfur mobility and seawater-crustal sulfur exchange during hydrothermal alteration: Geology, v. 23, n. 7, p. 585, https://doi.org/10.1130/0091-7613(1995)023<0585:SIPTTO>2.3.CO;2

Alt, J. C., Schwarzenbach, E. M., Früh-Green, G. L., Shanks, W. C. III, Bernasconi, S. M., Garrido, C. J., Crispini, L., Gaggero, L., Padrón-Navarta, J. A., and Marchesi, C., 2013, The role of serpentinites in cycling of carbon and sulfur: Seafloor serpentinization and subduction metamorphism: Lithos, v. 178, p. 40–54, https://doi.org/10.1016/j.lithos.2012.12.006

Arculus, R. J., 1985, Oxidation status of the mantle: past and present: Annual Review of Earth and Planetary Sciences, v. 13, p. 75–95, https://doi.org/10.1146/annurev.ea.13.050185.000451

Arvidson, R. S., 2006, MAGic: A Phanerozoic Model for the Geochemical Cycling of Major Rock-Forming Components: American Journal of Science, v. 306, n. 3, p. 135–190, https://doi.org/10.2475/ajs.306.3.135

Aulbach, S., and Stagno, V., 2016, Evidence for a reducing Archean ambient mantle and its effects on the carbon cycle: Geology, v. 44, n. 9, p. 751–754, https://doi.org/10.1130/G38070.1

Bach, W., and Edwards, K. J., 2003, Iron and sulfide oxidation within the basaltic ocean crust: implications for chemolithoautotrophic microbial biomass production: Geochimica et Cosmochimica Acta, v. 67, n. 20, p. 3871–3887, https://doi.org/10.1016/S0016-7037(03)00304-1

Ballhaus, C., Berry, R. F., and Green, D. H., 1990, Oxygen fugacity controls in the Earth's upper mantle: Nature, v. 348, p. 437–440, https://doi.org/10.1038/348437a0

Bebout, G. E., 1995, The impact of subduction-zone metamorphism on mantle-ocean chemical cycling: Chemical Geology, v. 126, n. 2, p. 191–218, https://doi.org/10.1016/0009-2541(95)00118-5

Bénard, A., Klimm, K., Woodland, A. B., Arculus, R. J., Wilke, M., Botcharnikov, R. E., Shimizu, N., Nebel, O., Rivard, C., and Ionov, D. A., 2018, Oxidising agents in sub-arc mantle melts link slab devolatilisation and arc magmas: Nature Communications, v. 9, p. 3500, https://doi.org/10.1038/s41467-018-05804-2

Bender, M., Sowers, T., and Labeyrie, L., 1994, The Dole Effect and its variations during the last 130,000 years as measured in the Vostok Ice Core: Global Biogeochemical Cycles, v. 8, n. 3, p. 363–376, https://doi.org/10.1029/94GB00724

Bergman, N. M., Lenton, T. M., and Watson, A. J., 2004, COPSE: A new model of biogeochemical cycling over Phanerozoic time: American Journal of Science, v. 304, n. 5, p. 397–437, https://doi.org/10.2475/ajs.304.5.397

Berner, R. A., 1982, Burial of organic carbon and pyrite sulfur in the modern ocean; its geochemical and environmental significance: American Journal of Science, v. 282, n. 4, p. 451–473, https://doi.org/10.2475/ajs.282.4.451

Berner, R. A., 1987, Models for carbon and sulfur cycles and atmospheric oxygen; application to Paleozoic geologic history: American Journal of Science, v. 287, n. 3, p. 177–196, https://doi.org/10.2475/ajs.287.3.177

Berner, R. A., 1991, A model for atmospheric CO_2 over Phanerozoic time: American Journal of Science, v. 291, n. 4, p. 339–376, https://doi.org/10.2475/ajs.291.4.339

Berner, R. A., 2001, Modeling atmospheric O_2 over Phanerozoic time: Geochimica et Cosmochimica Acta, v. 65, n. 5, p. 685–694, https://doi.org/10.1016/S0016-7037(00)00572-X

Berner, R. A., 2006, GEOCARBSULF: A combined model for Phanerozoic atmospheric O_2 and CO_2: Geochimica et Cosmochimica Acta, v. 70, n. 23, p. 5653–5664, https://doi.org/10.1016/j.gca.2005.11.032

Berner, R. A., 2009, Phanerozoic atmospheric oxygen: New results using the GEOCARBSULF model: American Journal of Science, v. 309, n. 7, p. 603–606, https://doi.org/10.2475/07.2009.03

Berner, R. A., and Caldeira, K., 1997, The need for mass balance and feedback in the geochemical carbon cycle: Geology, v. 25, n. 10, p. 955, https://doi.org/10.1130/0091-7613(1997)025<0955:TNFMBA>2.3.CO;2

Berner, R. A., and Canfield, D. E., 1989, A new model for atmospheric oxygen over Phanerozoic time: American Journal of Science, v. 289, n. 4, p. 333–361, https://doi.org/10.2475/ajs.289.4.333

Berner, R. A., and Raiswell, R., 1983, Burial of organic carbon and pyrite sulfur in sediments over phanerozoic time: a new theory: Geochimica et Cosmochimica Acta, v. 47, n. 5, p. 855–862, https://doi.org/10.1016/0016-7037(83)90151-5

Bird, P., 2003, An updated digital model of plate boundaries: Geochemistry, Geophysics, Geosystems, v. 4, n. 3, 1027, https://doi.org/10.1029/2001GC000252

Blamey, N. J. F., Brand, U., Parnell, J., Spear, N., Lécuyer, C., Benison, K., Meng, F., and Ni, P., 2016, Paradigm shift in determining Neoproterozoic atmospheric oxygen: Geology, v. 44, n. 8, p. 651–654, https://doi.org/10.1130/G37937.1

Blättler, C. L., Bergmann, K. D., Kah, L. C., Gómez-Pérez, I., and Higgins, J. A., 2020, Constraints on Meso- to Neoproterozoic seawater from ancient evaporite deposits: Earth and Planetary Science Letters, v. 532, 115951, https://doi.org/10.1016/j.epsl.2019.115951

Bouchez, J., Beyssac, O., Galy, V., Gaillardet, J., France-Lanord, C., Maurice, L., and Moreira-Turcq, P., 2010, Oxidation of petrogenic organic carbon in the Amazon floodplain as a source of atmospheric CO2: Geology, v. 38, n. 3, p. 255–258, https://doi.org/10.1130/G30608.1

Brocks, J. J., Jarrett, A. J. M., Sirantoine, E., Hallmann, C., Hoshino, Y., and Liyanage, T., 2017, The rise of algae in Cryogenian oceans and the emergence of animals: Nature, v. 548, p. 578–581, https://doi.org/10.1038/nature23457

Brounce, M., Kelley, K., and Cottrell, E., 2014, Variations in Fe3+/ΣFe of Mariana arc basalts and mantle wedge fO_2: Journal of Petrology, v. 55, n. 12, p. 2513–2536, https://doi.org/10.1093/petrology/egu065

Brounce, M., Stolper, E., and Eiler, J., 2017, Redox variations in Mauna Kea lavas, the oxygen fugacity of the Hawaiian plume, and the role of volcanic gases in Earth's oxygenation: Proceedings of the National Academy of Sciences of the United States of America, v. 114, n. 34, p. 8997–9002, https://doi.org/10.1073/pnas.1619527114

Brune, S., Williams, S. E., and Müller, R. D., 2017, Potential links between continental rifting, CO 2 degassing and climate change through time: Nature Geoscience, v. 10, p. 941–946, https://doi.org/10.1038/s41561-017-0003-6

Burgisser, A., and Scaillet, B., 2007, Redox evolution of a degassing magma rising to the surface: Nature, v. 445, p. 194-197, https://doi.org/10.1038/nature05509

Burgisser, A., Oppenheimer, C., Alletti, M., Kyle, P. R., Scaillet, B., and Carroll, M. R., 2012, Backward tracking of gas chemistry measurements at Erebus volcano: Geochemistry, Geophysics, Geosystems, v. 13, n. 11, p. Q11010, https://doi.org/10.1029/2012GC004243

Burgisser, A., Alletti, M., and Scaillet, B., 2015, Simulating the behavior of volatiles belonging to the C-O-H-S system in silicate melts under magmatic conditions with the software D-Compress: Computers & Geosciences, v. 79, p. 1–14, https://doi.org/10.1016/j.cageo.2015.03.002

Burke, A., Present, T. M., Paris, G., Rae, E. C. M., Sandilands, B. H., Gaillardet, J., Peucker-Ehrenbrink, B., Fischer, W. W., McClelland, J. W., Spencer, R. G., Voss, B. M., and Adkins, J. F., 2018, Sulfur isotopes in rivers: Insights into global weathering budgets, pyrite oxidation, and the modern sulfur cycle: Earth and Planetary Science Letters, v. 496, p. 168–177, https://doi.org/10.1016/j.epsl.2018.05.022

Campbell, I. H., and Allen, C. M., 2008, Formation of supercontinents linked to increases in atmospheric oxygen: Nature Geoscience, v. 1, p. 554–558, https://doi.org/10.1038/ngeo259

Canfield, D. E., 1989, Sulfate reduction and oxic respiration in marine sediments: implications for organic carbon preservation in euxinic environments: Deep Sea Research Part A. Oceanographic Research Papers, v. 36, n. 1, p. 121–138, https://doi.org/10.1016/0198-0149(89)90022-8

Canfield, D. E., 1993, Organic matter oxidation in marine sediments, *in* Wollast, R., Mackenzie, F. T., and Chou, L. editors, Interactions of C, N, P and S biogeochemical Cycles and Global Change, NATO ASI Series (Series I: Global Environmental Change): Berlin/Heidelberg, Germany, Springer, v. 4, p. 333–363, https://doi.org/10.1007/978-3-642-76064-8_14

Canfield, D. E., 1994, Factors influencing organic carbon preservation in marine sediments: Chemical Geology, v. 114, n. 3–4, p. 315–329, https://doi.org/10.1016/0009-2541(94)90061-2

Canfield, D. E., 1998, A new model for Proterozoic ocean chemistry: Nature, v. 396, p. 450–453, https://doi.org/10.1038/24839

Canfield, D. E., 2004, The evolution of the Earth surface sulfur reservoir: American Journal of Science, v. 304, n. 10, p. 839–861, https://doi.org/10.2475/ajs.304.10.839

Canfield, D. E., 2005, The early history of atmospheric oxygen: homage to Robert M. Garrels: Annual Review of Earth and Planetary Sciences., v. 33, p. 1–36, https://doi.org/10.1146/annurev.earth.33.092203.122711

Canfield, D. E., 2014, Proterozoic atmospheric oxygen, *in* Holland, H. D., and Turekian, K. K., editors, Treatise on Geochemistry (second edition): Amsterdam, the Netherlands, Elsevier, p. 197–216, https://doi.org/10.1016/B978-0-08-095975-7.01308-5

Canfield, D. E., Poulton, S. W., and Narbonne, G. M., 2007, Late-Neoproterozoic deep-ocean oxygenation and the rise of animal life: Science, v. 315, n. 5808, p. 92–95, https://doi.org/10.1126/science.1135013

Canfield, D. E., van Zuilen, M. A., Nabhan, S., Bjerrum, C. J., Zhang, S., Wang, H., and Wang, X., 2021, Petrographic carbon in ancient sediments constrains Proterozoic Era atmospheric oxygen levels: Proceedings of the National Academy of Sciences of the United States of America, v. 118, n. 23, e2101544118, https://doi.org/10.1073/pnas.2101544118

Carmichael, I. S., 1991, The redox states of basic and silicic magmas: a reflection of their source regions? Contributions to Mineralogy and Petrology, v. 106, p. 129–141, https://doi.org/10.1007/BF00306429

Catling, D. C., and Claire, M. W., 2005, How Earth's atmosphere evolved to an oxic state: a status report: Earth and Planetary Science Letters, v. 237, n. 1–2, p. 1–20, https://doi.org/10.1016/j.epsl.2005.06.013

Catling, D. C., and Kasting, J. F., 2017, Atmospheric Evolution on Inhabited and Lifeless Worlds: Cambridge, United Kingdom, Cambridge University Press, 592 p, https://doi.org/10.1017/9781139020558

Catling, D. C., Zahnle, K. J., and McKay, C. P., 2001, Biogenic methane, hydrogen escape, and the irreversible oxidation of early Earth: Science, v. 293, n. 5531, p. 839–843, https://doi.org/10.1126/science.1061976

Caves, J. K., Jost, A. B., Lau, K. V., and Maher, K., 2016, Cenozoic carbon cycle imbalances and a variable weathering feedback: Earth and Planetary Science Letters, v. 450, p. 152–163, https://doi.org/10.1016/j.epsl.2016.06.035

Charlou, J. L., Donval, J. P., Konn, C., Ondréas, H., Fouquet, Y., Jean-Baptiste, P., and Fourré, E., 2010, High production and fluxes of H2 and CH4 and evidence of abiotic hydrocarbon synthesis by serpentinization in ultramafic-hosted hydrothermal systems on the Mid-Atlantic Ridge, *in* Rona, P. A., Devey, C. W., Dyment, J., and Murton, B. J., editors, Diversity of hydrothermal systems on slow spreading

ocean ridges: Geophysical Monograph Series, v. 188, p. 265–296, https://doi.org/10.1029/2008GM000752
Chester, R., and Jickells, T., 2012, Marine Geochemistry: Hoboken, New Jersey, John Wiley & Sons, 424 p, https://doi.org/10.1002/9781118349083
Chowdhury, P., and Dasgupta, R., 2019, Effect of sulfate on the basaltic liquidus and sulfur Concentration at Anhydrite Saturation (SCAS) of hydrous basalts-Implications for sulfur cycle in subduction zones: Chemical Geology, v. 522, p. 162–174, https://doi.org/10.1016/j.chemgeo.2019.05.020
Clift, P. D., 2017, A revised budget for Cenozoic sedimentary carbon subduction: Reviews of Geophysics, v. 55, n. 1, p. 97–125, https://doi.org/10.1002/2016RG000531
Coggon, R. M., Teagle, D. A., Harris, M., Davidson, G. J., Alt, J. C., and Brewer, T. S., 2016, Hydrothermal contributions to global biogeochemical cycles: Insights from the Macquarie Island ophiolite: Lithos, v. 264, p. 329–347, https://doi.org/10.1016/j.lithos.2016.08.024
Cogné, J.-P., and Humler, E., 2006, Trends and rhythms in global seafloor generation rate: Geochemistry, Geophysics, Geosystems, v. 7, n. 3, Q03011, https://doi.org/10.1029/2005GC001148
Coogan, L. A., Parrish, R. R., and Roberts, N. M. W., 2016, Early hydrothermal carbon uptake by the upper oceanic crust: Insight from in situ U-Pb dating: Geology, v. 44, n. 2, p. 147–150, https://doi.org/10.1130/G37212.1
Cook-Kollars, J., Bebout, G. E., Collins, N. C., Angiboust, S., and Agard, P., 2014, Subduction zone metamorphic pathway for deep carbon cycling: I. Evidence from HP/UHP metasedimentary rocks, Italian Alps: Chemical Geology, v. 386, p. 31–48, https://doi.org/10.1016/j.chemgeo.2014.07.013
Cox, A. N., 2002, Allen's Astrophysical Quantities: New York, Springer, 721 p, https://doi.org/10.1007/978-1-4612-1186-0
Crisp, J. A., 1984, Rates of magma emplacement and volcanic output: Journal of Volcanology and Geothermal Research, v. 20, n. 3–4, p. 177–211, https://doi.org/10.1016/0377-0273(84)90039-8
Dahl, T. W., Hammarlund, E. U., Anbar, A. D., Bond, D. P. G., Gill, B. C., Gordon, G. W., Knoll, A. H., Nielsen, A. T., Schovsbo, N. H., and Canfield, D. E., 2010, Devonian rise in atmospheric oxygen correlated to the radiations of terrestrial plants and large predatory fish: Proceedings of the National Academy of Sciences of the United States of America, v. 107, n. 42, p. 17911–17915, https://doi.org/10.1073/pnas.1011287107
Daines, S. J., Mills, B. J. W., and Lenton, T. M., 2017, Atmospheric oxygen regulation at low Proterozoic levels by incomplete oxidative weathering of sedimentary organic carbon: Nature Communications, v. 8, 14379, https://doi.org/10.1038/ncomms14379
Dauphas, N., Craddock, P. R., Asimow, P. D., Bennett, V. C., Nutman, A. P., and Ohnenstetter, D., 2009, Iron isotopes may reveal the redox conditions of mantle melting from Archean to Present: Earth and Planetary Science Letters, v. 288, n. 1–2, p. 255–267, https://doi.org/10.1016/j.epsl.2009.09.029
de Hoog, J. C. M., Mason, P. R. D., and van Bergen, M. J, 2001, Sulfur and chalcophile elements in subduction zones: constraints from a laser ablation ICP-MS study of melt inclusions from Galunggung Volcano, Indonesia: Geochimica et Cosmochimica Acta, v. 65, n. 18, p. 3147–3164, https://doi.org/10.1016/S0016-7037(01)00634-2
de Ronde, C. E. J., Massoth, G. J., Baker, E. T., Lupton, J. E., Simmons, S. F., and Graham, I., 2003, Submarine Hydrothermal Venting Related to Volcanic Arcs, *in* Simmons, S. F, and Graham, I. editors, Volcanic, Geothermal, and Ore-Forming Fluids: Rulers and Witnesses of Processes within the Earth: Society of Economic Geologists Special Publication, v. 10, p. 91–110.
Derry, L. A., 2015, Causes and consequences of mid-Proterozoic anoxia: Geophysical Research Letters, v. 42, n. 20, 8538–8546, https://doi.org/10.1002/2015GL065333
Derry, L. A., and France-Lanord, C., 1996, Neogene growth of the sedimentary organic carbon reservoir: Paleoceanography, v. 11, n. 3, p. 267–275, https://doi.org/10.1029/95PA03839
Derry, L. A., Kaufman, A. J., and Jacobsen, S. B., 1992, Sedimentary cycling and environmental change in the Late Proterozoic: evidence from stable and radiogenic isotopes: Geochimica et Cosmochimica Acta, v. 56, n. 3, p. 1317–1329, https://doi.org/10.1016/0016-7037(92)90064-P
Des Marais, D. J., 2001, Isotopic evolution of the biogeochemical carbon cycle during the Precambrian: Reviews in Mineralogy and Geochemistry, v. 43, n. 1, p. 555–578, https://doi.org/10.2138/gsrmg.43.1.555
Dixon, J. E., and Stolper, E. M., 1995, An experimental study of water and carbon dioxide solubilities in mid-ocean ridge basaltic liquids. Part II: applications to degassing: Journal of Petrology, v. 36, n. 6. 1633–1646, https://doi.org/10.1093/oxfordjournals.petrology.a037268
Driesner, T., 2007, The system H2O-NaCl. Part II: Correlations for molar volume, enthalpy, and isobaric heat capacity from 0 to 1000 C, 1 to 5000 bar, and 0 to 1 XNaCl: Geochimica et Cosmochimica Acta, v. 71, n. 20, p. 4902–4919, https://doi.org/10.1016/j.gca.2007.05.026
Driesner, T., and Heinrich, C. A., 2007, The system H_2O-NaCl. Part I: Correlation formulae for phase relations in temperature-pressure-composition space from 0 to 1000°C, 0 to 5000 bar, and 0 to 1 X_{NaCl}: Geochimica et Cosmochimica Acta, v. 71, n. 20, p. 4880–4901, https://doi.org/10.1016/j.gca.2006.01.033
Ehhalt, D. H., and Rohrer, F., 2009, The tropospheric cycle of H_2: a critical review: Tellus B: Chemical and Physical Meteorology, v. 61, n. 3, p. 500–535, https://doi.org/10.1111/j.1600-0889.2009.00416.x
Elderfield, H., and Schultz, A., 1996, Mid-ocean ridge hydrothermal fluxes and the chemical composition of the ocean: Annual Review of Earth and Planetary Sciences, v. 24, p. 191–224, https://doi.org/10.1146/annurev.earth.24.1.191
Emerson, S., and Hedges, J. I., 1988, Processes controlling the organic carbon content of open ocean sediments: Paleoceanography, v. 3, n. 5, p. 621–634, https://doi.org/10.1029/PA003i005p00621

Emerson, S., Stump, C., Grootes, P. M., Stuiver, M., Farwell, G. W., and Schmidt, F. H., 1987, Estimates of degradable organic carbon in deep-sea surface sediments from ^{14}C concentrations: Nature, v. 329, p. 51–53, https://doi.org/10.1038/329051a0

Etiope, G., 2015, Natural Gas Seepage: The Earth's Hydrocarbon Degassing: Switzerland, Springer International Publishing, 199 p, https://doi.org/10.1007/978-3-319-14601-0

Etiope, G., and Sherwood Lollar, B., 2013, Abiotic methane on Earth: Reviews of Geophysics, v. 51, n. 2, p. 276–299, https://doi.org/10.1002/rog.20011

Evans, K. A., 2012, The redox budget of subduction zones: Earth-Science Reviews, v. 113, n. 1–2, p. 11–32, https://doi.org/10.1016/j.earscirev.2012.03.003

Evans, K. A., Elburg, M. A., and Kamenetsky, V. S., 2012, Oxidation state of subarc mantle: Geology, v. 40, n. 9, p. 783–786, https://doi.org/10.1130/G33037.1

Evans, K.-A., and Tomkins, A.-G., 2011, The relationship between subduction zone redox budget and arc magma fertility: Earth and Planetary Science Letters, v. 308, n. 3–4, p. 401–409, https://doi.org/10.1016/j.epsl.2011.06.009

Fakhraee, M., Hancisse, O., Canfield, D. E., Crowe, S. A., and Katsev, S., 2019, Proterozoic seawater sulfate scarcity and the evolution of ocean-atmosphere chemistry: Nature Geoscience, v. 12, p. 375–380, https://doi.org/10.1038/s41561-019-0351-5

Falkowski, P. G., Katz, M. E., Milligan, A. J., Fennel, K., Cramer, B. S., Aubry, M. P., Berner, R. A., Novacek, M. J., and Zapol, W. M., 2005, The rise of oxygen over the past 205 million years and the evolution of large placental mammals: Science, v. 309, n. 5744, p. 2202–2204, https://doi.org/10.1126/science.1116047

Farquhar, J., Bao, H., and Thiemens, M., 2000, Atmospheric influence of Earth's earliest sulfur cycle: Science, v. 289, n. 5480, p. 756–758, https://doi.org/10.1126/science.289.5480.756

Fiebig, J., Stefánsson, A., Ricci, A., Tassi, F., Viveiros, F., Silva, C., Lopez, T. M., Schreiber, C., Hofmann, S., and Mountain, B. W., 2019, Abiogenesis not required to explain the origin of volcanic-hydrothermal hydrocarbons: Geochemical Perspective Letters, v. 11, p. 23–27, https://doi.org/10.7185/geochemlet.1920

Fischer, T. P., Arellano, S., Carn, S., Aiuppa, A., Galle, B., Allard, P., Lopez, T., Shinohara, H., Kelly, P., Werner, C., Cardellini, A., and Chiodini, G., 2019, The emissions of CO_2 and other volatiles from the world's subaerial volcanoes: Scientific Reports, v. 9, 18716, https://doi.org/10.1038/s41598-019-54682-1

Foley, S. F., and Fischer, T. P., 2017, An essential role for continental rifts and lithosphere in the deep carbon cycle: Nature Geoscience, v. 10, p. 897–902, https://doi.org/10.1038/s41561-017-0002-7

Früh-Green, G. L., Connolly, J. A. D., Plas, A., Kelley, D. S., and Grobéty, B., 2004, Serpentinization of oceanic peridotites: implications for geochemical cycles and biological activity, *in* Wilcock, W. S. D., Delong, E. F., Kelley, D. S., Baross, J. A., and Cary, C., editors, The subseafloor biosphere at mid-ocean ridges: Geiphysical Monograph Series, v. 144, p. 119–136, https://doi.org/10.1029/144GM08

Gaillard, F., Scaillet, B., and Arndt, N. T., 2011, Atmospheric oxygenation caused by a change in volcanic degassing pressure: Nature, v. 478, p. 229–232, https://doi.org/10.1038/nature10460

Gale, A., Dalton, C. A., Langmuir, C. H., Su, Y., and Schilling, J.-G., 2013, The mean composition of ocean ridge basalts: Geochemistry, Geophysics, Geosystems, v. 14, n. 3, p. 489–518, https://doi.org/10.1029/2012GC004334

Galvez, M. E., 2020, Redox constraints on a Cenozoic imbalance in the organic carbon cycle: American Journal of Science, v. 320, n. 8, p. 730–751, https://doi.org/10.2475/10.2020.03

Galy, V., Beyssac, O., France-Lanord, C., and Eglinton, T., 2008, Recycling of graphite during Himalayan erosion: a geological stabilization of carbon in the crust: Science, v. 322, n. 5903, p. 943–945, https://doi.org/10.1126/science.1161408

Geopig, 2010: Available at: geopig3.la.asu.edu:8080/GEOPIG/pigopt1.html

Gill, J. B., 1981, Orogenic andesites and plate tectonics: Berlin/Heidelberg, Germany, Springer, 390 p, https://doi.org/10.1007/978-3-642-68012-0

Glasspool, I. J., and Scott, A. C., 2010, Phanerozoic concentrations of atmospheric oxygen reconstructed from sedimentary charcoal: Nature Geoscience, v. 3, p. 627–630, https://doi.org/10.1038/ngeo923

Greening, C., Constant, P., Hards, K., Morales, S. E., Oakeshott, J. G., Russell, R. J., Taylor, M. C., Berney, M., Conrad, R., and Cook, G. M., 2015, Atmospheric hydrogen scavenging: from enzymes to ecosystems: Applied and Environmental Microbiology, v. 81, n. 4, p. 1190–1199, https://doi.org/10.1128/AEM.03364-14

Halevy, I., and Bachan, A., 2017, The geologic history of seawater pH: Science, v. 355, n. 6329, p. 1069–1071, https://doi.org/10.1126/science.aal4151

Halverson, G. P., and Hurtgen, M. T., 2007, Ediacaran growth of the marine sulfate reservoir: Earth and Planetary Science Letters, v. 263, n. 1–2, p. 32–44, https://doi.org/10.1016/j.epsl.2007.08.022

Hansen, K. W., and Wallmann, K., 2003, Cretaceous and Cenozoic evolution of seawater composition, atmospheric O_2 and CO_2: a model perspective: American Journal of Science, v. 303, n. 2, p. 94–148, https://doi.org/10.2475/ajs.303.2.94

Hart, S., and Staudigel, H., 1978, Oceanic crust: age of hydrothermal alteration: Geophysical Research Letters, v. 5, n. 12, p. 1009–1012, https://doi.org/10.1029/GL005i012p01009

Hartmann, J., Dürr, H. H., Moosdorf, N., Meybeck, M., and Kempe, S., 2012, The geochemical composition of the terrestrial surface (without soils) and comparison with the upper continental crust: International Journal of Earth Sciences, v. 101, p. 365–376, https://doi.org/10.1007/s00531-010-0635-x

Hayes, J. M., and Waldbauer, J. R., 2006, The carbon cycle and associated redox processes through time: Philosophical Transactions of the Royal Society B: Biological Sciences, v. 361, n. 1470, p. 931–950, https://doi.org/10.1098/rstb.2006.1840

Hayes, J. M., Strauss, H., and Kaufman, A. J., 1999, The abundance of ^{13}C in marine organic matter and isotopic fractionation in the global biogeochemical cycle of carbon during the past 800 Ma: Chemical Geology, v. 161, n. 1–3, p. 103–125, https://doi.org/10.1016/S0009-2541(99)00083-2

Herzberg, C., Condie, K., and Korenaga, J., 2010, Thermal history of the Earth and its petrological expression: Earth and Planetary Science Letters, v. 292, n. 1–2, p. 79–88, https://doi.org/10.1016/j.epsl.2010.01.022

Hirschmann, M. M., 2018, Comparative deep Earth volatile cycles: The case for C recycling from exosphere/mantle fractionation of major (H_2O, C, N) volatiles and from H_2O/Ce, CO_2/Ba, and CO_2/Nb exosphere ratios: Earth and Planetary Science Letters, v. 502, p. 262–273, https://doi.org/10.1016/j.epsl.2018.08.023

Hofmann, A. W., 2003, Sampling mantle heterogeneity through oceanic basalts: isotopes and trace elements, *in* Holland, H. D., and Turekian, K. K., editors., Treatise on geochemistry: Amsterdam, the Netherlands, Elsevier, v. 2, p. 61–101, https://doi.org/10.1016/B0-08-043751-6/02123-X

Holland, H. D., 1978, The Chemistry of the Atmosphere and Oceans: New York, John Wiley & Sons, p. 351

Holland, H. D., 2002, Volcanic gases, black smokers, and the Great Oxidation Event: Geochimica et Cosmochimica Acta, v. 66, n. 21, p. 3811–3826, https://doi.org/10.1016/S0016-7037(02)00950-X

Holland, H. D., 2009, Why the atmosphere became oxygenated: a proposal: Geochimica et Cosmochimica Acta, v. 73, n. 18, p. 5241–5255, https://doi.org/10.1016/j.gca.2009.05.070

Holser, W. T., Schidlowski, M., Mackenzie, F. T., and Maynard, J. B., 1988, Geochemical Cycles of Carbon and Sulfur, *in* Gregor, C. B., Garrels, R. M., Mackenzie, F. T., and Maynard, J. B. editors, Chemical Cylces in the Evolution of the Earth: New York, John & Wiley, p. 105–173.

Horton, F., 2015, Did phosphorus derived from the weathering of large igneous provinces fertilize the Neoproterozoic ocean? Geochemistry, Geophysics, Geosystems, v. 16, n. 6, p. 1723–1738, https://doi.org/10.1002/2015GC005792

House, B. M., Bebout, G. E., and Hilton, D. R., 2019, Carbon cycling at the Sunda margin, Indonesia: A regional study with global implications: Geology, v. 47, n. 5, p. 483–486, https://doi.org/10.1130/G45830.1

Hunt, J. A., Zafu, A., Mather, T. A., Pyle, D. M., and Barry, P. H., 2017, Spatially Variable CO_2 Degassing in the Main Ethiopian Rift: Implications for Magma Storage, Volatile Transport, and Rift-Related Emissions: Geochemistry, Geophysics, Geosystems, v. 18, n. 10, p. 3714–3737, https://doi.org/10.1002/2017GC006975

Husson, J. M., and Peters, S. E., 2017, Atmospheric oxygenation driven by unsteady growth of the continental sedimentary reservoir: Earth and Planetary Science Letters, v. 460, p. 68–75, https://doi.org/10.1016/j.epsl.2016.12.012

Jarrard, R. D., Abrams, L. J., Pockalny, R., Larson, R. L., and Hirono, T., 2003, Physical properties of upper oceanic crust: Ocean Drilling Program Hole 801C and the waning of hydrothermal circulation: Journal of Geophysical Research: Solid Earth, v. 108, n. B4, 2188, https://doi.org/10.1029/2001JB001727

Johnson, J. E., Gerpheide, A., Lamb, M. P., and Fischer, W. W., 2014, O2 constraints from Paleoproterozoic detrital pyrite and uraninite: Geological Society of America Bulletin, v. 126, n. 5–6, p. 813–830, https://doi.org/10.1130/B30949.1

Johnson, H. P., and Semyan, S. W., 1994, Age variation in the physical properties of oceanic basalts: Implications for crustal formation and evolution: Journal of Geophysical Research: Solid Earth, v. 99, n. B4, p. 3123–3134, https://doi.org/10.1029/93JB00717

Johnston, D. T., Poulton, S. W., Dehler, C., Porter, S., Husson, J., Canfield, D. E., and Knoll, A. H., 2010, An emerging picture of Neoproterozoic ocean chemistry: Insights from the Chuar Group, Grand Canyon, USA: Earth and Planetary Science Letters, v. 290, n. 1–2, p. 64–73, https://doi.org/10.1016/j.epsl.2009.11.059

Jørgensen, B. B., 1982, Mineralization of organic matter in the sea bed-the role of sulphate reduction: Nature, v. 296, p. 643–645, https://doi.org/10.1038/296643a0

Jugo, P. J., 2009, Sulfur content at sulfide saturation in oxidized magmas: Geology, v. 37, n. 5, p. 415-418, https://doi.org/10.1130/G25527A.1

Kadko, D., Baker, E., Alt, J., and Baross, J., 1994, Global impact of submarine hydrothermal processes: Ridge, *in* Ridge/Vents Workshop, NSF RIDGE Initiative and NOAA Vents Program.

Kadko, D., and Moore, W., 1988, Radiochemical constraints on the crustal residence time of submarine hydrothermal fluids: Endeavour Ridge: Geochimica et Cosmochimica Acta, v. 52, n. 3, p. 659–668, https://doi.org/10.1016/0016-7037(88)90328-6

Kadoya, S., Catling, D. C., Nicklas, R. W., Puchtel, I. S., and Anbar, A. D., 2020a, Mantle cooling causes more reducing volcanic gases and gradual reduction of the atmosphere: Geochemical Perspectives Letters, v. 13, p. 25–29, https://doi.org/10.7185/geochemlet.2009

Kadoya, S., Catling, D. C., Nicklas, R. W., Puchtel, I. S., and Anbar, A. D., 2020b, Mantle data imply a decline of oxidizable volcanic gases could have triggered the Great Oxidation: Nature Communications, v. 11, 2774, https://doi.org/10.1038/s41467-020-16493-1

Kah, L. C., Lyons, T. W., and Frank, T. D., 2004, Low marine sulphate and protracted oxygenation of the Proterozoic biosphere: Nature, v. 431, p. 834–838, https://doi.org/10.1038/nature02974

Kasting, J. F., and Canfield, D. E., 2012, The global oxygen cycle, *in* Knoll, A. H., Canfield, D. E., and Konhauser, K. O., editors, Fundamentals of Geobiology: Blackwell publishing, p. 93–104, https://doi.org/10.1002/9781118280874.ch7

Kasting, J. F., Eggler, D. H., and Raeburn, S. P., 1993, Mantle redox evolution and the oxidation state of the Archean atmosphere: The Journal of Geology, v. 101, n. 2, p. 245–257, https://doi.org/10.1086/648219

Kasting, J. F., Catling, D. C., and Zahnle, K., 2012, Atmospheric oxygenation and volcanism: Nature, v. 487, p. E1, https://doi.org/10.1038/nature11274
Keir, R. S., 2010, A note on the fluxes of abiogenic methane and hydrogen from mid-ocean ridges: Geophysical research letters, v. 37, n. 24, p. L24609, https://doi.org/10.1029/2010GL045362
Kelemen, P. B., and Manning, C. E., 2015, Reevaluating carbon fluxes in subduction zones, what goes down, mostly comes up: Proceedings of the National Academy of Sciences of the United States of America, v. 112, n. 30, p. E3997–E4006, https://doi.org/10.1073/pnas.1507889112
Keller, C. B., Schoene, B., Barboni, M., Samperton, K. M., and Husson, J. M., 2015, Volcanic-plutonic parity and the differentiation of the continental crust: Nature, v. 523, p. 301–307, https://doi.org/10.1038/nature14584
Keller, C. B., Husson, J. M., Mitchell, R. N., Bottke, W. F., Gernon, T. M., Boehnke, P., Bell, E. A., Swanson-Hysell, N. L., and Peters, S. E., 2019, Neoproterozoic glacial origin of the Great Unconformity: Proceedings of the National Academy of Sciences of the United States of America, v. 116, n. 4, p. 1136–1145, https://doi.org/10.1073/pnas.1804350116
Kelley, K. A., and Cottrell, E., 2009, Water and the oxidation state of subduction zone magmas: Science, v. 325, n. 5940, p. 605–607, https://doi.org/10.1126/science.1174156
Killingley, J. S., and Muenow, D. W., 1975, Volatiles from Hawaiian submarine basalts determined by dynamic high temperature mass spectrometry: Geochimica et Cosmochimica Acta, v. 39, n. 11, p. 1467–1473, https://doi.org/10.1016/0016-7037(75)90148-9
Krissansen-Totton, J., Arney, G. N., and Catling, D. C., 2018, Constraining the climate and ocean pH of the early Earth with a geological carbon cycle model: Proceedings of the National Academy of Sciences of the United States of America, v. 115, n. 16, p. 4105–4110, https://doi.org/10.1073/pnas.1721296115
Kump, L. R., 1989, Chemical stability of the atmosphere and ocean: Global and Planetary Change, v. 1, n. 1–2, p. 123–136, https://doi.org/10.1016/0921-8181(89)90019-2
Kump, L. R., and Garrels, R. M., 1986, Modeling atmospheric O_2 in the global sedimentary redox cycle: American Journal of Science, v. 286, n. 5, p. 337–360, https://doi.org/10.2475/ajs.286.5.337
Kump, L. R., and Seyfried, W. E. Jr., , 2005, Hydrothermal Fe fluxes during the Precambrian: Effect of low oceanic sulfate concentrations and low hydrostatic pressure on the composition of black smokers: Earth and Planetary Science Letters, v. 235, n. 3–4, p. 654–662, https://doi.org/10.1016/j.epsl.2005.04.040
Laakso, T. A., and Schrag, D. P., 2014, Regulation of atmospheric oxygen during the Proterozoic: Earth and Planetary Science Letters, v. 388, p. 81–91, https://doi.org/10.1016/j.epsl.2013.11.049
Laakso, T. A., and Schrag, D. P., 2017, A theory of atmospheric oxygen: Geobiology, v. 15, n. 3, p. 366–384, https://doi.org/10.1111/gbi.12230
Laakso, T. A., Sperling, E. A., Johnston, D. T., and Knoll, A. H., 2020, Ediacaran reorganization of the marine phosphorus cycle: Proceedings of the National Academy of Sciences of the United States of America, v. 117, n. 22, p. 11961–11967, https://doi.org/10.1073/pnas.1916738117
Lasaga, A. C., 1989, A new approach to isotopic modeling of the variation of atmospheric oxygen through the Phanerozoic: American Journal of Science, v. 289, n. 4, p. 411–435, https://doi.org/10.2475/ajs.289.4.411
Lasaga, A. C., and Ohmoto, H., 2002, The oxygen geochemical cycle: dynamics and stability: Geochimica et Cosmochimica Acta, v. 66, n. 3, p. 361–381, https://doi.org/10.1016/S0016-7037(01)00685-8
Lécuyer, C., and Ricard, Y., 1999, Long-term fluxes and budget of ferric iron: implication for the redox states of the Earth's mantle and atmosphere: Earth and Planetary Science Letters, v. 165, n. 2, p. 197–211, https://doi.org/10.1016/S0012-821X(98)00267-2
Lee, C.-T. A., Leeman, W. P., Canil, D., and Li, Z.-X. A., 2005, Similar V/Sc systematics in MORB and arc basalts: implications for the oxygen fugacities of their mantle source regions: Journal of Petrology, v. 46, n. 11, p. 2313–2336, https://doi.org/10.1093/petrology/egi056
Lee, C.-T. A., Luffi, P., Le Roux, V., Dasgupta, R., Albaréde, F., and Leeman, W. P., 2010, The redox state of arc mantle using Zn/Fe systematics: Nature, v. 468, p. 681–685., https://doi.org/10.1038/nature09617
Lee, C.-T. A., Luffi, P., Chin, E. J., Bouchet, R., Dasgupta, R., Morton, D. M., Le Roux, V., Yin, Q.-Z., and Jin, D., 2012, Copper systematics in arc magmas and implications for crust-mantle differentiation: Science, v. 336, n. 6077, p. 64–68, https://doi.org/10.1126/science.1217313
Lee, C.-T. A., Yeung, L. Y., McKenzie, N. R., Yokoyama, Y., Ozaki, K., and Lenardic, A., 2016b, Two-step rise of atmospheric oxygen linked to the growth of continents: Nature Geoscience, v. 9, p. 417–424, https://doi.org/10.1038/ngeo2707
Lee, H., Muirhead, J. D., Fischer, T. P., Ebinger, C. J., Kattenhorn, S. A., Sharp, Z. D., and Kianji, G., 2016a, Massive and prolonged deep carbon emissions associated with continental rifting: Nature Geoscience, v. 9, p. 145–149, https://doi.org/10.1038/ngeo2622
Lenton, T. M., 2020, On the use of models in understanding the rise of complex life: Interface Focus, v. 10, n. 4, p. 20200018, https://doi.org/10.1098/rsfs.2020.0018
Lenton, T. M., and Watson, A. J., 2004, Biotic enhancement of weathering, atmospheric oxygen and carbon dioxide in the Neoproterozoic: Geophysical Research Letters, v. 31, n. 5, p. L05202, https://doi.org/10.1029/2003GL018802
Lenton, T. M., Boyle, R. A., Poulton, S. W., Shields-Zhou, G. A., and Butterfield, N. J., 2014, Co-evolution of eukaryotes and ocean oxygenation in the Neoproterozoic era: Nature Geoscience, v. 7, p. 257–265, https://doi.org/10.1038/ngeo2108
Lenton, T. M., Dahl, T. W., Daines, S. J., Mills, B. J. W., Ozaki, K., Saltzman, M. R., and Porada, P., 2016, Earliest land plants created modern levels of atmospheric oxygen: Proceedings of the National Academy of Sciences of the United of America, v. 113, n. 35, p. 9704–9709, https://doi.org/10.1073/pnas.1604787113

Lenton, T. M., Daines, S. J., and Mills, B. J. W., 2018, COPSE reloaded: an improved model of biogeochemical cycling over Phanerozoic time: Earth-Science Reviews, v. 178, p. 1–28, https://doi.org/10.1016/j.earscirev.2017.12.004

Le Voyer, M., Hauri, E. H., Cottrell, E., Kelley, K. A., Salters, V. J. M., Langmuir, C. H., Hilton, D. R., Barry, P. H., and Füri, E., 2019, Carbon Fluxes and Primary Magma CO2 Contents Along the Global Mid-Ocean Ridge System: Geochemistry, Geophysics, Geosystems, v. 20, n. 3, p. 1387–1424, https://doi.org/10.1029/2018GC007630

Li, G., and Elderfield, H., 2013, Evolution of carbon cycle over the past 100 million years: Geochimica et Cosmochimica Acta, v. 103, p. 11–25, https://doi.org/10.1016/j.gca.2012.10.014

Li, J.-L., Schwarzenbach, E. M., John, T., Ague, J. J., Huang, F., Gao, J., Klemd, R., Whitehouse, M. J., and Wang, X.-S., 2020, Uncovering and quantifying the subduction zone sulfur cycle from the slab perspective: Nature Communications, v. 11, p.514, https://doi.org/10.1038/s41467-019-14110-4

Li, Z.-X. A., and Lee, C.-T. A., 2004, The constancy of upper mantle fO_2 through time inferred from V/Sc ratios in basalts: Earth and Planetary Science Letters, v. 228, n. 3–4, p. 483–493, https://doi.org/10.1016/j.epsl.2004.10.006

Love, G. D., Grosjean, E., Stalvies, C., Fike, D. A., Grotzinger, J. P., Bradley, A. S., Kelly, A. E., Bhatia, M., Meredith, W., Snape, C. E., Bowring, S. A., Condon, D. J., and Summons, R. E., 2009, Fossil steroids record the appearance of Demospongiae during the Cryogenian period: Nature, v. 457, p. 718–721, https://doi.org/10.1038/nature07673

Lowenstein, T. K., Hardie, L. A., Timofeeff, M. N., and Demicco, R. V., 2003, Secular variation in seawater chemistry and the origin of calcium chloride basinal brines: Geology, v. 31, n. 10, p. 857–860, https://doi.org/10.1130/G19728R.1

Lu, W., Ridgwell, A., Thomas, E., Hardisty, D. S., Luo, G., Algeo, T. J., Saltzman, M. R., Gill, B. C., Shen, Y., Ling, H.-F., Edwards, C. T., Whalen, M. T., Gutchess, K. M., Jin, L., Rickaby, R. E. M., Jenkyns, H. C., Lynos, T. W., Lenton, T. M., Kump, L. R., and Lu, Z., 2018, Late inception of a resiliently oxygenated upper ocean: Science, v. 361, n. 6398, p. 174–177, https://doi.org/10.1126/science.aar5372

Lyons, T. W., Reinhard, C. T., and Planavsky, N. J., 2014, The rise of oxygen in Earth's early ocean and atmosphere: Nature, v. 506, p. 307–315, https://doi.org/10.1038/nature13068

Mallmann, G., and O'Neill, H. S. C., 2009, The crystal/melt partitioning of V during mantle melting as a function of oxygen fugacity compared with some other elements (Al, P, Ca, Sc, Ti, Cr, Fe, Ga, Y, Zr and Nb): Journal of Petrology, v. 50, n. 9, p. 1765–1794, https://doi.org/10.1093/petrology/egp053

Marty, B., and Tolstikhin, I. N., 1998, CO2 fluxes from mid-ocean ridges, arcs and plumes: Chemical Geology, v. 145, n. 3–4, p. 233–248, https://doi.org/10.1016/S0009-2541(97)00145-9

Métrich, N., Schiano, P., Clocchiatti, R., and Maury, R. C., 1999, Transfer of sulfur in subduction settings: an example from Batan Island (Luzon volcanic arc, Philippines): Earth and Planetary Science Letters, v. 167, n. 1–2, p. 1–14, https://doi.org/10.1016/S0012-821X(99)00009-6

Mills, B. J. W., Krause, A. J., Scotese, C. R., Hill, D. J., Shields, G. A., and Lenton, T. M., 2019, Modelling the long-term carbon cycle, atmospheric CO_2, and Earth surface temperature from late Neoproterozoic to present day: Gondwana Research, v. 67, p. 172–186, https://doi.org/10.1016/j.gr.2018.12.001

Mills, B., Lenton, T. M., and Watson, A. J., 2014, Proterozoic oxygen rise linked to shifting balance between seafloor and terrestrial weathering: Proceedings of the National Academy of Sciences of the United States of America, v. 111, n. 25, p. 9073–9078, https://doi.org/10.1073/pnas.1321679111

Miyazaki, Y., Planavsky, N. J., Bolton, E. W., and Reinhard, C. T., 2018, Making sense of massive carbon isotope excursions with an inverse carbon cycle model: Journal of Geophysical Research: Biogeosciences, v. 123, n. 8, p. 2485–2496, https://doi.org/10.1029/2018JG004416

Mjelde, R., Wessel, P., and Müller, R. D., 2010, Global pulsations of intraplate magmatism through the Cenozoic: Lithosphere, v. 2, n. 5, p. 361–376, https://doi.org/10.1130/L107.1

Moore, J. G., and Schilling, J.-G., 1973, Vesicles, water, and sulfur in Reykjanes Ridge basalts: Contributions to Mineralogy and Petrology, v. 41, p. 105–118, https://doi.org/10.1007/BF00375036

Mottl, M. J., Wheat, G., Baker, E., Becker, N., Davis, E., Feely, R., Grehan, A., Kadko, D., Lilley, M., Massoth, G., Moyer, C., and Sansone, F., 1998, Warm springs discovered on 3.5 Ma oceanic crust, eastern flank of the Juan de Fuca Ridge: Geology, v. 26, n. 1, p. 51–54, https://doi.org/10.1130/0091-7613(1998)026<0051:WSDOMO>2.3.CO;2

Mottl, M. J., Wheat, C. G., Fryer, P., Gharib, J., and Martin, J. B., 2004, Chemistry of springs across the Mariana forearc shows progressive devolatilization of the subducting plate: Geochimica et Cosmochimica Acta, v. 68, n. 23, p. 4915–4933, https://doi.org/10.1016/j.gca.2004.05.037

Moussallam, Y., Longpré, M.-A., McCammon, C., Gomez-Ulla, A., Rose-Koga, E. F., Scaillet, B., Peters, N., Gennaro, E., Paris, R., and Oppenheimer, C., 2019a, Mantle plumes are oxidised: Earth and Planetary Science Letters, v. 527, p. 115798, https://doi.org/10.1016/j.epsl.2019.115798

Moussallam, Y., Oppenheimer, C., and Scaillet, B., 2019b, On the relationship between oxidation state and temperature of volcanic gas emissions: Earth and Planetary Science Letters, v. 520, p. 260–267, https://doi.org/10.1016/j.epsl.2019.05.036

Müller, R. D., Seton, M., Zahirovic, S., Williams, S. E., Matthews, K. J., Wright, N. M., Shephard, G. E., Maloney, K. T., Barnett-Moore, N., Hosseinpour, M., Bower, D. J., and Cannon, J., 2016, Ocean basin evolution and global-scale plate reorganization events since Pangea breakup: Annual Review of Earth and Planetary Sciences, v. 44, p. 107–138, https://doi.org/10.1146/annurev-earth-060115-012211

Muth, M. J., and Wallace, P. J., 2021, Slab-derived sulfate generates oxidized basaltic magmas in the southern Cascade arc (California, USA): Geology, v. 49, n. 10, p. 1177–1181, https://doi.org/10.1130/G48759.1

Neal, C., and Stanger, G., 1983, Hydrogen generation from mantle source rocks in Oman: Earth and Planetary Science Letters, v. 66, p. 315–320, https://doi.org/10.1016/0012-821X(83)90144-9

Nicklas, R. W., Puchtel, I. S., and Ash, R. D., 2018, Redox state of the Archean mantle: Evidence from V partitioning in 3.5–2.4 Ga komatiites: Geochimica et Cosmochimica Acta, v. 222, p. 447–466, https://doi.org/10.1016/j.gca.2017.11.002

Nicklas, R. W., Puchtel, I. S., Ash, R. D., Piccoli, P. M., Hanski, E., Nisbet, E. G., Waterton, P., Pearson, D. G., and Anbar, A. D., 2019, Secular mantle oxidation across the Archean-Proterozoic boundary: Evidence from V partitioning in komatiites and picrites: Geochimica et Cosmochimica Acta, v. 250, p. 49–75, https://doi.org/10.1016/j.gca.2019.01.037

Nielsen, S. G., Rehkämper, M., Teagle, D. A. H., Butterfield, D. A., Alt, J. C., and Halliday, A. N., 2006, Hydrothermal fluid fluxes calculated from the isotopic mass balance of thallium in the ocean crust: Earth and Planetary Science Letters, v. 251, n. 1–2, p. 120–133, https://doi.org/10.1016/j.epsl.2006.09.002

Ohara, Y., Reagan, M. K., Fujikura, K., Watanabe, H., Michibayashi, K., Ishii, T., Stern, R. J., Pujana, I., Martinez, F., Girard, G., Ribeiro, J., Brounce, M., Komori, N., and Kino, M., 2012, A serpentinite-hosted ecosystem in the Southern Mariana Forearc: Proceedings of the National Academy of Sciences of the United States of America, v. 109, n. 8, p. 2831–2835, https://doi.org/10.1073/pnas.1112005109

Oppenheimer, C., Scaillet, B., and Martin, R. S., 2011, Sulfur degassing from volcanoes: source conditions, surveillance, plume chemistry and earth system impacts: Reviews in Mineralogy and Geochemistry, v. 73, n. 1, p. 363–421, https://doi.org/10.2138/rmg.2011.73.13

Oppenheimer, C., Scaillet, B., Woods, A., Sutton, A. J., Elias, T., and Moussallam, Y., 2018, Influence of eruptive style on volcanic gas emission chemistry and temperature: Nature Geoscience, v. 11, p. 678–681, https://doi.org/10.1038/s41561-018-0194-5

Parkinson, I. J., and Arculus, R. J., 1999, The redox state of subduction zones: insights from arc-peridotites: Chemical Geology, v. 160, n. 4, p. 409–423, https://doi.org/10.1016/S0009-2541(99)00110-2

Pavlov, A. A., and Kasting, J. F., 2002, Mass-independent fractionation of sulfur isotopes in Archean sediments: strong evidence for an anoxic Archean atmosphere: Astrobiology, v. 2, n.1, p. 27–41, https://doi.org/10.1089/153110702753621321

Petsch, S. T., Berner, R. A., and Eglinton, T. I., 2000, A field study of the chemical weathering of ancient sedimentary organic matter: Organic Geochemistry, v. 31, n. 5, p. 475–487, https://doi.org/10.1016/S0146-6380(00)00014-0

Planavsky, N. J., McGoldrick, P., Scott, C. T., Li, C., Reinhard, C. T., Kelly, A. E., Chu, X., Bekker, A., Love, G. D., and Lyons, T. W., 2011, Widespread iron-rich conditions in the mid-Proterozoic ocean: Nature, v. 477, p. 448–451, https://doi.org/10.1038/nature10327

Planavsky, N. J., Cole, D. B., Isson, T. T., Reinhard, C. T., Crockford, P. W., Sheldon, N. D., and Lyons, T. W., 2018, A case for low atmospheric oxygen levels during Earth's middle history: Emerging Topics in Life Sciences, v. 2, n. 2, p. 149–159, https://doi.org/10.1042/ETLS20170161

Plank, T., and Langmuir, C. H., 1998, The chemical composition of subducting sediment and its consequences for the crust and mantle: Chemical Geology, v. 145, n. 3–4, p. 325–394, https://doi.org/10.1016/S0009-2541(97)00150-2

Reekie, C. D. J., Jenner, F. E., Smythe, D. J., Hauri, E. H., Bullock, E. S., and Williams, H. M., 2019, Sulfide resorption during crustal ascent and degassing of oceanic plateau basalts: Nature communications, v. 10, 82, https://doi.org/10.1038/s41467-018-08001-3

Reinhard, C. T., Planavsky, N. J., Gill, B. C., Ozaki, K., Robbins, L. J., Lyons, T. W., Fischer, W. W., Wang, C., Cole, D. B., and Konhauser, K. O., 2017, Evolution of the global phosphorus cycle: Nature, v. 541, p. 386–389, https://doi.org/10.1038/nature20772

Richards, J. P., and Mumin, A. H., 2013, Magmatic-hydrothermal processes within an evolving Earth: Iron oxide-copper-gold and porphyry Cu±Mo±Au deposits: Geology, v. 41, n. 7, p. 767–770, https://doi.org/10.1130/G34275.1

Royer, D. L., Donnadieu, Y., Park, J., Kowalczyk, J., and Goddéris, Y., 2014, Error analysis of CO_2 and O_2 estimates from the long-term geochemical model GEOCARBSULF: American Journal of Science, v. 314, n. 9, p. 1259–1283, https://doi.org/10.2475/09.2014.01

Rudnick, R. L., and Gao, S., 2014, Composition of the continental crust, *in* Holland, H. D., and Turekian, K. K., editors, Treatise on Geochemistry (second edition): Amsterdam, the Netherlands, Elsevier, v. 4, p. 1–51, https://doi.org/10.1016/B978-0-08-095975-7.00301-6

Rye, R., and Holland, H. D., 1998, Paleosols and the evolution of atmospheric oxygen: a critical review: American Journal of Science, v. 298, n. 8, p. 621–672 https://doi.org/10.2475/ajs.298.8.621

Sahoo, S. K., Planavsky, N. J., Kendall, B., Wang, X., Shi, X., Scott, C., Anbar, A. D., Lyons, T. W., and Jiang, G., 2012, Ocean oxygenation in the wake of the Marinoan glaciation: Nature, v. 489, p. 546–549, https://doi.org/10.1038/nature11445

Sarmiento, J. L., and Gruber, N., 2006, Ocean Biogeochemical Dynamics: Princeton, Princeton University Press, 526 p, https://doi.org/10.1515/9781400849079

Sarmiento, J. L., Herbert, T. D., and Toggweiler, J. R., 1988, Causes of anoxia in the world ocean: Global Biogeochemical Cycles, v. 2, n. 2, p. 115–128, https://doi.org/10.1029/GB002i002p00115

Sawyer, G. M., Carn, S. A., Tsanev, V. I., Oppenheimer, C., and Burton, M., 2008, Investigation into magma degassing at Nyiragongo volcano, Democratic Republic of the Congo: Geochemistry, Geophysics, Geosystems, v. 9, n. 2, p. Q02017, https://doi.org/10.1029/2007GC001829

Scheuermann, P. P., Xing, Y., Ding, K., and Seyfried, W. E. Jr., 2020, Experimental measurement of $H_{2(aq)}$ solubility in hydrothermal fluids: application to the Piccard hydrothermal field, Mid-Cayman Rise: Geochimica et Cosmochimica Acta, v. 283, p. 22–39, https://doi.org/10.1016/j.gca.2020.05.020

Scholl, D. W., and von Huene, R., 2007, Crustal recycling at modern subduction zones applied to the past—Issues of growth and preservation of continental basement crust, mantle geochemistry, and supercontinent reconstruction, *in* Hatcher, R. D. Jr., Carlson, M. P., McBride, J. H., and Martínez Catalán, J. R.,

editors, 4-D Framework of Continental Crust: Geological Society of America Memoirs, v. 200, p. 9–32, https://doi.org/10.1130/2007.1200(02)
Seiter, K., Hensen, C., Schröter, J., and Zabel, M., 2004, Organic carbon content in surface sediments-defining regional provinces: Deep Sea Research Part I: Oceanographic Research Papers, v. 51, n. 12, p. 2001–2026, https://doi.org/10.1016/j.dsr.2004.06.014
Shanks, W. C. III, Böhlke, J. K., and Seal, R. II, , 1995, Stable Isotopes in Mid-Ocean Ridge Hydrothermal Systems, *in* Humphris, S. E., Zierenberg, R. A., Mullineaux, L. S., and Thomson, R.E. editors, Seafloor Hydrothermal Systems: Physical, Chemical, Biological, and Geological Interactions: Geophysical Monograph Series, Washington, DC, American Geophysical Union, v. 91, p. 194–221.
Sherwood Lollar, B., Onstott, T. C., Lacrampe-Couloume, G., and Ballentine, C. J., 2014, The contribution of the Precambrian continental lithosphere to global H_2 production: Nature, v. 516, p. 379–382, https://doi.org/10.1038/nature14017
Shields-Zhou, G., and Och, L., 2011, The case for a Neoproterozoic oxygenation event: geochemical evidence and biological consequences: GSA Today, v. 21, n. 3, p. 4–11, https://doi.org/10.1130/GSATG102A.1
Sides, I. R., Edmonds, M., Maclennan, J., Swanson, D. A., and Houghton, B. F., 2014, Eruption style at Kilauea Volcano in Hawai'i linked to primary melt composition: Nature Geoscience, v. 7, p. 464–469, https://doi.org/10.1038/ngeo2140
Sleep, N. H., and Bird, D. K., 2007, Niches of the pre-photosynthetic biosphere and geologic preservation of Earth's earliest ecology: Geobiology, v. 5, n. 2, p. 101–117, https://doi.org/10.1111/j.1472-4669.2007.00105.x
Sleep, N. H., Meibom, A., Fridriksson, T., Coleman, R. G., and Bird, D. K., 2004, H2-rich fluids from serpentinization: geochemical and biotic implications: Proceedings of the National Academy of Sciences of the United States of America, v. 101, n. 35, p. 12818–12823, https://doi.org/10.1073/pnas.0405289101
Sparkes, R. B., Hovius, N., Galy, A., and Liu, J. T., 2020, Survival of graphitized petrogenic organic carbon through multiple erosional cycles: Earth and Planetary Science Letters, v. 531, p. 115992, https://doi.org/10.1016/j.epsl.2019.115992
Spear, N., Holland, H. D., Garcia-Veígas, J., Lowenstein, T. K., Giegengack, R., and Peters, H., 2014, Analyses of fluid inclusions in Neoproterozoic marine halite provide oldest measurement of seawater chemistry: Geology, v. 42, n. 2, p. 103–106, https://doi.org/10.1130/G34913.1
Sperling, E. A., Pisani, D., and Peterson, K. J., 2007, Poriferan paraphyly and its implications for Precambrian palaeobiology: Geological Society, London, Special Publications, v. 286, p. 355–368, https://doi.org/10.1144/SP286.25
Sperling, E. A., Wolock, C. J., Morgan, A. S., Gill, B. C., Kunzmann, M., Halverson, G. P., Macdonald, F. A., Knoll, A. H., and Johnston, D. T., 2015, Statistical analysis of iron geochemical data suggests limited late Proterozoic oxygenation: Nature, v. 523, p. 451–454, https://doi.org/10.1038/nature14589
Stolper, D. A., and Bucholz, C. E., 2019, Neoproterozoic to early Phanerozoic rise in island arc redox state due to deep ocean oxygenation and increased marine sulfate levels: Proceedings of the National Academy of Sciences of the United States of America, v. 116, n. 18, p. 8746–8755, https://doi.org/10.1073/pnas.1821847116
Stolper, D. A., and Keller, C. B., 2018, A record of deep-ocean dissolved O_2 from the oxidation state of iron in submarine basalts: Nature, v. 553, p. 323–327, https://doi.org/10.1038/nature25009
Stolper, D. A., Bender, M. L., Dreyfus, G. B., Yan, Y., and Higgins, J. A., 2016, A Pleistocene ice core record of atmospheric O_2 concentrations: Science, v. 353, n. 6306, p. 1427–1430, https://doi.org/10.1126/science.aaf5445
Symonds, R. B., Rose, W. I., Bluth, G. J. S., and Gerlach, T. M., 1994, Volcanic-gas studies: Methods, results, and applications, *in* Carroll, M. R., and Holloway, J. R., editors, Volatiles in magma: Reviews in Mineralogy and Geochemistry, v. 30, p. 1–66, https://doi.org/10.1515/9781501509674-007
Syvitski, J. P. M., and Kettner, A., 2011, Sediment flux and the Anthropocene: Philosophical Transactions of the Royal Society A: Mathematical, Physical and Engineering Sciences, v. 369, n. 1938, p. 957–975, https://doi.org/10.1098/rsta.2010.0329
Tappert, R., McKellar, R. C., Wolfe, A. P., Tappert, M. C., Ortega-Blanco, J., and Muehlenbachs, K., 2013, Stable carbon isotopes of C3 plant resins and ambers record changes in atmospheric oxygen since the Triassic: Geochimica et Cosmochimica Acta, v. 121, p. 240–262, https://doi.org/10.1016/j.gca.2013.07.011
Thompson, K. J., Kenward, P. A., Bauer, K. W., Warchola, T., Gauger, T., Martinez, R., Simister, R. L., Michiels, C. C., Llirós, M., Reinhard, C. T., Kappler, A., Konhauser, K. O., and Crowe, S. A., 2019, Photoferrotrophy, deposition of banded iron formations, and methane production in Archean oceans: Science Advances, v. 5, n. 11, eaav2869, https://doi.org/10.1126/sciadv.aav2869
Tostevin, R., and Mills, B. J. W., 2020, Reconciling proxy records and models of Earth's oxygenation during the Neoproterozoic and Palaeozoic: Interface Focus, v. 10, n. 4, 20190137, https://doi.org/10.1098/rsfs.2019.0137
Turner, E. C., and Bekker, A., 2016, Thick sulfate evaporite accumulations marking a mid-Neoproterozoic oxygenation event (Ten Stone Formation, Northwest Territories, Canada): GSA Bulletin, v. 128, n. 1–2, p. 203–222, https://doi.org/10.1130/B31268.1
Van Cappellen, P., and Ingall, E. D., 1996, Redox stabilization of the atmosphere and oceans by phosphorus-limited marine productivity: Science, v. 271, n. 5248, p. 493–496, https://doi.org/10.1126/science.271.5248.493
Varne, R., Brown, A. V., and Falloon, T., 2000, Macquarie Island: its geology, structural history, and the timing and tectonic setting of its N-MORB to E-MORB magmatism, *in* Dilek, Y., Moores, E. M., Elthon, D., and Nicolas, A., editors, Ophiolites and oceanic crust: new insights from field studies and the Ocean

Drilling Program: Special Papers-Geological society of America, p. 301–320, https://doi.org/10.1130/0-8137-2349-3.301

Veizer, J., and Jansen, S. L., 1985, Basement and sedimentary recycling-2: time dimension to global tectonics: The Journal of Geology, v. 93, n. 6, p. 625–643, https://doi.org/10.1086/628992

Veizer, J., and Mackenzie, F. T., 2014, 9.15-Evolution of sedimentary rocks: *in* Holland, H. D., and Turekian, K. K., editors, Treatise on Geochemistry (second edition): Amsterdam, the Netherlands, Elsevier, v. 9, p. 399–435, https://doi.org/10.1016/B978-0-08-095975-7.00715-4

Volk, T., 1989, Sensitivity of climate and atmospheric CO_2 to deep-ocean and shallow-ocean carbonate burial: Nature, v. 337, p. 637–640, https://doi.org/10.1038/337637a0

von Huene, R., and Scholl, D. W., 1991, Observations at convergent margins concerning sediment subduction, subduction erosion, and the growth of continental crust: Reviews of Geophysics, v. 29, n. 3, p. 279–316, https://doi.org/10.1029/91RG00969

Walker, J. C. G., Hays, P. B., and Kasting, J. F., 1981, A negative feedback mechanism for the long-term stabilization of the Earth's surface temperature: Journal of Geophysical Research: Oceans, v. 86, n. C10, p. 9776–9782, https://doi.org/10.1029/JC086iC10p09776

Wallace, P. J., 2005, Volatiles in subduction zone magmas: concentrations and fluxes based on melt inclusion and volcanic gas data: Journal of Volcanology and Geothermal Research, v. 140, n. 1–3, p. 217–240, https://doi.org/10.1016/j.jvolgeores.2004.07.023

Wallace, P. J., and Edmonds, M., 2011, The sulfur budget in magmas: evidence from melt inclusions, submarine glasses, and volcanic gas emissions: Reviews in Mineralogy and Geochemistry, v. 73, n. 1, p. 215–246, https://doi.org/10.2138/rmg.2011.73.8

Wallace, M. W., Hood, A., Shuster, A., Greig, A., Planavsky, N. J., and Reed, C. P., 2017, Oxygenation history of the Neoproterozoic to early Phanerozoic and the rise of land plants: Earth and Planetary Science Letters, v. 466, p. 12–19, https://doi.org/10.1016/j.epsl.2017.02.046

Wallmann, K., 2001, Controls on the Cretaceous and Cenozoic evolution of seawater composition, atmospheric CO_2 and climate: Geochimica et Cosmochimica Acta, v. 65, n. 18, p. 3005–3025, https://doi.org/10.1016/S0016-7037(01)00638-X

Wheat, C. G., and Mottl, M. J., 2000, Composition of pore and spring waters from Baby Bare: Global implications of geochemical fluxes from a ridge flank hydrothermal system: Geochimica et Cosmochimica Acta, v. 64, n. 4, p. 629–642, https://doi.org/10.1016/S0016-7037(99)00347-6

Williams, J. J., Mills, B. J. W., and Lenton, T. M., 2019, A tectonically driven Ediacaran oxygenation event: Nature Communications, v. 10, 2690, https://doi.org/10.1038/s41467-019-10286-x

Wood, B. J., Bryndzia, L. T., and Johnson, K. E., 1990, Mantle oxidation state and its relationship to tectonic environment and fluid speciation: Science, v. 248, n. 4953, p. 337–345, https://doi.org/10.1126/science.248.4953.337

Yung, Y. L., Wen, J.-S., Moses, J. I., Landry, B. M., Allen, M., and Hsu, K.-J., 1989, Hydrogen and deuterium loss from the terrestrial atmosphere: A quantitative assessment of nonthermal escape fluxes: Journal of Geophysical Research: Atmospheres, v. 94, n. D12, p. 14971–14989, https://doi.org/10.1029/JD094iD12p14971

Zhang, H. L., Cottrell, E., Solheid, P. A., Kelley, K. A., and Hirschmann, M. M., 2018, Determination of $Fe^{3+}/\Sigma Fe$ of XANES basaltic glass standards by Mössbauer spectroscopy and its application to the oxidation state of iron in MORB: Chemical Geology, v. 479, p. 166–175, https://doi.org/10.1016/j.chemgeo.2018.01.006